ICE, CLOUD, and Land Elevation Satellite-2 (ICESat-2) Project

Algorithm Theoretical Basis Document (ATBD) for
Land Ice Along-Track Height Product (ATL06)

Prepared by: Benjamin Smith, University of Washington Applied Physics Lab

with

David Hancock, Kaitlin Harbeck, LeeAnne Roberts, Thomas Neumann, Kelly Brunt, Helen Fricker, Alex Gardner, Matthew Siegfried, Susheel Adusumilli, Beata Csathó, Nicholas Holschuh, Johan Nilsson, and Fernando Paolo

Maintained by: Denis Felikson, NASA Goddard Space Flight Center

Goddard Space Flight Center
Greenbelt, Maryland

**National Aeronautics and
Space Administration**

Abstract

This document describes the theoretical basis of the land ice height processing algorithms and the products that are produced by the ICESat-2 mission. It includes descriptions of the parameters that are provided with each product as well as ancillary geophysical parameters used in the derivation of the products.

CM Foreword

This document is an Ice, Cloud, and Land Elevation Satellite-2 (ICESat-2) Project Science Office controlled document. Changes to this document require prior approval of the Science Development Team ATBD Lead or designee. Proposed changes shall be submitted in the ICESat-II Management Information System (MIS) via a Signature Controlled Request (SCoRe), along with supportive material justifying the proposed change.

In this document, a requirement is identified by "shall," a good practice by "should," permission by "may" or "can," expectation by "will," and descriptive material by "is."

Questions or comments concerning this document should be addressed to:

ICESat-2 Project Science Office
Mail Stop 615
Goddard Space Flight Center
Greenbelt, Maryland 20771

Preface

This document is the Algorithm Theoretical Basis Document for the TBD processing to be implemented at the ICESat-2 Science Investigator-led Processing System (SIPS). The SIPS supports the ATLAS (Advance Topographic Laser Altimeter System) instrument on the ICESat-2 Spacecraft and encompasses the ATLAS Science Algorithm Software (ASAS) and the Scheduling and Data Management System (SDMS). The science algorithm software will produce Level 0 through Level 4 standard data products as well as the associated product quality assessments and metadata information.

The ICESat-2 Science Development Team, in support of the ICESat-2 Project Science Office (PSO), assumes responsibility for this document and updates it, as required, as algorithms are refined or to meet the needs of the ICESat-2 SIPS. Reviews of this document are performed when appropriate and as needed updates to this document are made. Changes to this document will be made by complete revision.

Changes to this document require prior approval of the Change Authority listed on the signature page. Proposed changes shall be submitted to the ICESat-2 PSO, along with supportive material justifying the proposed change.

Questions or comments concerning this document should be addressed to:

ICESat-2 Project Science Office
Mail Stop 615
Goddard Space Flight Center
Greenbelt, Maryland 20771

Review/Approval Page

Prepared by:

Benjamin Smith
Principal Researcher
University of Washington
Applied Physics Lab Polar Science Center
1013 NE 40th Street
Box 355640
Seattle, WA 98105

Reviewed by:

Alex Gardner
NASA Jet Propulsion Laboratory

Maintained by:

Denis Felikson
Research Scientist
NASA Goddard Space Flight Center
Cryospheric Sciences Laboratory
Code 615, Building 33, Room A209
8800 Greenbelt Rd.
Greenbelt, MD 20771

*** Signatures are available on-line at: https://ipdtdms.gsfc.nasa.gov *******

Change History Log

Revision Level	Description of Change	Date Approved
1.0	Initial Release	
4.0	Minor changes made to document front matter; added brief abstract; clarified description of corrections applied to land-ice height variable (*h_li*).	
5.0	Removed the parameter *h_robust_sprd* from the *ATL06_quality_summary* flag; updated Figures 8-1 and 8-2.	

List of TBDs/TBRs

Item No.	Location	Summary	Ind./Org.	Due Date

Table of Contents

List of Figures

List of Tables

1 INTRODUCTION

This document describes the theoretical basis and implementation of the level-3 land-ice processing algorithms. It currently includes ATL06, which provides geolocated land-ice surface heights, and ATL11, which provides time series of surface heights. The higher-level products, providing mapped height, and mapped height change will be described in supplements to this document available 2021.

The ATL06 product provides the most basic derived values from the ATLAS instrument on ICESat-2: the surface height at a given point on Earth's surface at a given time relative to the WGS-84 ellipsoid. ATL06 provides estimates of the ice-sheet surface height, and ancillary parameters needed to interpret and assess the quality of these height estimates. ATL06 heights represent the mean surface height averaged along 40-m segments of ground track, 20-m apart, for each of ATLAS's six beams. Segments within adjacent beams are aligned to facilitate estimation of the across-track surface slope; they are also aligned from orbit to orbit so that subsequent repeat tracks give height estimates for nearly the same location on the surface, simplifying the estimation of height changes made through repeat-track analysis. Height estimates from ATL06 can also be compared with other geodetic data and used as inputs to higher-level ICESat-2 products, particularly ATL11, 14, and 15.

Higher-level products are based on the height estimates in ATL06. ATL11 provides heights corrected for displacements between the reference tracks and the location of the ATLAS measurements. ATL14 provides gridded height maps for selected epochs during the mission, based on the corrected heights in ATL11. ATL15 provides height-change maps based on the ATL14 height maps and height differences derived from ATL11.

In this document, Section 2 provides an overview of land-ice products and gives a brief summary of the procedures used to derive products

Section 3 describes the algorithm used to generate the products.

Section 4 gives the processing steps and input data required to derive each parameter, and describes the products in detail.

Section 5 gives a detailed procedure for deriving selected parameters

Section 6 describes test data and specific tests that NASA's implementation of the algorithm should pass.

33 **2   BACKGROUND INFORMATION AND OVERVIEW**

34   This section provides a conceptual description of ICESat-2's ice-sheet height measurements and
35   gives a brief description of the derived products.

36   **2.1   Background**

37   ATLAS on ICESat-2 determines the range between the satellite and the Earth's surface by
38   measuring the two-way time delay of short pulses of laser light that it transmits in six beams. It
39   is different from previous operational ice-sheet altimeters in that uses a photon-counting
40   detector. Previous altimeters (e.g. GLAS on ICESat-1, ATM, and LVIS) have used full-
41   waveform digitizers that received millions or more photons for each transmitted pulse, allowing
42   the receiver to generate a waveform, *i.e.* the return power as a function of time. ATLAS instead
43   records a set of arrival times for individual photons, which are then analyzed to derive surface,
44   vegetation, and cloud properties. Although ATLAS measures much weaker signals than full-
45   waveform altimeters, it has three major design advantages over GLAS:

46   i)   ATLAS has six beams arranged in three pairs (Figure 2-1), so that it samples each of
47   three reference pair tracks with a pair of beams;
48   ii)   ATLAS transmits pulses at 10 kHz, giving approximately one pulse every 0.7 m
49   along track, more than two orders of magnitude finer than the 170-meter along-track
50   of GLAS;
51   iii)   ATLAS's expected pointing control will be better than 90 m RMS, better than the
52   100-200 m achieved by ICESat-1.

53   ATLAS's six beams are spread over a small angle so that their projection onto the surface of the
54   earth is a rectangular array with two rows and three columns, with about 3.3 km separation
55   between each column and its neighbors, and 2.5 km between the rows. As ICESat-2 moves
56   along its orbit, the ATLAS beams illuminate six tracks on the Earth's surface; the array is rotated
57   slightly with respect to the satellite's flight direction so that tracks for the fore and aft beams in
58   each column produce pairs of tracks, each pair separated by about 90 m (Figure 2-1). The
59   separation between beams in each pair allows for measurement of the local surface slope in the
60   across-track and along-track direction; this will allow ICESat-2 to make the most precise and
61   detailed repeat estimates of ice-sheet height of any satellite to date.

62   ATLAS pulses are short, about 1.6 ns long (FWHM), and are transmitted every 0.1 ms (10 kHz);
63   this fast repetition yields footprint centers separated by about 0.7 m in the along-track direction.
64   Each pulse illuminates an approximately circular area on the ground ~17 m in diameter.
65   ATLAS's strong beams detect at most 12 reflected photons from each transmitted pulse. Great
66   care is taken to detect only photons with the same wavelength as the transmitted laser pulse and
67   to limit the field of view of the detectors to a region slightly larger than the illuminated
68   "footprint" of each beam; therefore, ground-return photon events (PEs, meaning photons that are
69   detected) may readily be distinguished from solar background PEs because they are clustered in
70   time, while background PEs are distributed evenly in time and arrive much less frequently.

71   The high (~45-meter RMS) accuracy of ICESat-2's pointing control means that pairs for
72   consecutive repeats of each RPT (Reference Pair Track) are likely to overlap. The fine along-

73 track sampling and the multi-beam capability allow height products to be defined for segments
74 that are consistent in along-track position for repeated measurements along the same RPT.

75

 Schematic drawing showing the pattern made by ATLAS's 6-beam configuration on the ground, for a track running from lower left to upper right. The RPTs (Reference Pair Tracks, dashed lines) are defined in advance of launch; the central RPT follows the RGT (Reference Ground Track, matching the nadir track of the predicted orbit). The Ground Tracks are the tracks actually measured by ATLAS (GT1L, GT1R, etc, shown by green footprints). Measured Pair Tracks (PTs) are defined by the centers of the pairs of GTs, and deviate slightly from the RPTs because of inaccuracies in repeat-track pointing. The separation of GTs in each pair in this figure is greatly exaggerated relative to the separation of the PTs.

Figure 2-1. ICESat-2 repeat-track schematic

76
77 Further processing of ATL06 heights will produce heights corrected for surface slope and
78 curvature that give the estimated time-varying height for selected points on the RPTs and at
79 track-to-track crossover points (ATL11).These shape-corrected heights will be processed further
80 to give i) height maps for selected time intervals (semi-annual or annual, ATL14) and ii) annual
81 height-change maps for the Antarctic and Greenland ice sheets (ATL15)
82

83 **2.2 Physical Basis of Measurements**

84 **2.2.1 Height retrieval over approximately planar surfaces**

85 Light from the ATLAS lasers reaches the earth's surface as flat disks of down-traveling photons,
86 approximately 50 cm in vertical extent, and spread over about 17 m horizontally. On land ice,
87 photons are scattered once, or many times, by snow and ice grains, into every direction,
88 including towards the satellite; a tiny fraction return to the ATLAS telescope's focal plane, and a
89 few of these are counted by the detector electronics and recorded as Photon Events (PEs). Over
90 the vast majority of the earth's land ice, the surface is smooth, with small (single-degree)
91 variations in surface slopes at scales less than a few hundred meters. This allows us to
92 approximate the surface profiles measured by ATLAS with short linear segments. We aggregate
93 PEs received by ATLAS into 50% overlapping along-track segments of a fixed length (40 m),
94 whose centers are 20 m apart. We then fit these PEs with sloping line segments; for each
95 segment, we estimate both the along-track slope and the height at the center of the segment.
96 When both beams in a pair provide height measurements, we also calculate the across-track
97 slope for the pair. Any height variation not captured by this fitting process will be treated as
98 surface roughness.

99 The time variation in surface height is determined by fitting a simple spatial function to the
100 heights from multiple repeat measurements, and using this function to correct the measurements
101 for the height variations caused by spatial sampling of sloped and curving surfaces. This
102 function is fit to the subset of the repeat measurements that we assess to be of the highest quality,
103 but corrected height estimates are provided for all available repeats, and data-quality metrics are
104 provided to allow users to decide which heights to use.

105 *2.2.2* **Effects of surface slope and roughness**

106 Figure 2-2 shows how slope and roughness contribute to the shape of the return pulse. For many
107 areas of glaciers, the ground may be treated as a rough planar surface, and the laser pulse as
108 having a Gaussian distribution in space, with intensity falling to $1/e^2$ of its peak value over a
109 distance W/2. The laser pulses also have an approximate Gaussian distribution in time, with
110 standard deviation σ_{tx}. If the incident beam is not parallel to the surface normal, photons from the
111 edge of the footprint farthest from the satellite will be delayed relative to photons from the edge
112 nearest the satellite. At the same time, a rough surface will yield early photons and late photons,
113 further spreading the returned photons. If the angle between the beam and the surface normal is
114 φ, and the surface height within the footprint has a Gaussian distribution with RMS deviation R
115 relative to the plane of the surface, then the measured temporal distribution of the returned
116 photons will be Gaussian as well (Yi & Bentley, 1999), with a temporal standard deviation equal
117 to the quadratic sum of the spreads due to the transmitted pulse, the surface slope, and the
118 roughness:

$$\sigma_R = \left[\sigma_{tx}^2 + \left(\frac{2\sigma_{beam}}{c} \tan\varphi \right)^2 + \left(\frac{2R}{c} \right)^2 \right]^{1/2} \qquad\qquad 1$$

119 For ATLAS, σ_{beam} is expected to be around 4.25 m (one quarter of W), and σ_{tx} around 0.68 ns,
120 corresponding to a FWHM (Full Width at Half Maximum) of 1.6 ns, so spreading due to sloping

121   surfaces will be smaller than the transmit-pulse duration for slopes up to approximately 1.3
122   degrees.

Figure 2-2. Schematic of returns from different surface types

Top: Transmitted photon distribution. Middle: expected return photon distribution from a
flat surface, a rough surface, and a sloping surface. Bottom: surface types.
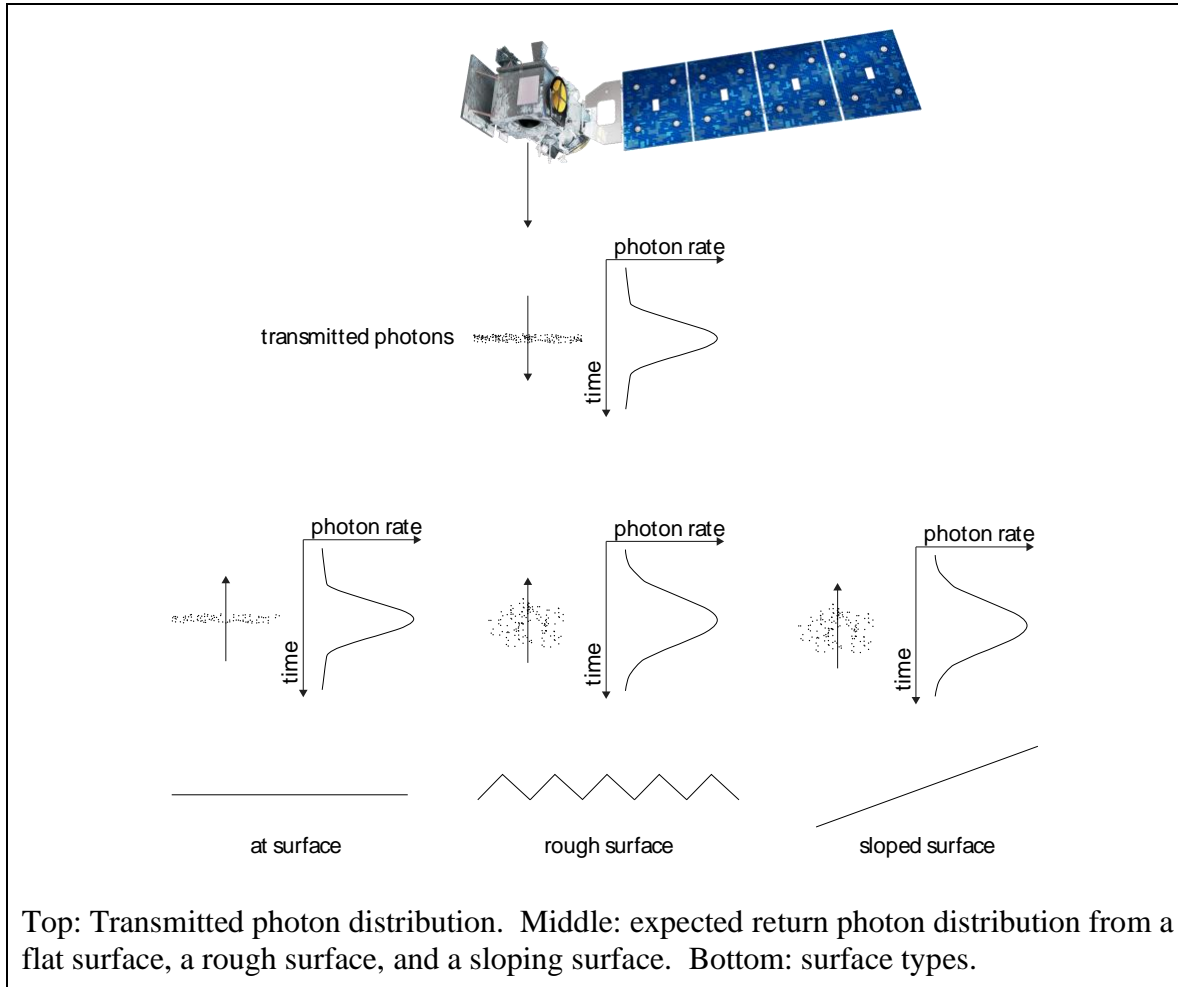
123   Surface roughness on a 17-m scale is likely to be small except in heavily crevassed glacier
124   margins and in heavily channeled ablation zones. Although analysis of the return pulse shape
125   does not allow us to distinguish the effects of roughness from those of slope, the geometry of
126   ATLAS's tracks, with pairs of beams separated by 90 m, allows estimates of the across-track
127   slope at scales modestly larger than a single footprint, while the along-track component of the
128   slope can be estimated from the along-track sequence of heights.

129   ### *2.2.3 Distinguishing return PEs and background PEs*

130   At the same time as signal photons are received by the ATLAS detector, background photons
131   from sunlight are continually entering the telescope. Most of these are eliminated by filters that
132   allow only photons with wavelengths close to the laser wavelengths through, but some pass these
133   filters, and their timing is also recorded. The time distribution of the returned signal photons
134   depends on the geometry and reflectance of the ice surface, and on scattering and attenuation in
135   the atmosphere. We distinguish signal PEs from background PEs by their clustering in time.

136 Sunlight scattered from bright (*i.e.* snow-covered) surfaces will produce detected PEs at rates up
137 to around 12 MHz. For comparison, a return with as few as three PEs distributed over one half
138 meter of range produces a brief return rate of 900 MHz. Signal returns are also distinct from the
139 background because they are spatially contiguous, so that PEs will be clustered in time in a
140 consistent way from one shot to the next.

141 **2.3   Potential Errors**

142 Errors in ATLAS land-ice products can come from a variety of sources:

143   1) Sampling error: ATLAS height estimates are based on a random sampling of the surface
144   height distribution;
145   2) Background noise: Random-noise PEs are mixed with the signal PEs, so sampled PEs
146   will include random outliers;
147   3) Complex topography: The along-track linear fit and across-track polynomial fit do not
148   always resolve complex surface topography.
149   4) Misidentified PEs: The ATL03 product will not always identify the correct PEs as signal
150   PEs;
151   5) First-photon bias: This is an error inherent to photon-counting detectors that results in a
152   high bias in the mean detected PE height that depends on signal strength;
153   6) Atmospheric forward scattering: Photons traveling downward through a cloudy
154   atmosphere may be scattered through small angles but still be reflected by the surface
155   within the ATLAS field of view; these will be delayed, producing an apparently lower
156   surface;
157   7) Subsurface scattering: Photons may be scattered many times within ice or snow before
158   returning to the detector; these will be delayed, producing a surface estimate with a low
159   bias.

160 These errors are each treated in a different way during the ATL06 processing:

161 1) and 2) are treated as random errors, and their effects are quantified in the error estimates
162 associated with the products.

163 3) and 4) will produce relatively large errors, and will need to be addressed with consistency
164 checks on the data during the generation of higher-level products.

165 5) will be corrected routinely during ATL06 processing (see Section 3.0).

166 6) and 7) require information about cloud structure and ice-surface conditions that will not be
167 available at the time of processing of ATL06. Correcting for these errors remains an active
168 avenue for research.

169 **2.4   Land-ice Level-3 products: ATL06: Land-Ice Height**

170 The ATL06 product provides surface height estimates organized by reference -pair track (RPT),
171 in a format designed to facilitate comparison between different repeat measurements on the same
172 RPT. It also combines information from the two beams in each PT to give across-track slope
173 estimates. A variety of parameters are provided that indicate the quality of the surface-height
174 estimates and the signal and noise levels associated with the measurement. Note that in cycles 1

175   and 2 of the mission, ICESat-2 did not point at the RPTS, and ICESat2's pairs are offset by up to
176   2 km from the RPT locations. The first cycle that was collected over the RPTS was the third.

177   We define ATL06 heights based on fits of a linear model to ATL03 height data from short
178   (40 m) segments of the ground track, centered on reference points spaced at 20-m intervals
179   along-track. We refer to height estimates for these short segments as "segment heights", and
180   segment's horizontal location is that of the reference point, displaced in a direction perpendicular
181   to the RGT to match the GT offset. The choice of 40 m for the segment length provides data
182   from slightly more than two independent (non-overlapping) ATL03 heights (based on 17-m
183   footprints) for the along-track slope estimate, so that this component of the slope can be
184   eliminated as a cause of vertical scatter in the PE height distribution. The spacing between
185   reference points is 20 m, so that each segment overlaps its neighbors by 50%. Defining
186   overlapping segments in this way increases the chances that a segment will overlap a locally
187   smooth area within a crevasse field, potentially improving elevation-rate recovery in these areas.

188   We use the same along-track sampling for both beams in each beam pair, and, for each cycle, use
189   the same reference point each time we calculate a segment height. This allows for direct
190   comparison between segment heights from the same RPT, without the need to interpolate in the
191   along-track direction. The ATL03 PE used for each segment can be determined by associating
192   the */gtxx/land_ice_segments/segment_id* parameter in ATL06 with the
193   */gtxx/geolocation/segment_id* parameter in ATL03: segment *m* in ATL06 includes PEs from
194   ATL03 segments *m-1* and *m* (here xx represents the ATLAS beam, with gt1l and gt1r providing
195   the left and right beams for pair 1).

196   A minimal representation of the data is given in datasets in the ATL06 product in the
197   */gtxx/land_ice_segments* groups. In these groups, we give the latitude, longitude, height, slope,
198   vertical error estimate, and a quality flag for each segment. This represents the minimum set of
199   parameters needed by most users; a wide variety of parameters describing the segment fit, the
200   input data, and the environmental conditions for the data are available in the subgroups within
201   the *gtxx* groups.

202 **3   ALGORITHM THEORY: DERIVATION OF ATL06 LAND ICE HEIGHT**
203 **PARAMETERS**

204   In this section, we describe the ATL06 height derivation from lower-level ATLAS data
205   (primarily the PE heights, locations, and times provided by ATL03). This process provides
206   height estimates and segment geolocations for a set of points (called reference points) spaced
207   every 20 m along each of ATLAS's pair tracks. One height is calculated for each beam in each
208   pair, for each reference point, for each cycle of ICESat-2's orbit.

Figure 3-1. Surface return shape

Left: power distribution for a strong beam transmit pulse, expressed as a function of height
above the surface, based on the mean of 3000 waveforms measured from an ATLAS
prototype laser, with a background noise rate of 10 MHz. Measured waveforms have been
smoothed, and noisy portions of the waveform at the beginning and end were replaced by a
smooth decay function. Inset: Power distribution on a log scale to better show the falloff in
power as a function of time. Right: Simulated PE heights for a 40 meter section of flat
ground track, based on the power distribution at left.

209 **1.1   Representation of the surface**

210

211   Figure 3-1 shows the expected surface-return power as a function of height above the surface,
212   based on waveforms measured from a prototype ATLAS laser, for sunlit ice-sheet conditions
213   with a background PE rate of 10 MHz, and a random set of photon heights generated based on

214   this waveform for a 40-meter along-track segment. The return has a sharp peak in power at the
215   ground, but it is asymmetric, with a leading edge (on the +z side) that is sharper than the trailing
216   edge (on the –z side), and with a long 'tail' of energy on the –z side caused by a slow decay in
217   laser power at the end of the pulse. This produces a dense collection of PEs at the surface height,
218   with scattered PEs above and below, some of which come from the sun and some of which come
219   from the tail of the waveform.

Figure 3-2. Mean and median height biases

Mean (red) and median (blue) heights for 1000 random collections of PEs for 40 meters
of along-track data over a flat surface, for weak and strong beams, for two different
background noise rates. Solid lines show the average height offset relative to the full-
waveform median and mean, colored patches show the 1-σ range.
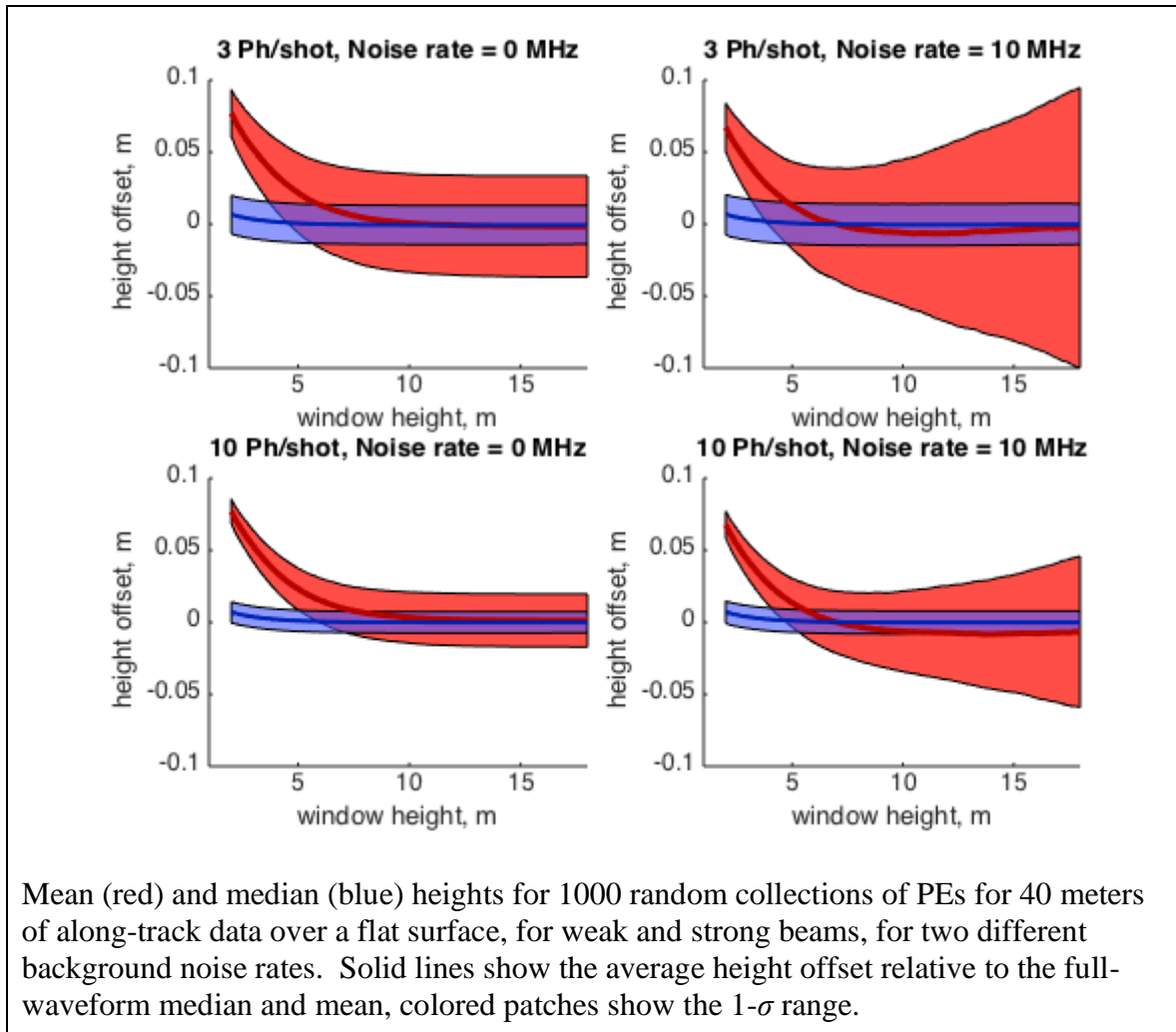
220

221   One way to characterize the surface height for this segment would be to calculate the mean of all
222   PE heights within a pre-determined height range (the 'surface window'). For simplicity, one
223   might choose a large surface window of 10-20 m to ensure the capture of all return PEs.
224   However, this choice would lead to significant noise and potential bias in the estimated surface
225   heights. The noise would come about because the mean of a distribution of heights is sensitive to
226   the extreme values of the distribution, so the photons at the edge of the distribution would
227   produce sampling errors in the recovered heights. The bias could come about if the shape of the

228 transmit pulse were to change over time, because of temperature changes or because of aging of
229 the lasers. If this were to happen, the mean recovered surface height could change even if the
230 true surface height did not, again because the mean is sensitive to outlying data. Figure 3-2
231 shows the expected bias and scatter magnitudes as a function of the width of the surface window
232 for the means of 1000 random collections of PEs based on the waveform in Figure 3-1.
233 Selecting a small surface window results in a narrow (2 cm or less) scatter of values around the
234 mean, because the range of PE heights in the window is small. However, this leads to a 7-8 cm
235 bias in the surface height, because the tail of the distribution is cut off.   Selecting a large surface
236 window leads to a small bias, but, particularly when background noise is large, it leads to scatter
237 in the surface heights, potentially as large as ±10 cm.

238 We ameliorate this problem in two ways: First, we use an iterative process to select a small
239 surface window that includes the majority of the signal PEs but few background PEs. Second,
240 we express the surface height as the median of the PE heights within the surface window. We
241 select the median instead of the mean because it is less sensitive to sampling error for
242 distributions containing a uniform, 'background' component. Median height offsets shown in
243 Figure 3-1 have a spread of less than 2 cm, have maximum biases less than 7 mm, and are nearly
244 independent of the surface-window height. This represents a large improvement in accuracy and
245 precision over the mean, and further processing (discussed in 3.5) can correct for the remaining
246 bias in the median heights.

247 In the course of processing photon-counting data, we frequently need to estimate the spread of a
248 distribution of PE heights. For other types of data, we might choose to make this estimate based
249 on the standard deviation of the sample of heights, but because our measurements contain a
250 mixture of signal and noise PEs, the standard deviation often overestimates the spread of the
251 data. Instead, we generally use the RDE (Robust Dispersion Estimator), which is equal to half
252 the difference between the 16th and the 84th percentiles of a distribution. For Gaussian-
253 distributed data, this statistic is approximately equal to the standard deviation, and for data
254 containing a mixture of a large fraction of signal and a small fraction of noise, it can give an
255 estimate of the spread of the signal that is relatively insensitive to the noise. In some cases, we
256 use a version of this statistic that estimates the spread of the signal component of a distribution
257 that contains a mixture signal (Gaussian- or near-Gaussian-distributed) PEs and background
258 (uniformly distributed) PEs. In these cases, we estimate the 50th and 75th percentiles of the signal
259 component and scale the difference between these percentiles based on the expected width of
260 these percentiles for a Gaussian distribution. We refer to this measure as "robust spread
261 including background" and describe its implementation in section 5.

262 **3.1.1   Land-ice height definition**

263 The land-ice height is defined as estimated surface height of the segment center for each
264 reference point, using median-based statistics. We calculate this the sum of the least-squares
265 height fit, the first-photon-bias median correction, and the pulse-truncation median correction.
266 Height increment values on the product allow removal of the corrections and calculation of the
267 segment mean height, and first-photon-bias and pulse-truncation corrections appropriate to the
268 segment mean.

269

270   **3.2   Outline of processing**

271   The outline of the process is as follows for each cycle for each along-track point. First, heights
272   and along-track slopes are calculated for each beam in each pair:

273   1. PEs from the current cycle falling into the along-track bin for the along-track point are
274   collected (3.3)
275   2. The heights and surface windows are iteratively refined (3.3.5.2)
276   3. Corrections and error estimates are calculated based on the edited PEs. (3.4, 3.5, 3.6)

277   Once these steps are complete, based on the height values for the two beams,

278   4. The across-track slope is calculated (3.7)

279   Each of these steps is described in turn below.

280   **3.3   PE selection**

281   ATL03 provides PE locations and timings for each beam. The first step in ATL06 processing is
282   to select groups of PEs that determine the segment height at each along-track point. Processing
283   is only carried out if the ATL03 *podppd_flag* indicates that the PE geolocation was of high
284   quality for all pulses in the segment, otherwise the segment is skipped.

285   **3.3.1   Along-track segments**

286   Our height- and height-change schemes rely on dividing the data into repeatable along-track
287   segments. We define these segments relative to the pre-defined RGT (see ATL06 Appendix A
288   for definitions related to the ICESat-2 ground and reference tracks) and use them to select groups
289   of PEs for each beam and each pass, and to define local coordinates relative to the RGT. We
290   define a set of reference points, spaced every 20 m in the along-track coordinate x along the
291   RGT, which specify the locations of the height estimates reported in ATL06. One set of
292   reference points is defined for each RPT (Reference Pair Track). An ATL06 segment of data
293   includes all PEs whose x coordinates are within approximately 20 m of that of a given reference
294   point, for a total length of 40 m, so that each segment overlaps its neighbors by 50%. Each
295   individual segment is fit with a least-squares model that gives the slope and height of the
296   segment (Figure 3-3 and Section 3.1.2.4), and height corrections are derived based on the
297   residuals to this model.

Figure 3-3. Reference point numbering schematic

Schematic drawing of two subsequent orbits in geographic (N,E) and along-track (x,y) coordinates. The rectangle shows the area of data included in a multiple-cycle repeat for reference point m.
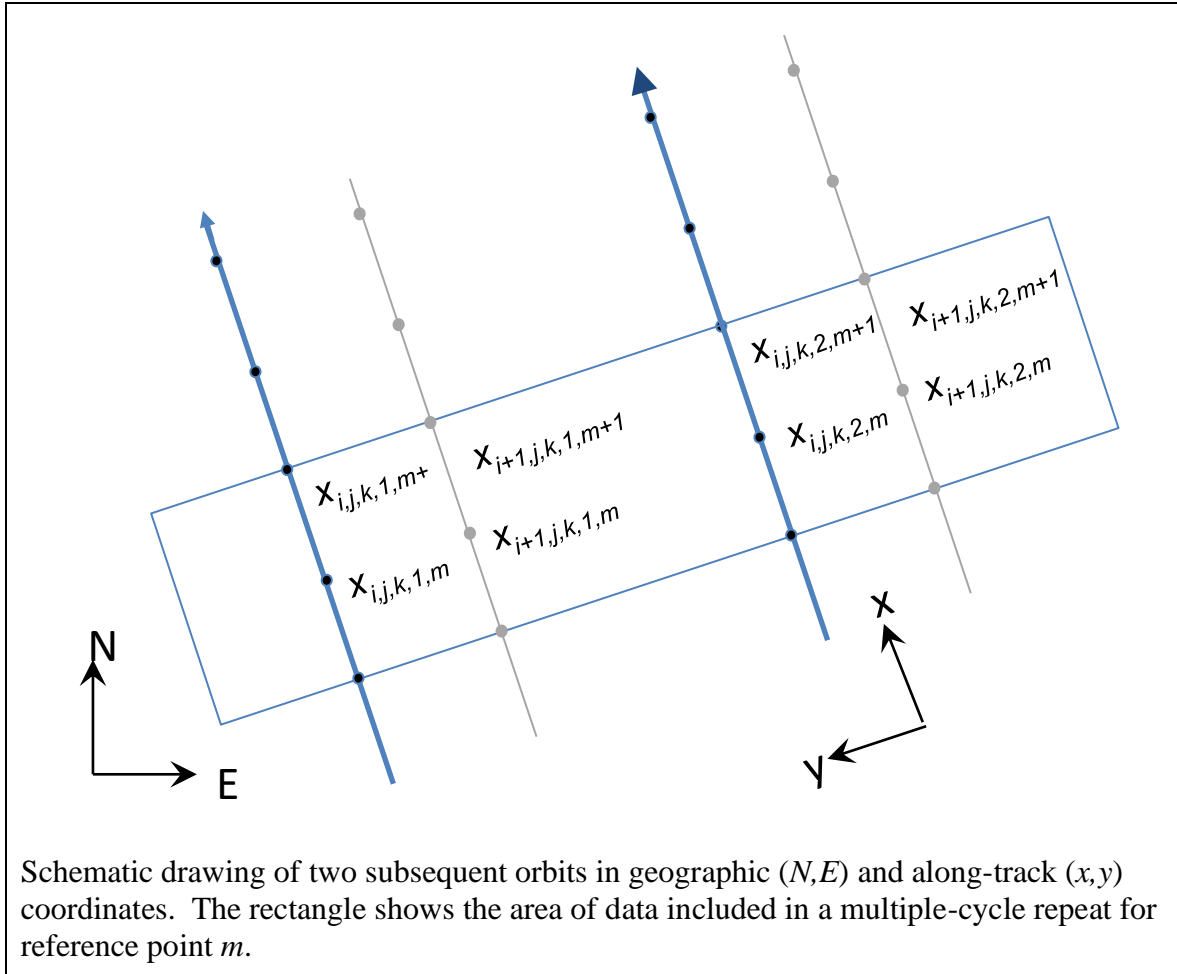
298

299 Along-track segments are designated by five subscripts (Figure 3-3):

300   -i, the cycle number, numbered from the start of the mission;

301   -j, the track number, numbered consecutively within the cycle;

302   -k, the pair number, numbered from left to right across the satellite swath;

303   -l, the beam number within the pair, numbered from left to right;

304   -m, the reference point number, counted from the equator crossing of the RGT.

305 An along-track repeat measurement for a segment is made up of segments with the same j, k, and
306 m, meaning that the track, the pair, and the along-track coordinates of the measurements are the

307   same. Each cycle, i, contributes measurements from two beams, with different l values, to the
308   repeat; these different measurements allow the across-track slope to be constrained
309   independently from the height change, and the along-track segment fitting procedure allows us to
310   correct for the along-track slope. Both ATL03 and ATL06 use this segment numbering scheme;
311   however, ATL06 segments are 40 m long and overlap their neighbors by 50%, while ATL03
312   segments are 20 m long and are disjoint. ATL06 segments are defined as including PE from pairs
313   of adjacent ATL03 segments, and are numbered to match the second of the two, so that ATL06

Figure 3-4. Example PE selection
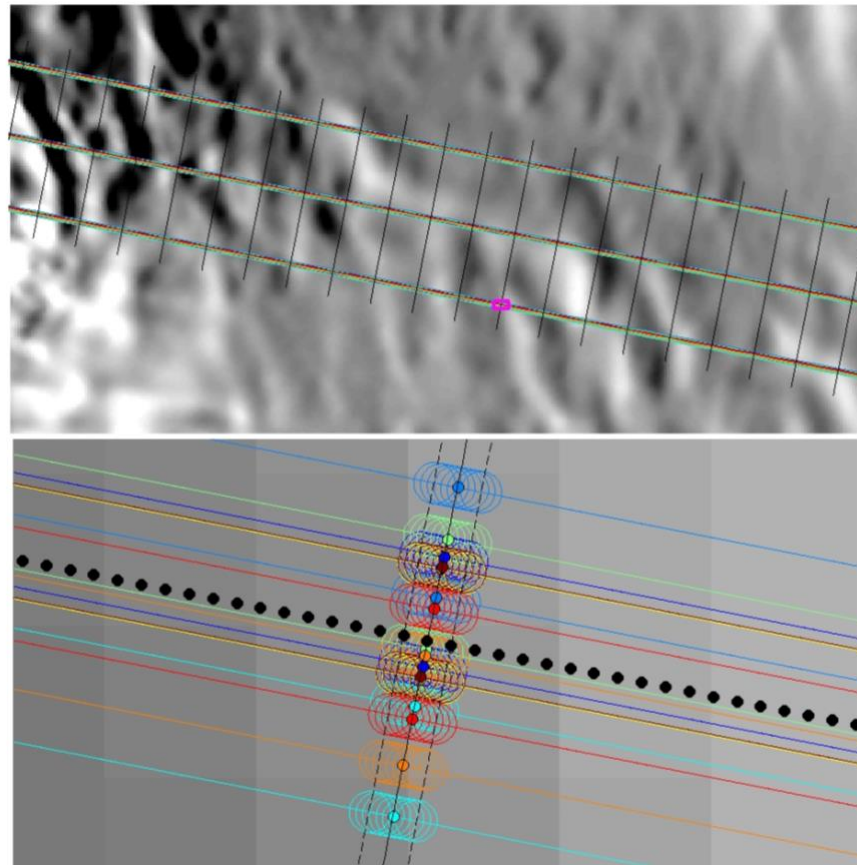
Selecting PEs for a reference point. Top: GT locations for eight simulated repeat measurement of track 188 (colored lines). Black lines are plotted every 2 km in the along-track coordinate x. Bottom: selected footprint locations for a reference point on PT 3 (circles, every 10th shown). Lines and circles are color coded by repeat. Solid points show reference-point locations, dashed lines show the 40-m along-track extent of the segments, filled circles show segment centers. Background image from (Scambos and others, 2007)

314   segment m includes ATL03 segments m and $m-1$.

315 **3.3.2   Local Coordinate Systems**

316   To select the PEs associated with each reference point, the height data are grouped in local
317   coordinates. The local coordinate system is defined in the ATL03G ATBD. Briefly, the
318   coordinate system is defined separately for each RGT with an x coordinate that follows the RGT,
319   starting at its equator crossing going north. The y coordinate is measured perpendicular to the x
320   coordinate and is positive to the left. Thus, the x coordinate runs from zero to around forty
321   thousand km for each track, the y coordinate runs from approximately -3.3 km for the right beam
322   pair to approximately 3.3 km for the left beam pair, although its values may be larger if ATLAS
323   is pointed off nadir.

324   To calculate along-track coordinates for any point P adjacent to an RGT, we define the x
325   coordinate to be equal to the x coordinate of the nearest point on the RGT, P_{RGT}. The y
326   coordinate is equal the distance between P and P_{RGT}, measured to the left of the along-track
327   direction (Figure 3-5). This calculation is carried out for each PE in ATL03: The x coordinate
328   for each PE is equal to the sum of the ATL03 parameters */geolocation/segment_dist_x* and
329   */heights/dist_ph_along*. The y coordinate is equal to the ATL03 *dist_ph_across* parameter.   Our
330   reference points are defined to be equal to the start of the first ATL03 segment, so that ATL06
331   segment m encompasses all PE from ATL03 segments *m-1* and *m.*

332

Figure 3-5. RGT coordinates

Along-track coordinates for point P relative to its RGT. The track drawn is ascending, in the northern hemisphere, so x is increasing from south to north. Y at P is negative.
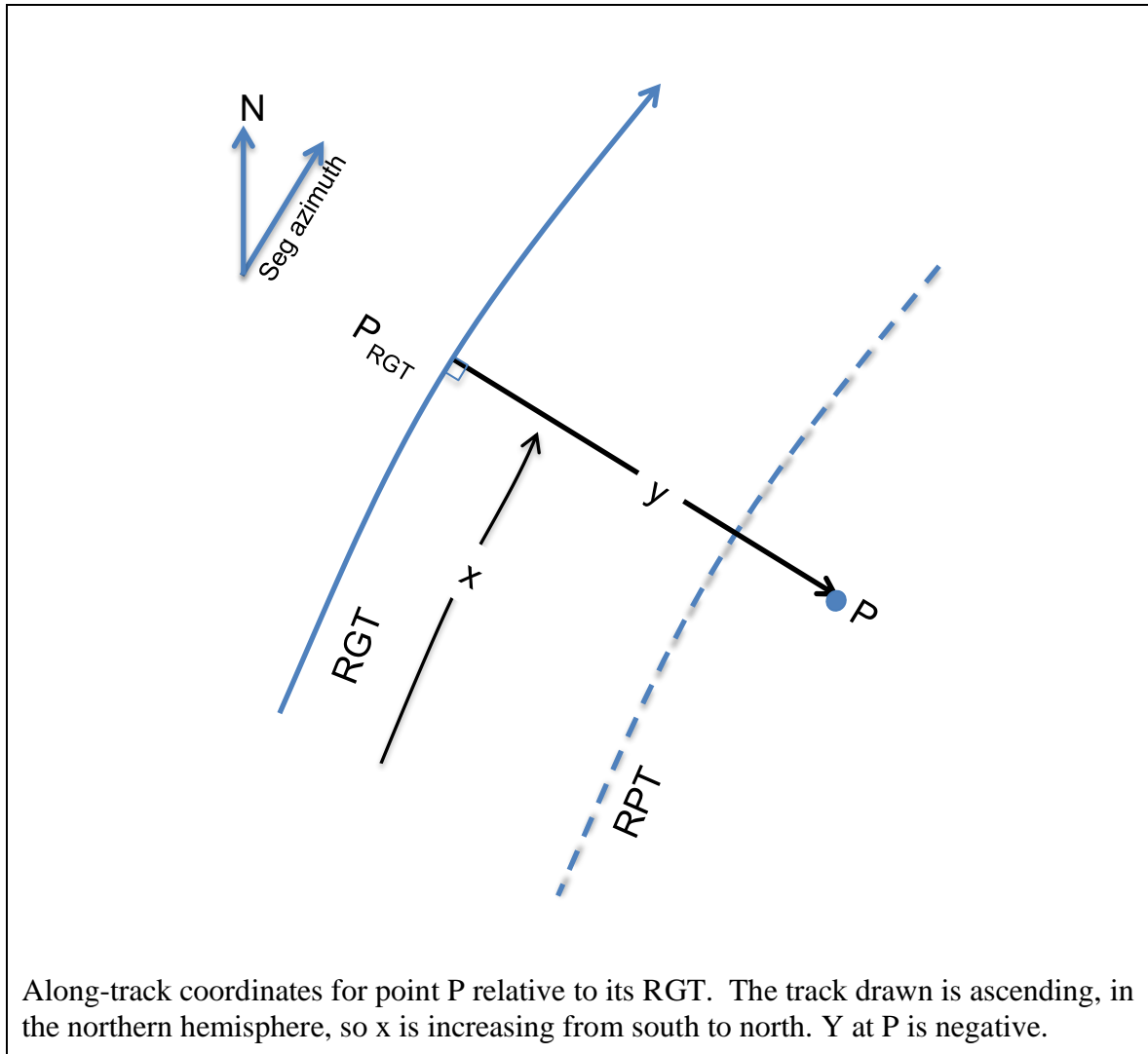
333

334   The AL06 along-track coordinate for each segment is given by the parameter *x_atc*. The across-
335   track coordinate is given by *y_atc*, and the angle between the along-track vector and local north
336   is given in the parameter *seg_azimuth*. To allow easy referencing between ATL06 and ATL03,
337   we provide the number for the second ATL03 segment in each ATL06 segment in the variable
338   *segment_id*.

339   **3.3.3   Parameters describing selected PEs**

340   ATL06 heights and slopes are estimated by piecewise-linear fits to PEs within each overlapping
341   40-m segment. Since ATL06 segments are 40-meters long and overlap by 50%, we can collect
342   the photons for each segment, *m*, by selecting all ATL03 PE that have *segment_id* equal to *m-1*
343   or *m*.

Figure 3-6 Segment fitting

Along-track segments fit to PE heights (points) as a function of along-track x for segment *m* (black line) and neighboring segments *m+1* and *m-1* (gray lines). PEs selected during ATL06 processing for reference point *m* are shown in black.
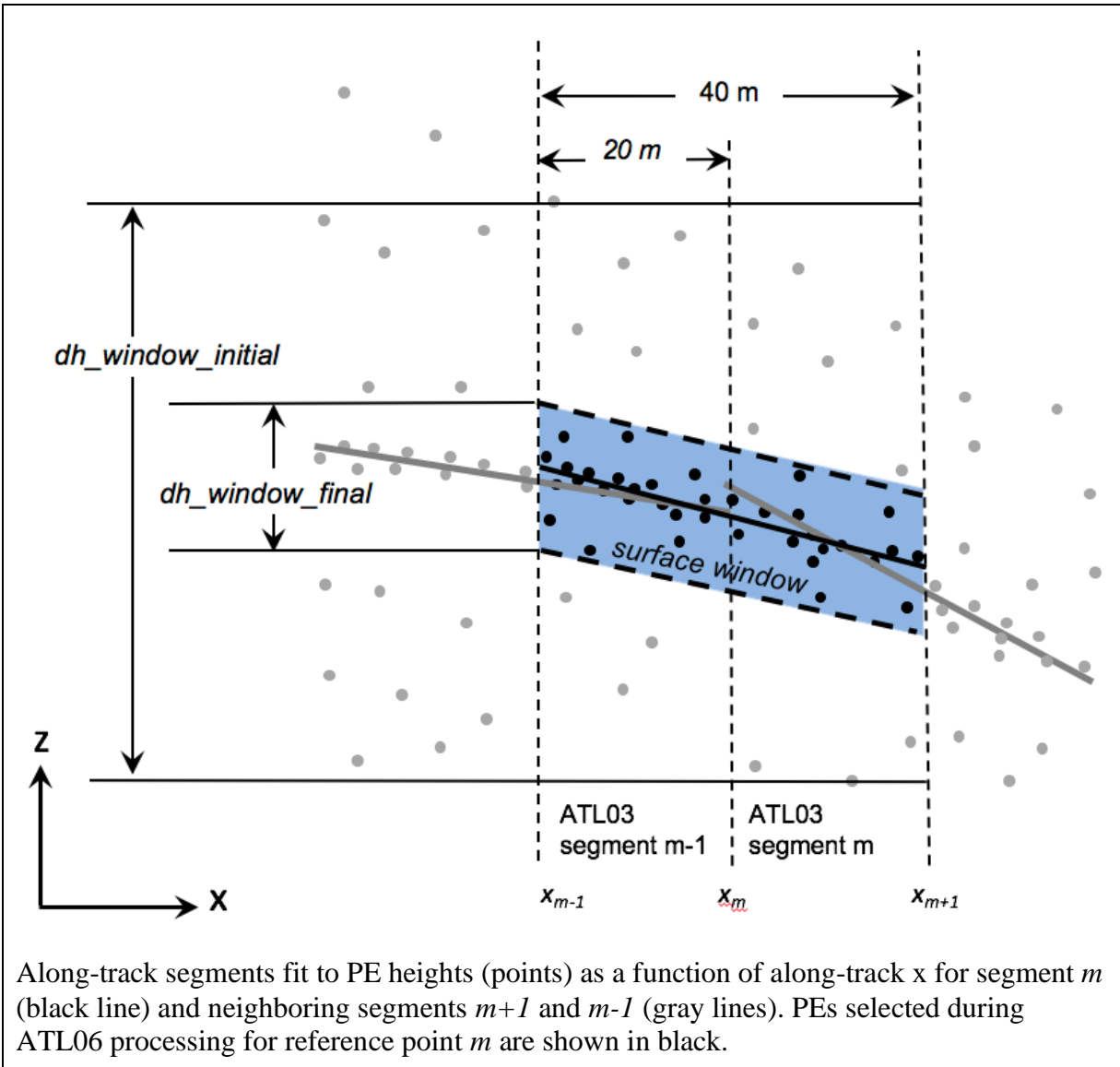
344

345 The initial PE selection is shown in Figure 3-6. ATL03 data give a ground-finding confidence
346 flag that indicates whether each PE was detected high confidence (SNR > 100, flag value of 4),
347 medium (100 < SNR < 40, flag value of 3) low confidence (SNR < 40, yet still passes threshold
348 test, flag value of 2), or is included because it falls within 10m of the detected surface (flag value
349 of 1).

350 An initial surface window is valid if it contains at least 10 PE, and if the along-track distance
351 between the first and last PE is greater than 20 m. This ensures that there are enough PE to
352 determine both the height and slope of the segment. We define three possible sources for signal-
353 selection data:

354   1. ATL03 confident PE (*signal_selection_source=0*): PE with *confidence_flag* values > 1
355   (low or better confidence)

356 2. All ATL03 detected PE (*signal_selection_source=1*): PE with *confidence_flag* flag
357   values ≥ 1 (including low or better, and pad PE).
358 3. A backup signal-finding algorithm (*signal_selection_source=2*)

359 3.3.3.1 Setting the surface window based on ATL03 flagged PE.

360 If sources 1 or 2 define a valid surface window, we calculate the slope of that window using an
361 initial least-squares fit to *h* as a function of *x* for the flagged PE. Based on the slope of this
362 window, we calculate *sigma_expected* using equation 1, and calculate the robust spread of the
363 residuals for the flagged PE (correcting for the background PE rate), *r_flagged*. If ATL03
364 confident PE define a window (case 1), the minimum surface window size, w_{min}, is set to 3 m,
365 and if ATL03 confident PE do not define a window but the combination of ATL03 detected and
366 pad PE do (case 2), w_{min} is set to 10 m.   The initial surface window, *w_surface_window_initial*
367 is then set to *max(*w_{min}, 6 *sigma_expected*, 6 *r_flagged*). The residuals for all of the segment PE
368 are then calculated, and PE with residuals within $\pm$*w_surface_window_initial/2* are selected and
369 passed on to the iterative along-track fitting.

370 3.3.3.2 Setting the surface window using the backup signal-finding algorithm

371 If any ATL03 PE are detected but they do not define a window or if no ATL03 PE are present, a
372 backup algorithm is used. First, if any ATL03-flagged PE are present, the along-track slope of
373 the initial window is set to zero, its width is set to 10 m, and it is centered vertically on the mean
374 height of the flagged PE. If the PE within this window fail the along-track-spread test or the ten-
375 PE test, then PE within 40 m along track of the reference point are examined to find the 10-
376 meter-high by 80-meter-long window, centered on the reference point, containing the largest
377 number of PE. Typically, there will be a range of center heights whose PE counts are not
378 significantly different from the maximum; if the maximum count is C_{max}, then any window with
379 a count greater than C_{max}-$C_{max}^{1/2}$ will be included. The initial window will extend from 5 m
380 below the minimum of these centers to 5 m above the top of these centers, and its length is set to
381 40 m. If this best window does not contain a good distribution of PE (i.e. more than 10 PE, with
382 a horizontal spread greater than 20 m), the segment is considered invalid. If C_{max} is less than 16
383 (the number of PE that would be detected in an 80-meter long window with a signal strength of
384 10 PE/40 m, minus one standard deviation), no PE are selected, and the signal selection is
385 marked as invalid.

Table 3-1 *signal_selection_source* values

Value	Meaning
0	Signal selection succeeded using ATL03 confident-or-better flagged PE
1	Signal selection failed using ATL03 confident-or-better flagged PE but succeeded using all flagged ATL03 PE

2	Signal selection failed using all flagged ATL03 PE, but succeeded using the backup algorithm
3	All signal-finding strategies failed.

386

387 The *signal_selection_source* parameter describes the success or failure of each step in this
388 process, and Table 3-1 describes the meaning of each value. For each signal-selection algorithm
389 that was attempted, the *signal_selection_status_confident, signal_selection_status_all,* and
390 *signal_selection_status_backup* parameters in the *segment_quality* group give details of the
391 success or failure of each part of the algorithm. The *signal_selection_source* parameter is
392 provided for all segments (successful or not) in the *segment_quality* group, and is provided for
393 segments for which at least one pair has an elevation in the *fit_statistics* subgroup.

Table 3-2 Status parameters for signal-selection algorithms

Signal_selection_status_confident	
0	Signal selection succeeded using ATL03 low-or-better confidence PEs
1	Signal selection using ATL03 low-or-better confidence PEs failed the 20-meter-spread test
2	Signal selection using ATL03 low-or-better confidence PEs failed the 10-photon-count test
3	Signal selection using ATL03 low-or-better confidence PEs failed both tests
Signal_selection_status_all	
0	Signal selection succeeded using all ATL03 flagged PEs (or algorithm not attempted)
1	Signal selection using all ATL03 flagged PEs failed the 20-meter-spread test
2	Signal selection using all ATL03 flagged PEs failed the 10-photon-count test
3	Signal selection using all ATL03 flagged PEs failed both tests

Signal_selection_status_backup	
0	Signal selection succeeded using the backup signal finder after centering the window on flagged PE (or backup signal finder not attempted)
1	Signal selection succeeded using the backup signal finder after searching for the strongest-signal window using four adjacent ATL03 segments
2	Signal selection using the backup signal finder failed the 20-meter-spread test
3	Signal selection using the backup signal finder failed the 10-photon-count test
4	Signal selection using the backup signal finder failed both tests

394

395 The final, refined window is described in the *fit_statistics* subgroups. The height of the window
396 is given as *dh_window_final,* and the number of pulses that might contribute PE to the ATL06
397 segment is given in the *n_seg_pulses* parameter. Note that not all of the pulses in the segment
398 necessarily contribute to the received PEs if the signal strength is low. We calculate
399 *n_seg_pulses* based on the speed of the nadir point, $v_{nadir,}$ of the spacecraft along the ground
400 track, the pulse repetition frequency, and the nominal 40-m length of the ATL06 segment:
401 $N_{seg_{pulses}} = PRF \times 40\ m/v_{nadir}$. This parameter has non-integer values, because it is intended
402 to represent the expected number of pulses in each segment. There is no straightforward way to
403 determine exactly which pulses might have targeted a particular ground segment.

404 ### 3.3.4 Handling of invalid segments

405 Segments must pass a series of tests before their elevations are reported in the ATL06
406 *gtxx*/*land_ice_segments* groups. The signal selection routines must return at least 10 PE, spread
407 over at least 20 m. Fitting does not proceed if these criteria are not met. For segments that
408 continue to the surface window refinement routine, after the surface window refinement is
409 complete, the final PE count and surface-window height are checked against the *snr_significance*
410 parameter, to ensure that the probability of the measured signal-to-noise ration resulting from a
411 random signal selection is small. Only segments with *snr_significance <0.05* (indicating that,
412 given a random-noise input, the algorithm would converge to the calculated SNR less than 5% of
413 the time) proceed to the next stage.

414 These criteria allow a significant number of low-quality segment heights to be reported in
415 ATL06. This intended for the benefit of users who need to measure surface heights under
416 marginal conditions. To help other users remove these segments, the

417   *land_ice_segments/ATL06_quality_summary* parameter gives a synopsis of the parameters
418   relevant to segment quality (Table 4-3), any one of which could indicate unusable data. The
419   subset of segments with *ATL06_quality_summary* = 0 are unlikely to contain blunders due to
420   signal-finding errors. This choice of parameters may reject useful elevations collected over
421   rough, strongly sloping, or low-reflectivity surfaces and under clouds so obtain more height
422   estimates, users may need to examine additional parameters in ATL06, or regenerate a similar
423   flag for themselves based on a less-stringent set of parameters.

424   A variety of data flags are available to indicate why a particular segment does not have a
425   reported height parameter. In many cases, the strong-beam segment in a pair will have a
426   reported height, and the weak beam will not; in these cases, a full record is available for the
427   weak-beam segment, providing all parameters up to the step where the fitting process failed. In
428   cases where neither the strong nor the weak beam returned a surface height, the *segment_quality*
429   group provides the *signal_selection_source* parameter, which will show a value of 3 if all signal-
430   selection strategies failed. Only in cases where both segments passed the signal-selection tests
431   but did not pass the *snr_signifcance < 0.05* test will there be an entry in *segment_quality* and no
432   entry in the remainder of the ATL06 records.

433

434   Users wishing to apply more- or less-stringent criteria to the data than those described above can
435   examine the refined surface window width *fit_statistics/w_surface_window_final,* the signal-to-
436   noise ratio, *fit_statistics/snr*, the range-based-error parameter, *land_ice_segments/h_li_sigma* and
437   the uncorrected reflectance, *r_eff*, to ensure that they are within expected ranges.

438   **3.3.5   Surface-window refinement and least-squares height estimate**

439   The ATL06 ground-finding algorithm refines the ATL03 surface detection estimate by iterative
440   fitting of the initially-selected ATL03 PEs with the along-track segment model, rejecting PEs
441   with large residuals to the model at each step (3.3.5.2). After the iterations are terminated, the
442   final model height, based on this fit, *h_mean,* is used as an input to the next stage of the
443   algorithm, in which the model residuals are used to derive corrections to the model height.

444   *3.3.5.1   Least-squares fitting*

445   For each segment, we first calculate a least-squares best-fitting segment to the initially selected
446   ATL03 PEs, then use an iterative procedure based on the least-squares fit to refine this window.

447   Each time we perform the least-squares fit, we construct a design matrix, $\mathbf{G_0}$, from the vector x,
448   of along-track coordinates for the selected PEs:

$$\mathbf{G}_0 = [1 \; x] \qquad 2$$

449   The segment height and along-track slope are calculated based on $\mathbf{G_0}$ and the vector of ATL03
450   heights, h, as:

20

$$[h_{fit}, \frac{dh}{dx}] = (\mathbf{G}_0^T \mathbf{G}_0)^{-1} \mathbf{G}_0^T \mathbf{h} \qquad 3$$

451 The residuals to this model are then calculated:

$$r_o = h - \mathbf{G_0}[h_{fit}, \frac{dh}{dx}] \qquad 4$$

452

453 *3.3.5.2 Iterative ground-window refinement*

454 The initial surface window height may be as large as 20 meters from top to bottom, larger in
455 rough terrain or when the signal-to-noise ratio is small. This means that it may include many
456 noise PEs mixed with the signal PEs. If included in the calculation, these will lead to large
457 random errors in the surface slope and height. We can increase the proportion of signal PEs by
458 shrinking the surface window, but need to avoid shrinking it so much that we lose signal PEs.
459 To do this, we seek to find a window centered on the median height of the surface-return PEs,
460 whose height is three times the spread of the surface PE height residuals. Because the spread and
461 the median of the surface PEs are not initially known, we use an iterative procedure to shrink the
462 size of the surface window, estimating the median and spread at each step.

463 We have two ways of calculating a value for the spread of the surface return, which we combine
464 as part of our calculation of the width of the surface window. The first is to predict the RMS
465 spread of the surface return using an initial estimate of the surface-slope vector and Equation 1 to
466 give *h_expected_RMS,* assuming zero roughness. The second is to calculate it based on the
467 spread of the residuals to the current model, σ_o. In low-signal-to-noise conditions, we include a
468 correction for the background signal level in this calculation (described in 3.11). Since either of
469 these might provide a good estimate of the spread of the surface PEs we take the maximum of
470 these two values as our spread estimate. To avoid excessive trimming, we eliminate PEs only if
471 their residual magnitude is greater than the maximum of 1.5 m and three times our spread
472 estimate.

473 We initialize the iterative procedure with the PE selection described in the previous two sections.
474 In cases where the signal selection was initialized with flagged PE (*signal_selection_source=0*
475 *or 1)*, the iterative ground-window refinement is forced to use only PE included in the initial
476 selection. In all other cases, iterations after the first may include PE that were not included in the
477 initial selection, so the window may expand or migrate as iterations progress. In either case the
478 PE that might be selected are the *selectable* PE.

479 At each step, we

480 a) Perform a least-squares fit to the currently selected PEs using equation 3, giving a current
481   model estimate, [*h_mean, dh/dx*] and residuals to the model, *r*.
482 b) Calculate the median and background-corrected RDE (see 3.11) of the distribution of the
483   residuals for the selected PEs, r_{med} and σ_o, and update *h_expected_RMS* based on the
484   current *dh/dx* estimate. The residual spread (σ_o) is limited to a maximum value of 5 m.
485 c) Calculate the residuals of all of the *selectable* PEs to the current model estimate, *r*.

486   d) Select PEs from among the *selectable* PEs for which $|r\text{-}r_{med}| < H\_window/2$, where
487          $H\_window = \max(6\,\sigma_o,\ 6\,h\_expected\_RMS,\ 0.75\,H\_window\_last,\ 3\text{ m})$.

488   The iterations are terminated if no further PEs are eliminated in a given step. If a given iteration
489   eliminates PE such that the selected PE no longer define a window, then that step is reversed,
490   and the iterations are terminated. The inclusion of 0.75 *H_window_last* as the minimum size of
491   the window in each step of the calculation attempts to ensure that the calculation does not
492   converge too fast to a spurious value of *h_mean.*

493

494   The window width after the final step is reported as *w_surface_window_final*, and the number of
495   PEs in the window is reported as *n_fit_photons*. The final slope of the along-track segment is
496   reported as *dh_fit_dx*. The median residual to the along-track fit is given in the parameter
497   *med_r_fit*, and is used to convert between a mean-based height estimate for each segment and a
498   median-based estimate.

499   **3.4   First-Photon Bias**

Figure 3-7. First-photon bias correction

Simulated rates of photon arrivals at the detector (gray) and of detected photons (red) for
a strong beam over a flat surface (at 0 ns). The first-photon bias correction gives a
corrected histogram (blue outline) and an estimate of the effective detector gain (green).
The actual effective gain of the detector (black) is shown for comparison.
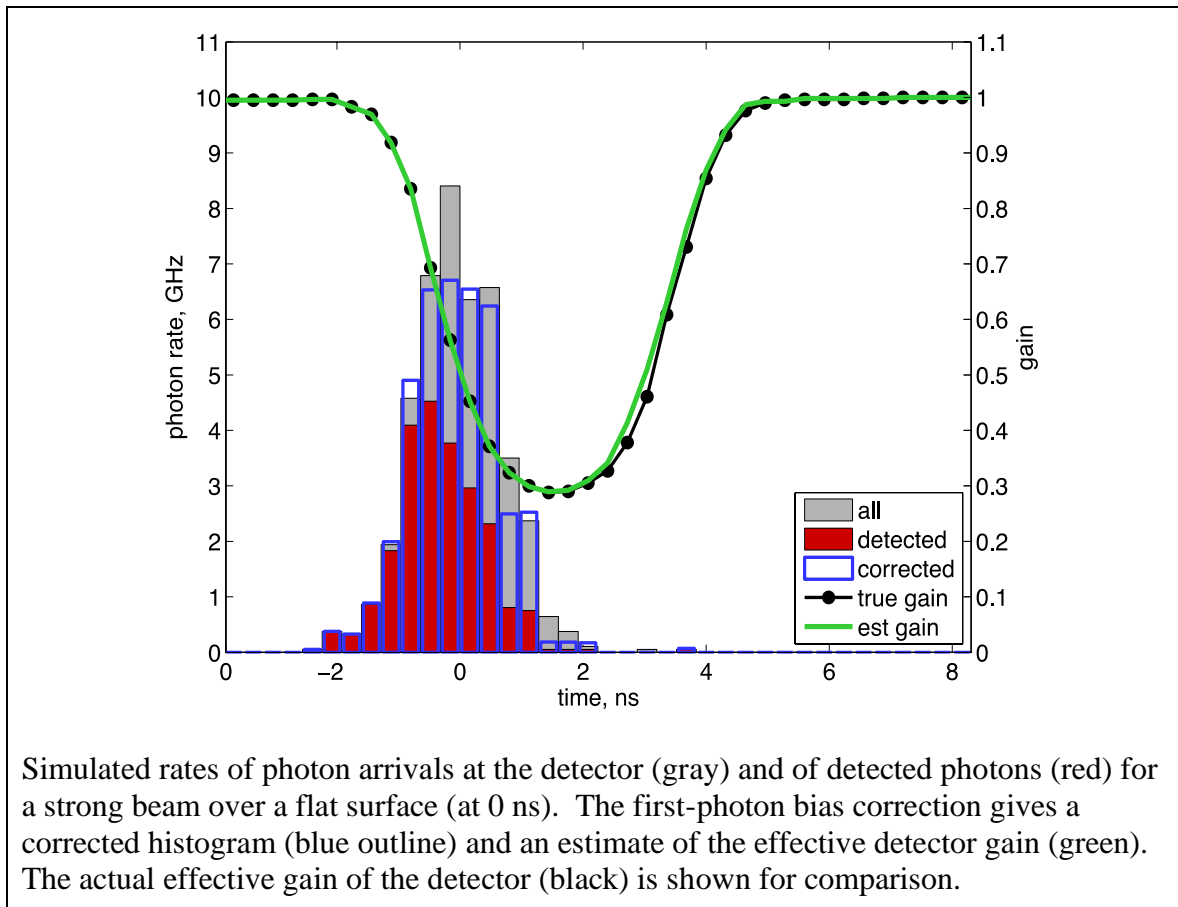
500

501 The first-photon bias (FPB) results from an inherent problem with the photon-counting detectors
502 selected for ATLAS. For a short time, t_{dead}, after an individual pixel of each detector detects a
503 photon, it cannot detect another. This means that photons early in a ground return are more
504 likely to be detected than those later on, and, for a symmetric return-photon distribution, the
505 mean surface height estimate is biased upwards, an effect that is largest for more intense pulses
506 and for pulses from flat surfaces where the return energy is concentrated in a short period of
507 time. Note that for ATLAS's asymmetric transmit pulse, the first-photon bias may result in either
508 positive or negative height errors, because for small roughness values, the FPB suppresses
509 detection the early, intense part of the waveform, while the tail of the waveform is unaffected,
510 resulting in a negative height bias. For larger roughness values, FPB affects the tail and the peak
511 more equally, and the bias becomes positive. For clarity, we will describe modeling results using
512 a simulated symmetric Gaussian transmit pulse, but the corrections provided on the ATL06
513 products may have either positive or negative signs.

514 For ATLAS, t_{dead} is quite short, at approximately 3.2 ns, and there are multiple pixels in each
515 detector (16 for the strong beams, 4 for the weak), to which photons are assigned at random as
516 they reach the detector, resulting in fewer photons reaching each pixel while it is inactive.
517 Despite this, up to several cm of bias may be observed for flat bright surfaces. Figure 3-7 shows
518 simulated instantaneous photon rates for photons incident on the detector, and of detected
519 photons for returns from a flat, smooth surface for a strong spot, under moderately saturated
520 conditions (1.2 photons per pixel per pulse), aggregated over 40 m. Background PE are not
521 included in the simulation, but their effect is likely to be minor, because their contribution to the
522 total PE count is, in strong-signal conditions, a small fraction of the total, and the correction is
523 negligible if the signal is not strong.

524 We have found that we can generate a correction for the first-photon bias based on a model of
525 the detector for PEs aggregated over a 40-m ground-track segment. In this algorithm, we
526 generate a histogram representing the distribution of heights around the ground return for the
527 segment, as represented by the histogram of PE residuals to the best-fitting sloping segment
528 model. We then estimate the effective gain of the detector, a function that represents the
529 probability that a photon would have been detected if it reached the detector. We use this
530 function to correct the received histogram to an estimate of the histogram of all the photons,
531 detected and undetected. Statistics of this histogram are used to improve estimates of the
532 surface height.

533 Using the residuals to the best-fitting segment in this calculation assumes that each pulse
534 experiences the same distribution of photon-arrival times, shifted in time by the along-track
535 surface slope, so that a typical distribution can be found by correcting for the along-track slope.
536 If the surface slope or the reflectance has strong variations within a segment this assumption will
537 fail, but for segments where the correction is large (i.e., in the interior of the ice sheets), it should
538 not introduce large errors because ice-sheet surfaces are typically very homogeneous.

539 **3.4.1 Mathematical Description for the First-Photon Bias**

540 The photon distribution incident on the detectors is written as a function of t_i-t_g, where t_i is the
541 PE time and t_{gi} is the time of the ground return. In practice, this is calculated as t_i-t_{gi}=-r $c/2$,

542   where r is the height residual to the best-fitting segment. We can express the histogram over N
543   PE times as:

$$N\big(t;\ t_i - t_{gi}\big) = \sum_{i=1:N} \sum_{t_i - t_{gi} \in (t, t+\Delta t]} 1 \qquad\qquad 5$$

544   Only some of these photons are detected: After a photon hits a detector, that detector cannot
545   detect another photon until it becomes active, after receiving no photons for a time t_{dead}. This can
546   be expressed by a function giving the status of each pixel for each pulse at time t:

$$A(t, p, pixel) = \begin{bmatrix} 1 & if\ pixel\ is\ active\ at\ time\ t\ for\ pulse\ p \\ 0 & if\ pixel\ is\ inactive\ at\ time\ t\ for\ pulse\ p \end{bmatrix} \qquad 6$$

547   The detected photon distribution is then:

$$N_d\big(t;\ t - t_g\big) = \sum_{i=1:N} \sum_{t_i - t_{gi} \in (t, t+\Delta t]} A(t_i - t_{gi}, pixel_i, P_i) \qquad 7$$

548   If the photon distribution in $t\text{-}t_g$ is constant over the pulses and over all pixels, then we can write:

$$N_d\big(t - t_g;\ \Delta t\big) = G\big(t - t_g\big) N\big(t - t_g;\ \Delta t\big) \qquad\qquad 8$$

549   Where:

$$G\big(t - t_g\big) = \frac{1}{N_{pulses} N_{pixels}} \sum_{pulses, pixels} A(t - t_g) \qquad\qquad 9$$

550   This function is effectively a gain for this collection of pulses. It ranges between zero, when all
551   pixels are inactive, and one, when all pixels are active. The detector gain is shown by the black
552   line in Figure 3-7. It falls rapidly from unity to about 0.3 during the early part of the surface
553   return, then recovers gradually over a period slightly longer than t_{dead}, about 3.2 ns.

554   **3.4.2   Correction Formulation for the First-Photon Bias**

555   We implement the gain correction based on channel dead-time estimates from ATL03 and a
556   histogram of residual times relative to the best-fitting segment model from 3.3.5.2, truncated by
557   ±*h_window_final*/2. We represent the deadtime for the detector with the mean deadtime for all
558   channels in the detector, and assume that all pixels (and channels) have identical sensitivity.
559   Although the algorithm's function does not depend strongly on the spacing of the histogram bins,
560   our test software has used a bin spacing of 0.05 ns. We express the timing for the correction as a
561   function of time relative to the ground-return time, under the assumption that for an entire
562   segment, the return shape will be consistent relative to the ground-return time:

$$\tau = t - t_g \qquad\qquad 10$$

563   Our strategy in this calculation is to correct an initial histogram of PE arrivals for the effects of
564   detector dead time ($G<1$) by dividing $N_d(\tau)$ by $G(\tau)$:

$$N_{est}(\tau;\ \Delta t) = \frac{1}{G(\tau)} N_d(\tau, \Delta t) \hspace{3cm} 11$$

565   To correct waveforms for the effects of dead time, we can use an *a posteriori* estimate of $G(\tau)$
566   calculated with a simple model of the detector. In this model, we calculate a detected
567   distribution, N_d, as the histogram of PE arrivals relative to the ground bin for a single-segment
568   (40 m) section of track. For each bin in the histogram, we then determine the average number of
569   pixels in the detector that were inactive. This is calculated:

$$P_{dead}(\tau) = \frac{number\ of\ photons\ in\ [\tau - t_{dead}, \tau)}{N_{pix} N_{puses}} \hspace{2cm} 12$$

570

571   The estimated gain is then *1-P_{dead}*. This calculation can be carried out efficiently by convolving
572   the histogram of residuals with a rectangular window of height $1/N_{pix}N_{pulses}$, and shifting the
573   result by the width of the window.

574   For our simulated example (in Figure 3-7) the recovered gain (green) is approximately equal to
575   the true detector gain; this example is fairly typical of other simulations of this process, where
576   the estimated gain is usually within a few percent of the true gain. There are visible differences
577   between the corrected photon-timing histogram (blue) and the incident photon histogram, but the
578   effects of these variations on the recovered heights are relatively small and have approximately
579   zero bias.

580   **3.4.3   Statistics Derived from the First-Photon-Bias Correction**

581   The output of the gain estimation is a corrected histogram of height differences relative to a
582   reference surface. Statistics of this histogram (e.g. its vertical centroid, its median) can be
583   calculated as they would for the uncorrected PE heights. Since these statistics are calculated on
584   the histogram of uncorrected photon residuals, their values give the correction relative to the
585   mean of the PE heights. Thus, to calculate the corrected mean or median surface height, we add
586   the gain-corrected mean or median of the residuals, respectively, to the uncorrected mean height.
587   Because we expect the transmitted pulse to be skewed, we expect the median height correction to
588   be much larger than the mean height correction.

589

590   *3.4.3.1   Mean Height Correction*

591   The mean height correction based on the corrected histogram is:

$$fpb\_mean\_corr = \sum \frac{N_{corr,i}}{N_{tot}} dz_i \hspace{3cm} 13$$

592 Here dz_i are the bin centers of the histogram of the PE residuals (i.e. the difference between the
593 PE heights and the linear segment fit. The error in the mean correction is found using the error
594 propagation formula for a centroid, assuming that the measured PE counts are Poisson
595 distributed and ignoring the error in the gain estimate. For each bin in the corrected histogram,
596 the corrected count at that bin has an error:

$$\sigma_{N,corr,i} = \frac{N_{0,i}^{1/2}}{G_i} \qquad 14$$

597 The error in the mean height based on the corrected counts is then:

$$\sigma_{fpb-corr} = \left[\sum \left(\sigma_{N,corr,i} \frac{dz_i - fpb\_corr}{N_{corr,tot}} \right)^2 \right]^{1/2} \qquad 15$$

598 *3.4.3.2 Median Height Correction*

599 The median correction and its error are calculated from the CDF (Cumulative Distribution
600 Function) of the corrected histogram as a function of dz:

$$CDF(dz_0) = \sum_{dz_i < dz_0} \frac{N_{corr,i}}{N_{corr,tot}} \qquad 16$$

601 The median of the corrected histogram is found by interpolating into *dz* as a function of CDF(*dz*)
602 at an abscissa value of 0.5:

$$median\ fpb = CDF^{-1}(0.5) \qquad 17$$

603 Because CDF is a function of the residuals to the linear segment-fit model, the median calculated
604 in this way gives an offset relative to *h_mean*.

605 The uncertainty of the median interpolated from the CDF is the slope of the inverse function of
606 CDF(*dz*) with respect to CDF times the statistical uncertainty in the CDF at the median point:

$$\sigma_{med} = \frac{dz}{dCDF}\bigg]_{CDF=0.5} \sigma_{CDF}(h_{med}) \qquad 18$$

607 The statistical uncertainty in the CDF achieves half its total variance at the median, so we can
608 calculate its uncertainty at the median as:

$$\sigma_{cdf}(dz_{med}) = \left[\frac{1}{2} \sum \frac{\sigma_{N,corr,i}^2}{N_{tot,corr}^2} \right]^{1/2} \qquad 19$$

609   We estimate the slope of the CDF based on the 60th and 40th percentiles of dz, calculated from
610   the CDF of dz, and noting that 20% of the residuals should fall within this range. The error in
611   the median correction is then:

$$fpb\_md\_corr\_sigma = \frac{dz_{60} - dz_{40}}{0.2} \sigma_{cdf}(dz_{med}) \qquad\qquad 20$$

612   For both the mean and the median corrections, the error calculated in this way gives the total
613   error in the surface height due to the Poisson sampling in the data. It does not take into account
614   the effects of the along-track distribution of the photons, as the propagated least-squares error
615   (equation 19) does, so the error in the final, corrected height measurement (*h_li_sigma*) is the
616   maximum of *sigma_h_mean* and *fpb_med_corr_sigma*. Note that neither the combined error nor
617   the median error calculated above are rigorous estimates of the error guaranteed to work under
618   all circumstances. However, numerical experiments have shown that these error estimates match
619   the RMS spread of recovered values to within ~10% for numbers of PEs greater than ~20. For
620   smaller numbers of PE, the error estimates may be up to 20% too small.

621   **3.4.3.3   Corrected Return Count**

622   The corrected number of returned photons is calculated:

$$fpb_{N\_photons} = \sum N_{corr} \qquad\qquad 21$$

623   This sum is carried out over the ground window calculated during ground-bin refinement
624   (3.3.5.2). This is similar to the dead-time correction on ATL03.

625   **3.4.3.4   Correction Validity**

626   The correction should provide accurate height and signal-strength corrections as long as there are
627   at least a few active detector pixels during each time increment. If the estimated detector gain for
628   a segment falls below 2/(*N_seg_pulses x n_pixels*), the correction values are set to their invalid
629   value (*NaN*), so that any value that uses these corrections (e.g. *h_li, fpb_n_corr)* will also be
630   marked invalid.

631

632   **3.4.3.5   Accuracy of the first-photon bias correction**

Figure 3-8. Accuracy of first-photon bias correction elevation recovery
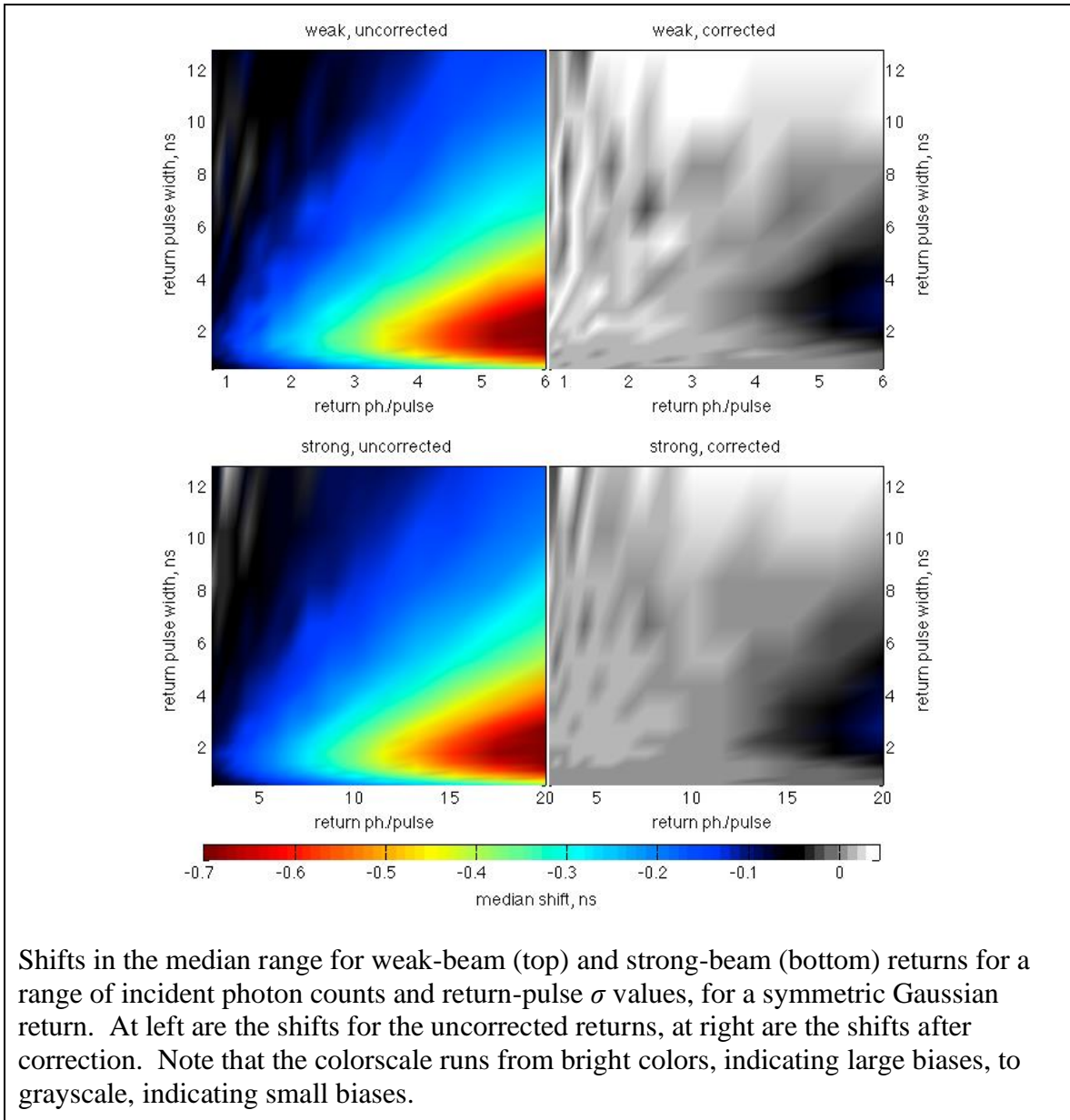
Shifts in the median range for weak-beam (top) and strong-beam (bottom) returns for a range of incident photon counts and return-pulse σ values, for a symmetric Gaussian return. At left are the shifts for the uncorrected returns, at right are the shifts after correction. Note that the colorscale runs from bright colors, indicating large biases, to grayscale, indicating small biases.

633 We assess the potential accuracy of this calculation with a simple simulation of elevation
634 recovery for a strong and a weak ATLAS beam. For each realization of this simulation, we
635 generate random arrival times for a collection of N_{inc} incident return-pulse photons, with
636 standard deviation σ_{inc}. These photons are assigned at random to detector pixels (4 pixels for a
637 weak beam, 16 for a strong beam) and are labeled as detected or undetected based on the detector
638 model described in 3.4 with a dead time of 3.2 ns. Based on these PE times, we then calculate a
639 corrected arrival-time histogram as described in 3.4.2 and calculate statistics for this distribution
640 as described in 3.4.3.

Figure 3-9. Accuracy of first-photon-bias-correction signal strength recovery
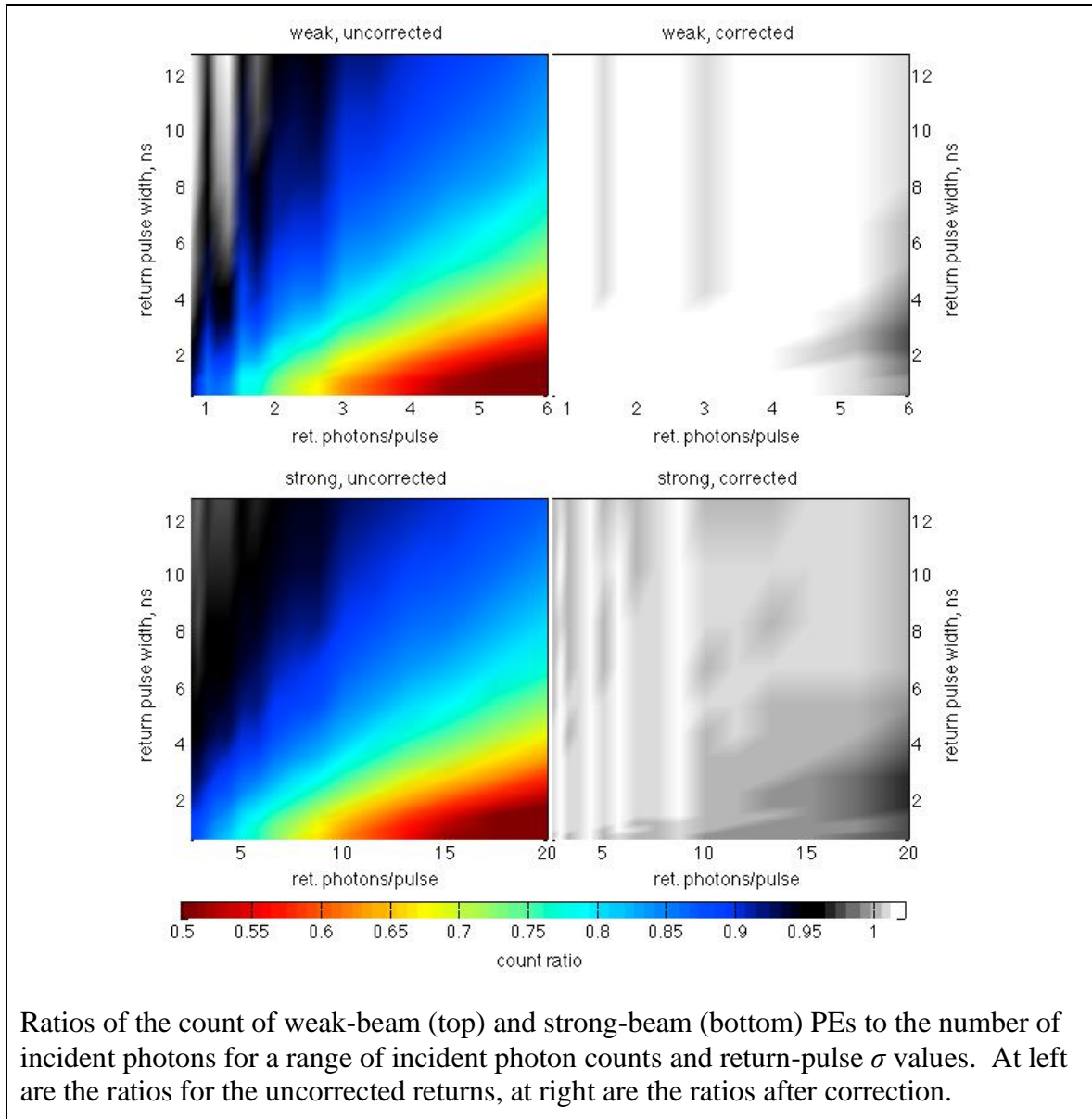
Ratios of the count of weak-beam (top) and strong-beam (bottom) PEs to the number of incident photons for a range of incident photon counts and return-pulse σ values. At left are the ratios for the uncorrected returns, at right are the ratios after correction.

641

642 Results of this simulation are shown in Figure 3-8 and Figure 3-9. For the strongest simulated
643 returns, with around two photons per pulse per detector pixel, uncorrected time biases are as
644 large as -0.7 ns, corresponding to positive elevation biases of about 0.1 m. For these returns,
645 only about 60% incident photons are detected. For expected return strengths, of 0.8 photons per
646 pulse per pixel, elevation biases are smaller, around -0.2 ns, and about 85% of incident photons
647 are detected. The largest elevation errors come for return-pulse widths of around 2 ns, and the
648 largest loss of signal photons happens for the smallest pulse widths and the strongest returns.

649 Applying the correction removes the majority of the bias, both for return times and for signal
650 strengths. Corrected returns have much smaller time biases, accurate to 0.1 ns (1.5 cm) for the

651   strongest (2 photons/pixel/pulse) returns, and 0.02 ns (0.03 cm) for expected (0.8 ph/pixel/pulse)
652   return strengths. Corrected PE counts are within 2% of the incident counts.

653   **3.5   Transmit-pulse shape correction**

Figure 3-10. Transmit-pulse-shape correction

Transmit-pulse shape correction example. Left: Transmit (Tx) waveform from a prototype
ATLAS laser and a simulated return (Rx) from a rough (0.25 m RMS) surface. The Tx pulse
is aligned so that its centroid is at 0 ns (black dashed line), the medians of the Tx and Rx
pulses are shown by dotted gray and black lines, respectively, and the centroid of the
truncated Rx pulse is shown by a dashed gray line. Right: average bias between the centroid
of the Tx pulse and the median and centroid of the windowed Rx pulse, both with (solid) and
without (dashed) the transmit-pulse-shape correction applied.

654

655   The ATL06 surface-fitting routine and the ATL06 first-photon bias correction both give
656   estimates of the median height of the surface for each segment, relative to the centroid of the
657   transmit pulse, for a 'windowed' collection of photons of limited vertical extent (typically ±1.5
658   m around the median height). However, the ATL03 PE heights are calculated relative to an
659   estimate of the centroid of the entire transmit pulse.   Because the transmitted pulse is not
660   symmetric in time around its centroid, its median is different from its mean, and the centroid of
661   any truncated subset of the photons from this pulse will have a nonzero bias relative to those
662   from the full waveform. This introduces a potential bias in ATL06 height estimates.

663   The magnitude of the bias depends on three factors: the shape of the 'tail' of the transmitted
664   waveform, the width of the surface window, and the effective surface roughness (i.e. the total
665   broadening introduced by surface slope and roughness). The effects of the tail shape and the

666 surface-window height were described previously (1.1). The effect of increasing effective
667 surface roughness is to increase the scatter in the PEs, producing returns that are closer to
668 symmetrical, as shown for 0.25 m noise in Figure 3-10 (left panel). This larger scatter results in
669 return-waveform medians that have smaller biases than those from a smooth surface, and in
670 smaller biases in the truncated-waveform centroids. Figure 3-10 (right panel) shows the
671 magnitude of biases in return centroids and medians for prototype-laser waveforms, broadened to
672 simulate the effects surface roughness values between 0 and 1.5 meters. For each waveform, we
673 calculated the centroid and median surface height relative to the centroid and median of the
674 transmitted pulse, using a surface window height of a maximum of 3 m and three times the RDE
675 of the returned PEs. The worst of the biases, for the zero-roughness median, is around 15 cm,
676 and biases decrease with increasing roughness. The bias in the centroid is smaller than that of the
677 median, but both are large relative to other expected instrumental biases.

678 We have found that we can correct for this effect by modeling expected return-pulse shapes and
679 calculating the biases for these shapes, then subtracting the bias from the measured height
680 estimates. The model is based on transmitted-waveform shapes measured periodically during the
681 ICESat-2 orbit using the transmitter-echo-pulse (TEP). Using this TEP waveform and the width
682 of the return, we estimate the extent to which reflection from the sloped, rough surface has
683 broadened the return, and smooth the TEP waveform to broaden it to the same width. We then
684 truncate the broadened synthetic waveform around its mean using the surface window
685 determined in 3.3, then calculate the median and centroid of the broadened, truncated waveform.
686 This gives corrections to the median and mean surface heights.

687 Note that at the time of writing of this document the relationship between the absolute values of
688 the photon times measured in the TEP and the transmit times of the lasers has not been
689 established. On-orbit calibration exercises and further analysis of pre-launch calibration data
690 should be helpful in this regard, but for now, we take the TEP as a measurement of the shape of
691 the waveform, not the timing of the transmission. Accordingly, we shift the time values on the
692 TEP measurements obtained from ATL03 so that the centroid of the signal photons arrival times
693 is equal to zero, and assume that this shifted TEP represents the transmit pulse.

694 To estimate the broadened transmit-pulse shape, we begin with an estimate of the transmitted
695 pulse shape derived from ATL03, $P_{tx}(t)$, and $RDE(t_i)$, our estimate of the degree to which the
696 distribution of surface returns, t_i, has been spread by its reflection from a rough or sloping
697 surface:

$$\sigma_s^2 = \max\left((0.01\ ns)^2, RDE(t_i)^2 - RDE\left(P_{tx}(t)\right)^2\right) \qquad 22$$

698 The *max((0.01 ns)², ...)* function here is included to ensure that the broadening estimate is
699 positive. From this we generate an estimate of the surface broadening function S(t):

$$S(t) = \exp\left(-\frac{t^2}{2\sigma_s^2}\right) \qquad 23$$

700 The estimated broadened pulse shape, $P_B(t)$ is the temporal convolution of $P_{tx}(t)$ and S(t):

$$P_B(t) = P_{tx}(t) * S(t)$$
<div align="right">24</div>

701 We apply a windowing function, $W_s(t)$, to account for the truncation of the surface return during
702 the ground-bin-selection process:

$$W_s(t) = \begin{bmatrix} 0 & |t - mean(P_B(t))| > h\_window\_final/2 \\ 1 & |t - mean(P_B(t))| \le h\_window\_final/2 \end{bmatrix}$$
<div align="right">25</div>

703

704 The height correction for the median based on this waveform estimate is then:

$$dh_{tx} = \frac{c}{2} median_t(P_B(t)W_s(t))$$
<div align="right">26</div>

705 Here $median_t()$ represents the temporal median of a function:

$$median_t(f(t)) \equiv t \; such \; that \int_{-\infty}^{t} f(t')dt' = \frac{1}{2}\int_{-\infty}^{\infty} f(t')dt'$$
<div align="right">27</div>

706 The correction for the mean is identical, but uses the mean instead of the median in equation 26.
707 Figure 3-10 shows that after applying this correction, the remaining bias in the median and mean
708 heights is less than 3 mm.   The value calculated in equation 26 is included in the standard
709 surface-height estimate, h_li, and is provided in the *tx_median_corr* and *tx_mean_corr* fields in
710 the *bias_correction* parameter subgroup.

711

3.6   Signal, Noise, and Error Estimates

713 Before we can calculate the error in the retrieved surface height, we must form estimates of
714 relative contributions of signal and noise PEs to the observed PE count. Under ideal conditions,
715 when the signal level is high and the background count rate is low, few noise PEs will be present
716 among those selected by editing process described above. However, under cloudy conditions
717 when the sun is above the horizon this will often not be true, and it is important that the error
718 estimates reflect the potential presence of background PEs.

3.6.1   Background PE rate

720 The background PE rate (*bckgrd* in the *geophysical* subgroup) is derived from the ATL03
721 parameter */bckgrd_atlas/bckgrd_rate*, and is derived from a 50-shot, 200Hz count of PE within
722 the ATLAS signal-finding window, corrected for the number of PE detected by the ATL03
723 ground-finding algorithm. In general, we expect this parameter to be sufficiently accurate to
724 allow us to predict the number of PE within 10 m of the ground to a precision of better than 10
725 PE/segment.

726 The expected background rate, *E_bckgrd*, is also predicted based the solar elevation, assuming a
727 flat, Lambertian surface at the ground. The calculation of this parameter is described in the
728 ATL07 ATBD, section 4.2.3.1. This parameter, when compared against the measured *bckgrd*, is
729 a potential indicator of the surface reflectance and cloud properties.

730 **3.6.2   Signal PE count**

731 The total number of PEs selected in the window, as a function of the number of signal PEs, the
732 background rate, the number of pulses in the window, and the background window height is:

$$N_{tot} = N_{sig} + N_{BG} \qquad\qquad 28$$

733 The number of background PEs in the window has a mean value:

$$N_{BG} = 2\ N_{pulses} h_{window}\ BGR/c \qquad\qquad 29$$

734 Subtracting the two gives an estimate of the number of signal PE, *N_signal*. Because the number of
735 background PE is a Poisson random variable, the calculated *N_signal* may be less than zero in
736 weak-signal conditions. The ratio between the number of signal and noise photons is reported as
737 *fit_statistics/snr*.

738   To help distinguish high-quality surface returns from returns that are likely a result of
739 signal-finding blunders, we provide the *fit_statistics/snr_significance*, which gives the
740 probability that in the absence of any real ground signal, a segment with at least the observed
741 SNR would be found by the ATL06 signal-selection routine, for the initial range of heights,
742 *h_range_initial* and background rate *bckgrd*.   If ATL03 detected photons were used in the signal
743 selection (*signal_selection_source* of 0 or 1, or *signal_selection_status_backup* of 0),
744 *h_range_input* is equal to the range of photon heights. Otherwise it is set to the full range of PE
745 heights provided from ATL03 for the segment. The values of *snr_significance* are calculated
746 from a look-up table based on 1,000,000 realizations of random noise for background-noise
747 values, *bckgrd_table*, between 1 and 10 MHz, and for initial window sizes, *w_table*, between 3
748 and 80 meters. For each set of random-noise PE, the backup signal-selection algorithm is run to
749 select the input PE for the iterative ground-window refinement routine (3.3.5.2), which is then
750 run to convergence, and the final SNR is recorded. Then, for each value of *bckgrd_table* and
751 *w_table,* the probability of reporting a segment with an SNR value greater than a set of values
752 between -10 and 10, in steps of 0.1, is calculated, and the value is stored in *F_table*. To find
753 *snr_significance* for each segment, we interpolate into *F_table* as a three-dimensional linear
754 function of *h_range_input*, *bckgrd*, and *snr* for that segment.

755 **3.6.3   Per-Photon Errors**

756 Noise PEs are vertically distributed throughout the window with a standard deviation of
757 approximately

$$\sigma_{BG} = 0.287\ h_{window} \qquad\qquad 30$$

758   where the factor 0.287 equals the standard deviation of a uniform random variable on a unit
759   interval.

760   The signal PEs have an approximate skewed Gaussian distribution, whose width depends on the
761   transmit-pulse duration, the surface roughness, the surface slope, and the footprint width, as
762   described in equation 1, with additional broadening possible due to atmospheric or subsurface
763   scattering. For ice-sheet surfaces and near-vertical beams we assume that the angle between the
764   beam and the surface slope is equal to the magnitude of the surface slope. The total standard
765   deviation of the surface return heights, $\sigma_{photon,est}$ is then:

$$\sigma_{photon,est} = \left(\frac{N_{BG}\sigma_{BG}^2 + N_{signal}\sigma_{signal}^2}{N_{BG} + N_{signal}} \right)^{1/2} \qquad 31$$

766   With the exception of the surface roughness, all of the quantities needed for this equation are
767   estimated from the data: the slope spreading is estimated from the along-track component of the
768   surface slope and the transmitted pulse width using equation 1, and the background and signal
769   PE counts are estimated from the total number of PEs and the background rate. If we assume the
770   roughness to be zero, and neglect atmospheric and subsurface scattering errors, equation 31 gives
771   a minimum error estimate. An alternate estimate of the per-PE error is the vertical spread of PEs
772   relative to the along-track fit, *h_rms_misfit*. We combine these two estimates by setting our error
773   estimate, σ_{photon}, to the maximum of *h_rms_misfit* and $\sigma_{photon,est}$.

774   **3.6.4 Propagated Height Errors:**

775   Given the established per-PE error, σ_{photon}, the error propagation for the linear fitting equation
776   gives an estimate of the covariance matrix for the fit (Menke, 1989):

$$\mathbf{C}_{fit} = ((\mathbf{G}^T\mathbf{G})^{-1}\ \mathbf{G}^T)((\mathbf{G}^T\mathbf{G})^{-1}\ \mathbf{G}^T)^T \sigma_{photon}^2 \qquad 32$$

777   The height error estimate, *sigma_h_mean* is the square root of the upper-left element of $\mathbf{C}_{fit}$.
778   This error is combined with the sampling error estimated during the first-photon-bias calculation
779   to give the total surface ranging error, *h_li_sigma.* The error in the along-track slope
780   *sigma_dh_fit_dx* , is equal to the square root of the lower-right element of $\mathbf{C}_{fit}$.

781   **3.6.5 Uncorrected reflectance**

782   The uncorrected reflectance gives the ratio of the measured return energy to the energy expected
783   from a white surface, through a nominal clear atmosphere (Yang and others, 2013). Following
784   the strategy outlined in the ATL09 ATBD, we calculate:

$$r_{eff} = \frac{\pi E_{RX} r^2 F}{N_{seg\_pulses} E_{TX} A T_{opt}} \qquad 33$$

785   Here E_{RX} is the received energy, *r* is the range to the surface, *A* is the telescope area, and T_{opt} is a
786   factor that combines the optical efficiency of the instrument optics and the detector sensitivity. *F*
787   is a calibration factor that will be determined and maintained as part of the atmospheric science

788   operations. E_{TX} is the transmitted energy per pulse from the ATL03 parameter *tx_pulse_e*. We
789   calculate E_{RX} based on the number of returned PE as:

$$E_{RX} = (fpb_N - N_{BG}) \frac{hc}{\lambda} \qquad 34$$

790   Here fpb_N is the dead-time-corrected segment signal photon count, N_{BG} is the background-photon
791   count (from equation 29), and hc/λ is the energy received per photon. Note that this is the same
792   calculation as equation 4.7 in the ATL09 ATBD, except that we use the ATL06 first-photon-
793   bias-corrected photon count, instead of the correction factor used in ATL09. For an atmospheric
794   transmittance 0.95, we expect to see r_{eff} of about 0.88 over unit-reflectance surfaces.

3.7   Across-track slope calculation

796   After the iterative editing process is complete, the across-track slope is computed for the pair
797   based on the first-photon-bias-corrected median heights for the two segments:

$$\frac{dh}{dy} = \frac{h_{LI,R} - h_{LI,L}}{y_{ATC,R} - y_{ATC,L}} \qquad 35$$

798   If only one beam has returned a height, then *across_track_slope* is set to *invalid* for both beams.

3.8   Subsurface-Scattering Bias

800   The subsurface-scattering, or volume-scattering, bias comes from photons that experience
801   multiple scattering within the snow or ice before returning to the satellite. Ice absorbs green
802   light only weakly, with attenuation lengths of tens of meters or more, but ice grains in firn and
803   air bubbles in ice both scatter green light strongly (Warren and others, 2006). While most
804   photons from an ATLAS pulse are expected to exit the surface of a firn pack within a fraction of
805   a nanosecond, others will likely be delayed significantly, producing a long tail on the histogram
806   of return times. Averaging return times of PEs from this tail with PEs from the surface return
807   leads to a delay in the mean PE return time, and a downward bias in the apparent surface height.
808   The median surface height is modestly less sensitive than the mean, because it less sensitive to
809   outlying data values far from the central peak of the return distribution. This error and its
810   temporal variability is expected to be small for fine-grained snow surfaces such as those found
811   on the Antarctic Plateau and in central Greenland, but it may be more significant in coastal areas
812   where seasonal snow melt leads to large temporal variations in the surface grain size.

813   The magnitude of the subsurface-scattering bias delay depends in part on the scattering density
814   of the snow and its bulk absorbance, both of which are determined by the density and grain or
815   bubble size close to the surface, and on the impurity content of the snow or ice. Since none of
816   these properties may be known at the time of ATLAS processing, each must be determined
817   independently using external information about the snow, such as meteorological model output
818   or infrared reflectance data.

819   We do not expect to be able to offer an accurate correction for this effect with our current
820   understanding of the process. This remains an area of active research.

821 **3.9 Atmospheric-Scattering Bias**

822 A second important source of bias in ATLAS height measurements may come from atmospheric
823 scattering of the down-going laser pulse. Scattering by ice particles in the atmosphere redirects
824 much of the light through small angles, often less than about one degree. These photons may fall
825 outside the field of view of the ATLAS detectors, in which case they will be lost and will have
826 no impact on altimetry beyond attenuation of the received pulse, or they may reflect from the
827 surface within the field of view, in which case they may then be detected by ATLAS. However,
828 because their down-going path was longer than the assumed straight down-and-back path
829 assumed in the PRD model, they will give erroneously long ranges, and therefore low surface
830 heights. This effect is increasingly severe for thicker clouds, which scatter more photons, and for
831 clouds closer to the surface, where photons scattered through large angles may still remain in the
832 field of view.

833 Under cloudy conditions, the received pulse contains a mixture of scattered and unscattered
834 photons, yielding a tail of delayed photons on the downward side of the return pulse; mean and
835 median delays for a segment's aggregate PEs will depend on the relative fraction of the two
836 groups of photons, and the mean path delay per photon. This process has been modeled and
837 found to produce 1-cm level biases on ATLAS height retrievals under most circumstances (Yang
838 and others, 2011) but since the bias may be correlated over large spatial scales it may have a
839 non-negligible impact on continental-scale surface-change retrievals.

840 As is the case with the subsurface-scattering bias, parameters relating to a possible correction
841 must be determined from datasets external to ATLAS, likely from atmospheric models that give
842 an estimate of the cloud optical depth and the particle size. Potential corrections and data editing
843 strategies for this effect remain an active topic of research.

844

845 **3.10 Segment geolocation**

846 After ground-window refinement we calculate the final location of the segment. The segment
847 location is defined as the reference-point location plus the across-track unit vector times the
848 mean across-track coordinate of the selected PEs.

849 To calculate the latitude and longitude of each segment, including the offset between the
850 segment and the reference point, we use the latitude, longitude, and along-track distance
851 provided by ATL03 for the selected PE. We assume that latitude and longitude for the selected
852 PE in the segment are linear functions of along-track distance, and fit a linear function, f_{lat}, to the
853 PE latitudes, and a second linear function, f_{lon}, to the PE longitudes, each as a function of x-x_0.
854 The intercepts of these functions give the segment latitude and longitude.

855 Geolocation errors in the along- and across-track direction are calculated based on the ATL03
856 parameters *sigma_geo_AT,* and *sigma_geo_XT* and the radial orbit error, *sigma_geo_r*.

857 With the surface-slope vector and the geolocation estimate we can calculate the geolocation
858 contribution to the uncertainty in the surface height:

$$\sigma_{geo,h} = \left(sigma_{geo,r}^2 + \left(sigma_{geo,AT} \frac{dh}{dx} \right)^2 + \left(sigma_{geo,XT} \frac{dh}{dy} \right)^2 \right)^{1/2} \qquad 36$$

859   This value is reported in the *land_ice_segments* group as *sigma_geo_h*, and the contributing
860   *sigma_geo_r, sigma_geo_xt, and sigma_geo_at* are reported in the *ground_track* group.

861   **3.11 Noise-corrected robust estimators of spread**

862   Many of the parameters in this document are based on ordinal statistics. These statistics use the
863   percentiles of a distribution, which are defined based on the cumulative distribution function
864   (CDF) of the distribution. We define the CDF of a discrete sample of values S as:

$$C(x;S) = \frac{the\ number\ of\ values\ in\ S\ that\ are\ less\ than\ x}{the\ number\ of\ values\ in\ S} \qquad 37$$

865   For a binned distribution (e.g. a histogram or a probability distribution function), $C(x; D(x_o))$, we
866   define the CDF as

$$C(x; D(x_0)) = \frac{\int_{x_1}^{x} D(x')dx'}{\int_{x_1}^{x_2} D(x')dx'} \qquad 38$$

867   Here are x_1 and x_2 are the bounds over which the distribution is defined. The percentiles of a
868   distribution are found by calculating the inverse function of the CDF of the distribution:

$$p(r; D) = C^{-1}\left(\frac{r}{100}; D \right) \qquad 39$$

869   Thus the median of a distribution D is:

$$Median(D) = x\ such\ that\ \ C(x; D) = 0.5 \qquad 40$$

870   We also define the robust dispersion estimate (RDE) of a distribution as

$$RDE(D) = \frac{p(0.84; D) - p(0.16; D)}{2} \qquad 41$$

871   This is analogous to the standard deviation of a normal distribution, which is equal to half the
872   difference between its 84th and 16th percentiles, but is less influenced by outlying background
873   values.

874

875   In most cases, distributions of ATLAS PEs include a mix of signal and noise PEs. In these
876   cases, the noise PEs and the signal PEs both contribute to the distribution D. We expect the
877   noise PEs are generally uniformly distributed, so we can assume that

$$C(x; D) = \frac{BGR(x - x_1) + \int_{x_1}^{x} D_{signal}(x')dx'}{\int_{x_1}^{x_2} D(x')dx'} \qquad 42$$

878   Here D_{signal} is the distribution of the signal PEs, and BGR is the background PE rate, in units of
879   x^{-1}. We can solve this for C_{signal}:

$$C(x; D_{signal}, BGR) = \frac{\int_{x_1}^{x} D_{signal}(x')dx'}{N_{signal}} = \frac{\int_{x_1}^{x} D(x')dx' - \frac{BGR(x - x_1)}{N_{total}}}{N_{signal}} \qquad 43$$

880   Here $N_{total} = \int_{x_1}^{x_2} D(x')dx'$ and $N_{signal} = N_{total} - (x_2 - x_1)BGR$.

881   Estimating the percentiles of D_{signal} is complicated because C(x; D_{signal}, bckgrd) generally does
882   not have an inverse function in x. However, if we evaluate C(x; D_{signal}, bckgrd) for a set of
883   values, x_i, we can find x_{LT}, the largest value of x_i for which C(x; D_{signal}, bckgrd) < r/100 and x_{GT},
884   the first value of x_i for which C(x; D_{signal}, bckgrd) >r/100, and interpolate linearly into [x_{LT}, x_{GT}]
885   as a function of [C(x_{LT}; D_{signal}, bckgrd), C(x_{GT}; D_{signal}, bckgrd)] at the point r/100.

886   The above procedure defines the background-corrected percentiles of a distribution. Based on
887   this we define the noise-corrected median of a distribution, which we designate: median(D;
888   bckgrd). We define the noise-corrected RDE of a distribution somewhat differently from its
889   uncorrected counterpart. For low-noise distributions, the standard deviation of the population
890   can accurately be estimated as half the difference between its 16th and 84th percentiles. In the
891   presence of significant noise, the standard deviation can be estimated more accurately based on
892   the difference between the 25th and 50th percentiles of the distribution, divided by a correction
893   factor of 1.349, equal to the width of the central 50% of a normalized Gaussian distribution.

894

895   The surface-window-refinement procedure in section 3.3.5 uses least-squares fitting and the
896   RDE to progressively narrow the surface window. This procedure will not converge under all
897   circumstances. Consider an initial surface window spanning from $-H_i/2$ to $H_i/2$, with noise rate
898   R (in PE/m) , containing *s* signal PEs at the center of the window. The normal (non-background-
899   corrected) RDE will find a spread of:

$$\hat{\sigma} = 0.34\,H - \frac{s}{R} \qquad 44$$

900   If s is small, $\hat{\sigma} \approx 0.34\,H$ so the three-sigma interval will have a width of 2.04 H, and the
901   refinement will not converge. Convergence requires $6\hat{\sigma} < H$, or:

$$s > 1.73HR \qquad 45$$

902   For a background rate of 10MHz (0.067 PE/m) and a weak beam (three surface PE per pulse),
903   the procedure will converge if H < 26 m. For a strong beam (10 PE per pulse), it will converge if
904   H<86m. The convergence intervals become smaller in proportion to the signal PE count as the
905   surface return is weakened by cloud attenuation or by reduced surface reflectance.

906   The noise-corrected RDE and median improve on the performance of their uncorrected
907   counterparts, but their performance is limited by the accuracy of the signal-level estimate. The
908   estimate of N_{signal} has an approximate error of $(N_{pulses} (HR+s))^{1/2}$ due to the Poisson statistics of
909   the PE. In contrast to the non-robust RDE and median, the process works increasingly well as
910   more shots are aggregated, because N_{signal} increases in proportion to N_{pulses}, while its error
911   increases in proportion to $N_{pulses}^{1/2}$. If we require that $N_{pulses} s > a\sigma_n$, we find convergence
912   intervals:

$$H < \frac{N_{pulses} s^2 - a^2 s}{a^2 R} \qquad\qquad 46$$

913   For 10 MHz noise, 3 PE/pulse, and for 57 pulses, this gives $s > 3\sigma_n$ for $H < 806$ m, implying
914   that the accuracy of the signal-level estimate will not be the limiting factor for any reasonable
915   initial window size.

916

917

918 **4   ATL06 DATA PRODUCT DESCRIPTION**

919 Here we describe how the parameters appear in the ATL06 product. The ATL06 parameters are
920 arranged by beam, and within each beam in a number of groups and subgroups. Where
921 parameter descriptions in the ATL06 data dictionary are considered adequate, they are not
922 repeated in this document.

923 **4.1   Data Granules**

924 ATL06 data are provided as HDF5 files. The HDF format allows several datasets of different
925 spatial and temporal resolutions to be included in a file. ATL06 files contain data primarily at the
926 single-segment resolution, divided into different groups to improve the conceptual organization
927 of the files. Each file contains data from a single cycle and a single RGT.

928 Within each file there are six top-level groups, each corresponding to data from GT: *gt1l, gt1r,*
929 *gt2l*, etc. The subgroups within these *gtxx* groups are *segment_quality*, *land_ice_segments,* and
930 *residual_histogram.*

931 In the *segment_quality* group, the data are nearly dense, providing signal-selection and location
932 information for every segment attempted (i.e. those that contain at least one ATL03 PE) in the
933 granule, at the 20-meter along-track segment spacing. Datasets in this group can be used to check
934 the geographic distribution of data gaps in the ATL06 record.

935 In the *land_ice_segments* group, data are sparse, meaning that values are reported only for those
936 pairs for which adequate signal levels (i.e. more than 10 PE, *snr_significance > 0.05*) were found
937 for at least one segment: This means that within each pair, every dataset has the same number of
938 values, and that datasets are pre-aligned between pairs, with invalid values (NaNs) posted where
939 the algorithm provided a value for only one beam in a pair. Conversely, if neither beam in a pair
940 successfully obtained a value for *h_li*, that segment is skipped for both beams in the pair. The
941 *segment_id*, timing, and geolocation fields for the valid segments should allow the along-track
942 structure of the data to be reconstructed within these sparse groups. For segments without valid
943 heights that still appear on the product (because the other beam in the pair did contain a valid
944 height) the latitude and longitude are reported for the mean location of all PE for the segment (if
945 any PE are present) or as the location for the valid segment in the pair, displaced by the 90-meter
946 within-pair separation (if no PE are present).

947 The *residual_histogram* group is at lower resolution than the other groups, giving the distribution
948 of PE relative to the segment heights at a horizontal resolution of 200 m, or around 280 pulses.
949 The *segment_id_list, x_atc_mean, lat_mean,* and *lon_mean* fields in this group all can be used to
950 connect the *residual_histogram* group to the per-segment groups.

951 In the native format archived at the National Snow and Ice Data Center (NSIDC), each granule
952 (file) of data contains segments from a single pass over a one-degree increment of latitude for a
953 particular RGT, with corresponding data from all six beams. Over most of the globe, ICESat-2
954 travels in a roughly north-south direction, so each granule will contain approximately 111 km of
955 data for each beam, or approximately 5660 segments. The granules containing the southernmost
956 extent of Antarctica, south of 87S, will contain a considerably longer stretch of data, but because
957 this area will likely be of most interest to researchers investigating continental-scale Antarctic
958 mass balance, the additional coverage will likely be desirable. We expect that because most

959 users will obtain their data through subsetting services provided by the NSIDC, the native
960 granule structure will be of minor importance.

961 **4.2 Segment_quality group**

962 The segment_quality group contains a nearly dense record of the success or failure of the
963 surface-finding strategies, and gives the locations of the ref erence points on the RPTs. It
964 contains a record of the success or failure of the surface-finding strategies, and gives the
965 locations of the reference points on the RPTs.

966 Locations provided within this group are for the reference points on the pair tracks, not for the
967 segments themselves. This means that both beams in a pair will have the same location (because
968 they are not displaced relative to the reference point), and that the actual segment locations will
969 usually be displaced from the values in *reference_pt_lat* and *reference_pt_lon* in this group by
970 more than 45 m in the across-track direction. The laser beam and spot numbers corresponding to
971 the ground tracks are available in the attributes of the *ground_track* group.

972

Table 4-1 *Segment_quality* group

Parameter	Units	Description
delta_time	seconds	Elapsed GPS seconds since the reference epoch. Use the metadata attribute *granule_start_seconds* to compute the full GPS time.
segment_id	unitless	segment number corresponding to the second of two ATL03 segments in the ATL06 segment, counted from the RGT equator crossing
reference_pt_lat	degrees	Latitude of the reference segment location on the RPT
reference_pt_lon	degrees	Longitude of the reference segment location on the RPT
record_number	unitless	For those segments that have adequate signal strength, this parameter gives the record for the pair within the other groups in the granule.
signal_selection_source	unitless	Indicates the last algorithm attempted to select the signal for ATL06 fitting, see table Table 3-1.

		A value of 3 indicates that all algorithms failed.

973

974 **4.2.1 Signal_selection_status subgroup**

975 This subgroup includes the *Signal_selection_status_confident, Signal_selection_status_all,* and
976 *Signal_selection_status_backup* parameters. Their values are described in Table 3-2. Its density
977 structure matches that of the *segment_quality* group.

978

979 **4.3 *Land_ice_segments* group**

980 The primary set of derived ATL06 parameters are given in the *land_ice_segments* group (Table
981 4-2). This group contains geolocation, height, and standard error and quality measures for each
982 segment. This group is sparse, meaning that parameters are provided only for pairs of segments
983 for which at least one beam has a valid surface-height measurement. This group contains the
984 *bias correction*, *fit statistics*, *ground_track*, and *geophysical* subgroups, which all have the same
985 sparsity structure as the *land_ice_segments* group.

986

987 **Table 4-2 *land_ice_segments* group**

Parameter	Units	Description	Defined
ATL06_quality_summary	Unitless	Flag indicating: 0: No likely problems identified for the segment 1: One or more likely problems identified for the segment	4.3
delta_time	Seconds	Elapsed GPS seconds since the reference epoch. Use the metadata attribute granule_start_seconds to compute the full gpstime.	Interpolated to the segment center from ATL03
h_li	Meters	Standard land-ice segment height determined by land ice algorithm, corrected for first-photon bias, representing the median-based height of the selected PEs	Equation 47

h_li_sigma	Meters	Propagated error due to sampling error and FPB correction from the land ice algorithm	Equation 48
sigma_geo_h	meters	Total vertical geolocation error due to PPD and POD, including the effects of horizontal geolocation error on the segment vertical error	3.10
latitude	degrees north	Latitude of segment center, WGS84, North=+	3.10
longitude	degrees east	Longitude of segment center, WGS84, East=+	3.10
segment_id	counts	Segment number, counting from the equator. Equal to the *segment_id* for the second of the two 20-m ATL03 segments included in the 40-m ATL06 segment	ATL03

988

989   The standard surface height will be given on the ATL06 product as *h_li*. This height is the
990   segment-center height obtained from the along-track slope fit, with the mean-median correction
991   applied so that it represents the median surface height for the segment. By default, *h_li* will be
992   corrected for all height increments in the *geophysical* parameter group except for the ocean tide,
993   the equilibrium tide, and the dynamic atmosphere correction (*dac*); this includes earth, load, and
994   pole tides, and troposphere corrections. Since these parameters are included in the standard
995   ATL03 PE height, no correction is applied at the ATL06 stage. Using the names for product
996   variables:

$$h\_li = h\_mean + fpb\_med\_corr + tx\_med\_corr \qquad 47$$

997   Tide and troposphere corrections may be removed from *h* by adding the values provided in the
998   ATL06 *geophysical* group. The correction values for the waveform-based corrections are
999   provided in the *bias_correction* group, so that users may convert, for example, from a median-
1000 based height estimate to a mean-based estimate.

1001 The errors in the standard land-ice height product are calculated as the maximum of the median
1002 error (calculated during the first-photon-bias correction) and the linear-fit error (calculated in
1003 3.6), ignoring errors in the tidal and atmospheric corrections.

$$h\_li\_sigma = \max(sigma\_h\_fit, \ fpb\_med\_corr\_sigma) \qquad 48$$

1004 This value does not include the effects of geolocation errors on the height estimate, because
1005 while the components of *h_li_sigma* should be uncorrelated at the segment-to-segment scale, the
1006 geolocation errors are likely to be correlated on much longer scales. The vertical component of
1007 the geolocation error, as calculated from the surface-slope vector and the mean horizontal
1008 geolocation accuracies of the selected PEs are given in parameter *sigma_geo_h* (see 3.10). The
1009 error on a single segment height measurement taken independently of all adjacent measurements
1010 should be $(h\_li\_sigma^2 + sigma\_geo\_h^2)^{1/2}$. Averaged over several tens of segments with a
1011 consistent surface slope, the error should approach *sigma_geo_h,* but the relative scatter between
1012 individual adjacent segments should be *h_li_sigma.*

1013 The geolocation of the segment is given in geographic coordinates by parameters *latitude* and
1014 *longitude*. These each represent the horizontal centers of the segments. The corresponding
1015 along-track coordinates are given in the *ground_track* group as *x_atc* and *y_atc.*

1016 The *land_ice_segments* group includes the *ATL06_quality_summary* parameter, which indicates
1017 the best-quality subset of all ATL06 data. A zero in this parameter implies that no data-quality
1018 tests have found a problem with the segment, a one implies that some potential problem has been
1019 found. Users who select only segments with zero values for this flag can be relatively certain of
1020 obtaining high-quality data, but will likely miss a significant fraction of usable data, particularly
1021 in cloudy, rough, or low-surface-reflectance conditions. Table 4-3 gives the parameter values
1022 needed for *ATL06_quality_summary* to be reported as zero. The last of these characteristics, the
1023 vertical density of photons, helps remove the effects of a common problem where the ATL03
1024 photon selection identifies a cloud top as a likely surface return. In these cases, ATL06 can
1025 converge to a large (10+ m) vertical window containing tens of signal photons. Requiring a
1026 minimum ratio between the number of photons and the height of the window eliminates most
1027 clouds, and eliminates only a few returns from rough or steep surfaces.

Table 4-3 Segment characteristics for *ATL06_quality_summary* to be zero

Characteristic	Threshold	Description
h_li_sigma	< 1 m	Errors in surface height are moderate or better
snr_significance	< 0.02	Surface detection blunders are unlikely
signal_selection_source	<=1	Signal selection must be based on ATL03 photons
n_fit_photons / w_surface_window_final	>1 PE /m for weak beams, > 4 PE/m for strong beams	The vertical density of photons in the final surface window.

1028

1029

1030

1031   **4.3.1   geophysical subgroup**

1032   The *geophysical* group (Table 4-4) contains tidal and atmospheric corrections that may be added
1033   to or removed from *h_li,* and inferred atmospheric properties that may be used to determine
1034   whether the elevation of a given segment might be affected by atmospheric forward scattering.
1035   Note that the *neutat_delay* parameter and all *tide_* parameters in this group are applied by default
1036   except for *tide_ocean* and *dac* (dynamic atmosphere correction).. The sign of the parameters is
1037   such that adding the parameter value to *h_IS* removes the correction (for applied corrections) and
1038   subtracting the parameter includes the correction (for *tide_ocean*). These parameters are
1039   interpolated from the corresponding ATL03 parameters for the 'nominal photons', interpolated
1040   as a piecewise linear function of along-track distance to the segment centers. This group is
1041   sparse, meaning that parameters are provided only for pairs of segments for which at least one
1042   beam has a valid surface-height measurement.

1043   The ocean-tide value (*tide_ocean*) and dynamic atmosphere correction(*dac)* are provided to
1044   allow interested users to correct for tides and the inverse-barometer effect over ice shelves.
1045   These parameter are not applied because the locations of ice-sheet grounding lines (defining the
1046   inland extent of floating ice shelves) are not always precisely known, and may change over time.
1047   Different users will want to apply the ocean-tide model to different areas within the grounding
1048   zone.

1049   This group also include parameters related to solar background and parameters indicative of the
1050   presence or absence of clouds. Some of these parameters are derived from the ATLAS
1051   atmospheric channel, and should help identify segments strongly affected by clouds or blowing
1052   snow: parameters *cloud_flg_asr* and *cloud_flg_atm* give estimates of the probability of clouds
1053   between ATLAS and the ground, based on the apparent surface reflectance and on atmospheric
1054   backscatter, respectively. Their values are described in the ATL09 ATBD, and should be
1055   evaluated against the standard that cloud optical thickness greater than 0.5 in the lower 3 km of
1056   the atmosphere is required to produce a substantial altimetry error. (Yang and others, 2011) .
1057   Note that over surfaces other than bright snow (e.g. over blue ice or dirty snow) the
1058   *cloud_flg_asr* may indicate clouds when none are present.

1059   Blowing snow has a larger potential to produce altimetry errors, and has been assigned its own
1060   flag; the estimated height of a detected blowing-snow layer is given in *bsnow_h*, which is set to
1061   zero if no such layer can be detected; the confidence with which a blowing-snow layer can be
1062   detected or ruled out is given in *bsnow_conf*. For both flags, cautious users may require a value
1063   of 0 or 1 (clear with high/medium confidence) but under sunlit conditions, neither flag may
1064   clearly indicate cloud-free conditions.   The estimated optical thickness of blowing snow layers,
1065   if found, is given in *bsnow_od*.

1066

1067

1068

1069
Table 4-4 *geophysical* subgroup

Parameter	Units	Description	Defined
bckgrd	Hz	Background count rate, derived from the ATL03 50-shot average, interpolated to the segment center.	Interpolated from ATL03
bsnow_conf	unitless	Blowing snow confidence. -3=surface not detected; -2=no surface wind;-1=no scattering layer found; 0=no top layer found; 1=none-little; 2=weak; 3=moderate; 4=moderate-high; 5=high; 6=very high	ATL09
bsnow_od	unitless	Blowing snow layer optical depth	ATL09
bsnow_h	meters	Blowing snow layer top height	ATL09
cloud_flg_asr	counts	Cloud flag (probability) from apparent surface reflectance. 0=clear with high confidence; 1=clear with medium confidence; 2=clear with low confidence; 3=cloudy with low confidence; 4=cloudy with medium confidence; 5=cloudy with high confidence	ATL09
cloud_flg_atm	counts	Number of layers found from the backscatter profile using the DDA layer finder.	ATL09
layer_flag	counts	This flag is a combination of multiple flags (cloud_flag_atm, cloud_flag_asr, and bsnow_con) and takes daytime/nighttime into consideration. A value of 1 means clouds or blowing snow are likely present. A value of 0 indicates the likely absence of clouds or blowing snow.	ATL09

e_bckgrd	Hz	Expected background count rate based on sun angle, surface slope, for unit surface reflectance	Calculated following ATL07
msw_flag	unitless	Multiple Scattering warning flag. The multiple scattering warning flag (ATL09 parameter msw_flag) has values from -1 to 5 where zero means no multiple scattering and 5 the greatest. If no layers were detected, then msw_flag = 0. If blowing snow is detected and its estimated optical depth is greater than or equal to 0.5, then msw_flag = 5. If the blowing snow optical depth is less than 0.5, then msw_flag = 4. If no blowing snow is detected but there are cloud or aerosol layers detected, the msw_flag assumes values of 1 to 3 based on the height of the bottom of the lowest layer: < 1 km, msw_flag = 3; 1-3 km, msw_flag = 2; > 3km, msw_flag = 1. A value of -1 indicates that the signal to noise of the data was too low to reliably ascertain the presence of cloud or blowing snow. We expect values of -1 to occur only during daylight.	ALT09
r_eff	unitless	Effective reflectance, uncorrected for atmospheric effects.	Equation 33
solar_azimuth	degrees_east	The direction, eastwards from north, of the sun vector as seen by an observer at the laser ground spot.	ATL03 solar_azimuth parameter, interpolated to the segment center from the reference photons
solar_elevation	degrees	Solar Angle above or below the plane tangent to the ellipsoid surface at the laser spot. Positive values mean the sun is above the horizon, while negative values mean it is below the horizon. The effect of atmospheric refraction is not included. This is a low-precision value,	ATL03 solar_elevation parameter, interpolated to the segment center from the reference photon

		with approximately TBD degree accuracy.	
tide_earth	meters	Earth tide	Inherited from ATL03
dac	meters	dynamic atmosphere correction	Inherited from ATL03
tide_load	meters	Load Tide	Inherited from ATL03
tide_ocean	meters	Ocean Tide	Inherited from ATL03
tide_pole	meters	Pole Tide	Inherited from ATL03
tide_equilibrium	meters	Equilibrium tide	Inherited from ATL03
neutat_delay_total	meters	Total neutral atmospheric delay correction (wet+dry)	Inherited from ATL03

1070

1071 In some circumstances, the estimated background rate may also give an indication of cloud
1072 conditions. The estimated background rate is provided in parameter *bckgrd*, which may be
1073 compared with the background rate expected for a unit-reflectance Lambertian surface, with a
1074 slope equal to the measured surface slope, *E_bckgrd*. In sunlit conditions, these parameters
1075 together allow an estimate of the total sub-satellite reflectance. The effective, uncorrected surface
1076 reflectance, *r_eff*, based on first-photon-bias-corrected PE count and the range to the ground,
1077 may be compared to these numbers; if *bckgrd* is approximately equal to *e_bckgrd*, the
1078 atmosphere and the surface must together have a reflectance close to unity; if *r_eff* is
1079 approximately equal to unity, this indicates that the surface below the satellite is likely snow, and
1080 likely cloud free; if *bckgrd* is approximately equal to *e_bckgrd* and *r_eff* is small, clouds must be
1081 present, and if *bckgrd* is less than *e_bckgrd,* the surface must be dark, and, most likely not snow
1082 covered.

1083 Also included in this group are the solar azimuth (*solar_azimuth*) and elevation
1084 (*solar_elevation*), used in estimating the expected background rates.

1085 **4.3.2   ground_track subgroup**

1086 The *ground_track* subgroup (Table 4-5) contains parameters describing the GT and RGT for
1087 each segment, as well as angular information about the beams. All the components needed to
1088 identify a given segment's orbit number, reference track, pair track, and beam number are given,
1089 along with the azimuth and elevation of the beam relative to the ellipsoid surface normal. The
1090 orientation of the RPT with respect to local north is given in *seg_azimuth.*

1091 Note that in land-ice products, the ground tracks and pair tracks are numbered separately from
1092 the laser beams: the ground tracks are numbered from left to right relative to RGT, and the
1093 ground track number is associated with group names within the product: From left to right, they
1094 are *gt1l, gt1r, gt2l, gt2r, gt3l, and gt3r*. The laser beams are numbered from left to right relative
1095 to the spacecraft flight direction. When the spacecraft is flying with its x axis pointing forwards,
1096 the beam numbers are in the same order (beam numbers 1…6 correspond to tracks *gt1l...gt3r*),
1097 but when it is in the opposite orientation, the laser-beam numbers are reversed relative to the
1098 ground-track numbers (beam numbers 1…6 correspond to tracks *gt3r...gt1l*).

1099 This group is sparse, meaning that parameters are provided only for pairs of segments for which
1100 at least one beam has a valid surface-height measurement. Data-set attributes give:

1101   -the reference ground track number

1102   -the correspondence between laser beam numbers and ground tracks

1103   -the cycle number

1104 The RMS accuracy of the horizontal geolocation for the segment is described by the geolocation
1105 error ellipse, which is calculated based on the PE-medians of the ATL03 parameters
1106 *sigma_geo_xt*, *sigma_geo_at* and *sigma_geo_r*. The along-track and across-track coordinates of
1107 the segments are provided by parameters *x_atc* and *y_atc*.

Table 4-5 *ground_track* subgroup

Parameter	Units	Description	Derived
ref_azimuth	degrees	The direction, eastwards from north, of the laser beam vector as seen by an observer at the laser ground spot viewing toward the spacecraft (i.e., the vector from the ground to the spacecraft).	ATL03
ref_coelv	degrees	Coelevation (CE) is direction from vertical of the laser beam as seen by an observer located at the laser ground spot.	ATL03
seg_azimuth	degrees	The azimuth of the pair track, east of local north	3.1.2.2
sigma_geo_at	meters	Geolocation error in the along-track direction	3.10
sigma_geo_xt	meters	Geolocation error in the across-track direction	3.10

sigma_geo_r	Meters	Radial orbit error	3.10
x_atc	meters	The along-track x-coordinate of the segment, measured parallel to the RGT, measured from the ascending node of the equatorial crossing of a given RGT	3.1.2.2
y_atc	meters	Along-track y coordinate of the segment, relative to the RGT, measured along the perpendicular to the RGT, positive to the right of the RGT.	3.1.2.2

1108

1109   **4.3.3   bias_correction subgroup**

1110   The *bias_correction* subgroup (Table 4-6) contains information about the estimated first-photon
1111   bias, and the transmit-pulse-shape bias. The standard correction applied in *h_li* is
1112   *fpb_med_corr+tx_med_corr*, and its error is *fpb_med_corr_sigma*. The alternate, mean-based
1113   correction, is *fpb_mean_corr,* with error *fpb_mean_corr_sigma.* The median-based elevation,
1114   without the first-photon-bias correction, may be recovered by subtracting *fpb_med_corr* and
1115   adding *med_r_fit.* For example, users who prefer to use the mean statistics instead of the median
1116   statistics would use *h_li - fpb_med_corr –tx_med_corr+ fpb_mean_corr +tx_mean_corr* as their
1117   height estimate.

1118   The corrected photon count is given as *fpb_n_corr*; this gives an estimate of the number of
1119   photons in the surface window as estimated during the FPB correction. The transmit-pulse-shape
1120   corrections (*tx_med_corr* and *tx_mean_corr*) are also given.

1121

Table 4-6 *bias_correction* subgroup

Parameter	Units	Description	Derived
fpb_mean_corr	meters	First-photon bias correction to the mean segment height	3.4.3.1
fpb_mean_corr_sigma	meters	Estimated error in *fpb_mean_corr*	3.4.3.1
fpb_med_corr	meters	First-photon-bias correction giving the difference between the	3.4.3.2

		mean segment height and the corrected median height	
fpb_med_corr_sigma	meters	Estimated error in *fpb_med_corr*	3.4.3.2
fpb_n_corr	counts	Estimated window photon count after first-photon-bias correction	3.4.3.3
med_r_fit	meters	Difference between uncorrected mean and median of linear-fit residuals	3.3.5.2
tx_med_corr	meters	Estimate of the difference between the full-waveform transmit-pulse mean and the median of a broadened, truncated waveform consistent with the received pulse	3.5
tx_mean_corr	meters	Estimate of the difference between the full-waveform transmit-pulse mean and the mean of a broadened, truncated waveform consistent with the received pulse	3.5

1122

4.3.4 fit_statistics subgroup

1124 The *fit_statistics* subgroup gives a variety of parameters describing the segment fit and its
1125 residuals. These parameters may be used to determine whether a particular segment is
1126 potentially usable if it is not identified as problem-free in the
1127 *land_ice_segments/ATL06_quality_summary* flag.

Table 4-7 *fit_statistics* subgroup

Parameter	units	Description
dh_fit_dx	unitless	Along-track slope from along-track segment fit

dh_fit_dx_sigma	Unitless	Propagated error in the along-track segment slope
dh_fit_dy	Unitless	Across-track slope from segment fits to weak and strong beams; the same slope is reported for both laser beams in each pair
signal_selection_source	Unitless	Flag describing the source of the information used to select the signal PE. See Table 3-1
signal_selection_source_status	Unitless	Indicates the status of the last signal selection algorithm attempted (see *signal_selection_source*). Values for this flag are given in the sections of Table 3-2.
h_mean	meters	Mean surface height, not corrected for first-photon bias or pulse truncation.
sigma_h_mean	meters	Propagated height error due to PE-height sampling error for height from the along-track fit, not including geolocation-induced error
h_expected_rms	meters	Expected RMS misfit between PE heights and along-track segment fit
h_rms_misfit	meters	RMS misfit between PE heights and along-track segment fit
h_robust_sprd	meters	RDE of misfit between PE heights and the along-track segment fit.
n_seg_pulses	counts (pulse ID)	The number of pulses potentially included in the segment (floating-point number)

n_fit_photons	counts	Number of PEs used in determining h_li after editing
w_surface_window_final	meters	Width of the surface window, top to bottom
snr	unitless	Signal-to-noise ratio in the final refined window
snr_significance	unitless	Probability that signal-finding routine would converge to at least the observed SNR for a random-noise input. Small values indicate a small likelihood of a surface-detection blunder.

1128

4.3.5 *DEM* subgroup

This subgroup (Table 4-8) contains DEM elevations interpolated at the segment centers. It contains only three parameters: the DEM elevation (*dem_h*), the geoid height (*geoid_h*), and the DEM source (*dem_flag*). The best DEMs available in time for the ICESat-2 launch may be significantly better than those available at present (February 2015), but the best current choices are:

- For Antarctica, the REMA DEM : https://www.pgc.umn.edu/data/rema/, filtered to 40-m resolution before interpolation to the ICESat-2 segment centers, with gaps filled with ATL06 data from cycles 1 and 2.
- For the Arctic, the Arctic DEM, based on stereophotogrammetry https://www.pgc.umn.edu/data/arcticdem. The DEM should be filtered to 40-m resolution before interpolation to the ICESat-2 reference points.
- For areas outside the poles, a multi-sensor global DEM, posted at 7.5 arcsec (http://topotools.cr.usgs.gov/gmted_viewer).

This group is sparse, meaning that parameters are provided only for pairs of segments for which at least one beam has a valid surface-height measurement.

Table 4-8 *DEM sub*group

Parameter	Description
dem_h	Height of the DEM, interpolated by cubic-spline interpolation in the DEM coordinate system to the PE location

dem_flag	source for the DEM.1=Antarctic DEM, 2=Arctic DEM, 3=global DEM.
geoid_h	Geoid height, meters

1145

4.4 *residual_histogram* group

1147 This group contains histograms of the residuals between PE heights and the least-squares fit
1148 segment heights, at 200-meter along-track resolution. It is intended to allow visualization of the
1149 surface-return shapes, and investigation of changes in the return pulse shape or of near-surface
1150 scattering, such as that due to dense blowing snow. Each column of the histogram gives the
1151 number of PE in a set of bins distributed between -50 and +50 m around the surface. The
1152 distribution of these bins is as follows:

1153 From 50 to 20 m below the surface, bins are spaced at 1 m

1154 From 20 m to 10 m below the surface, bins are spaced at 0.5 m

1155 From 10 m to 4 m below the surface, bins are spaced at 0.25 m

1156 From 4 m to 2 m below the surface, bins are spaced at 2 cm

1157 From 2 m below the surface to 2 m above the surface, bins are spaced at 1 cm

1158 From 2 m to 4 m above the surface, bins are spaced at 2 cm

1159 From 4 to 10 m above the surface, bins are spaced at 0.25 m

1160 From 10 to 20 m above the surface, bins are spaced at 0.5 m

1161 From 20 m above the surface to 50 m above the surface, bins are spaced at 1 m.

1162 This distribution of bin edges gives 749 (*N_bins*) vertical bins, with 750 edges. The heights of
1163 the bin tops are given in the *bin_top_h* parameter, listed in order from bottom to top. For any bin
1164 in the histogram, the bottom elevation is equal to the top of the previous bin, and the elevation of
1165 the bottom of the bottom bin is 1 m below its top. The residuals from collections of 10 along-
1166 track ATL06 segments are combined into each histogram; because adjacent ATL06 segments
1167 overlap by 50%, only those PE within 10 m of each segment center in the along-track direction
1168 are included in the histograms. Only those segments with high-quality signals
1169 (ATL06_quality_summary =0) are included in the histogram, and a list of the *segment_id* values
1170 of included segments is provided in the group (recall that the *segment_id* for a segment
1171 corresponds to the second of the two ATL03 segments included in each ATL06 segment). To
1172 allow reconstruction of the per-pulse signal levels, the sum of the number of pulses in the valid
1173 segments is given for each histogram, and the *background_per_m* parameter is given to indicate
1174 the number of background photons expected in each vertical meter of each histogram. The
1175 expected number of photons in each histogram bin can be found by multiplying the height
1176 difference between the edges of the bin by *background_per_m*. The counts for any histogram

1177   bins that are not entirely encompassed by at least one of the two possible telemetry band window
1178   ranges are marked as invalid.
1179

Table 4-9 Parameters in the *residual_histogram* group

Parameter	Dimensions	Description
count	N_bins x N_hist	Residual count in 1-cm bins, for PE within 10 (horizontal) m of segment centers for each histogram. Bin-top heights may be found in *residual_histogram/bin_top_h.*
delta_time	1xN_hist	Elapsed GPS seconds since the reference epoch. Use the metadata attribute granule_start_seconds to compute the full gpstime. Calculated from the mean of the *delta_time* for the segments in each histogram bin.
bin_top_h	N_bins	Height of the top of each histogram bin, listed in increasing order. The bottom of each bin is equal to the top of the next-lowest bin, and the bottom of the lowest bin is 1 m below its top
bckgrd_per_m	1xN_hist	Number of background PE expected for each vertical meter of the histogram based on the observed background rate (bckgrd)
segment_id_list	10xN_hist	Segments ids included in each column of the histogram
lat_mean	1x N_hist	Mean latitude of the segments included in the histogram
lon_mean	1x N_hist	Mean longitude of the segments included in the histogram
pulse_count	1xN_hist	Number of pulses potentially included in the histogram (pulses are counted if they are in the central 20 m of each segment, even if no PE from the pulse are selected)

x_atc_mean	1x N_hist	Mean along-track coordinate of the segments included in the histogram.

1180

1181

1182 **5   ALGORITHM IMPLEMENTATION: LAND ICE HEIGHT (ATL 06/L3A)**

1183   This section gives detailed procedures for estimating heights from ATL03 PEs. The procedures
1184   are presented as an outline of the steps that need to be programmed to calculate the main
1185   parameters from each group; we assume that after interaction with the programming team these
1186   outlines will be updated to ensure their accuracy and consistency with the rest of this document.

1187   **5.1   Outline of Procedure**

1188   The following steps are performed for each along-track reference point:

1189   1. PEs from the current cycle falling into the along-track bin for the along-track point are
1190   collected
1191   2. The initial height and along-track slope are estimated for each beam in the pair
1192   3. The heights and surface windows are iteratively refined for each beam in the pair
1193   4. Corrections for subsurface scattering, first-photon bias, median offsets, and error
1194   estimates are calculated for each beam based on the edited PEs
1195   5. The across-track slope is calculated

1196   Steps 1-5 are described in the "Processing Procedure" subsection.

1197   **5.2   Input Parameters**

1198   Steps 1-6 in 5.1.1 can be calculated based on ATL03 inputs. Steps 5 and 6 require information
1199   about the background rate, which is provided with the atmospheric data

1200   **Table 5**-**1** lists parameters needed from ATL03 and ATL09 for generation of ATL06.

1201   Individual PE heights, times, IDs, and geolocations are provided by ATL03. A variety of tidal
1202   and atmospheric-delay parameters are derived from subsamples of ATL03 fields or by
1203   interpolation into data tables used during ATL03 processing. Some ATL03 parameters are
1204   provided for every PE (e.g. height and horizontal position). These are averaged over the selected
1205   PEs for each segment. Others are provided for 'reference' photons spaced approximately every
1206   40 m along track. For these fields, ATL06 values are interpolated as a function of along-track x
1207   from the values for the 'nominal' photons to the segment centers.

1208   In addition, parameters from the atmospheric channel are used to define the blowing-snow height
1209   parameter, the blowing-snow confidence parameter, and the cloud-flag confidence parameter.

1210   The 200-Hz background-rate parameter is used to estimate background rates for each segment, as
1211   is the 50-Hz background-rate parameter based on the full atmospheric window. An estimate of
1212   the optical depth for the 3 km above the ground and a blowing-snow height estimate and
1213   confidence flag are also calculated based on ATL09 parameters.

1214   The transmit-pulse shape is used to correct the truncated means and medians used in estimating
1215   the surface shape to reduce potential biases in the recovered surface height.

Table 5-1. Inputs for ATL06

Parameter	Source	Description	
podppd flag	*/gtxx/geolocation/podppd_flag*	Flag indicating low/high quality geolocation	
Segment_ID	ATL03: /gtxx/geolocation	ATL03 segment ID	
Ph_index_beg	ATL03: /gtxx/geolocation	First photon in the segment	
Segment_ph_cnt	ATL03: /gtxx/geolocation	Number of PE in each segment	
Segment_dist_x	ATL03: /gtxx/geolocation	Along-track distance for each ATL03 segment	
Segment_length	ATL03: /gtxx/geolocation	Along-track length of each ATL03 segment.	
Velocity_sc	ATL03: /gtxx/geolocation	Spacecraft ground speed	
Sigma_across	ATL03: /gtxx/geolocation	across-track component of geolocation error	
Sigma_along	ATL03: /gtxx/geolocation	Along-track component of geolocation error	
Sigma_h	ATL03: /gtxx/geolocation	Vertical component of geolocation error	
Delta_time	ATL03: /gtxx/geolocation	Time for each PE	
H_ph	ATL03: /gtxx/heights	WGS-84 PE height	
Lat_ph	ATL03:	PE latitude	

	/gtxx/heights	
Lon_ph	ATL03: /gtxx/heights	PE longitude
Signal_conf_ph	ATL03: /gtxx/heights	Signal-classification confidence
Ph_id_channel	ATL03: /gtxx/heights	Channel number for each PE
Ph_id_pulse	ATL03: /gtxx/heights	Pulse number for the current PE
Pce_mframe_cnt	ATL03: /gtxx/heights	Major frame number for the current PE
Dist_ph_along	ATL03: /gtxx/heights	Along-track distance relative to the current segment start
Dist_ph_across	ATL03: /gtxx/heights	Along-track distance relative to the RGT
bckgrd_rate	ATL03: /gtxx/bckgrd_atlas	Background rate calculated from the 50-pulse altimetric histogram
delta_time (corresponding to bckgrd_rate)	ATL03: /gtxx/bckgrd_atlas	Time for the first shot in the 50-pulse altimetric histogram
DEM elevation	Standard DEMs	Best-available DEMs (see 4.3.5) interpolated to each segment location
Tide model values	ATL03: /gtxx/geophys_corr	Various tide-model parameters
Tep_hist	ATL03: Atlas_impulse_response/ beam_x/histogram	Transmitter-echo-pulse histogram for the strong/weak spot (should match current spot)

Tep_hist_x	ATL03: Atlas_impulse_response/ beam_x/histogram	Times for transmitter-echo-pulse histogram bins
Tep_bckgrd	ATL03: Atlas_impulse_response/ beam_x/histogram	Transmitter-echo-pulse per-bin background count
Tep_tod	ATL03: Atlas_impulse_response/ beam_x/histogram	Day/time for the TEP measurement used
Channel dead-time estimates	ATL03	dead-time estimates for each channel, from ATL03 parameters /atlas_impulse_response/dead_time
Blowing-snow flag	ATL09	Blowing-snow flag
Blowing-snow confidence	ATL09	Blowing-snow confidence
Cloud flag	ATL09	Cloud flag and confidence

1216

1217 Note that some parameters that are provided for each segment in ATL03 are needed for each PE
1218 in ATL06. For example, the along-track distance for a PE is the sum of *segment_dist_x*
1219 (provided per segment) and *dist_ph_along* (provided for each PE). To allow us to access these
1220 fields, we generate an internal *ph_seg_num* variable, based on the ATL03
1221 *geolocation/ph_index_beg* variables, assigning all photons between the *i*-th value of
1222 *geolocation/ph_index_beg* and 1 less than the *i+1*-th value a *ph_seg_num* value of *i*. The
1223 background rate is provided in ATL03 on a 50-shot sampling interval; we convert this to the per-
1224 PE rate by interpolating as a function of *delta_time*.

1225

1226 **5.3   Processing Procedure for Parameters**

1227 In this section, we give pseudocode for the calculation of ATL06 parameters. The flow chart for
1228 this process is summarized in Figure 5-1. The code is made up of several functions that call one
1229 another, following the process described in Section 5.1.

Figure 5-1. Flow chart for top-level ATL06 processing

Processing chain showing inputs and outputs for ATL06 fitting routine.
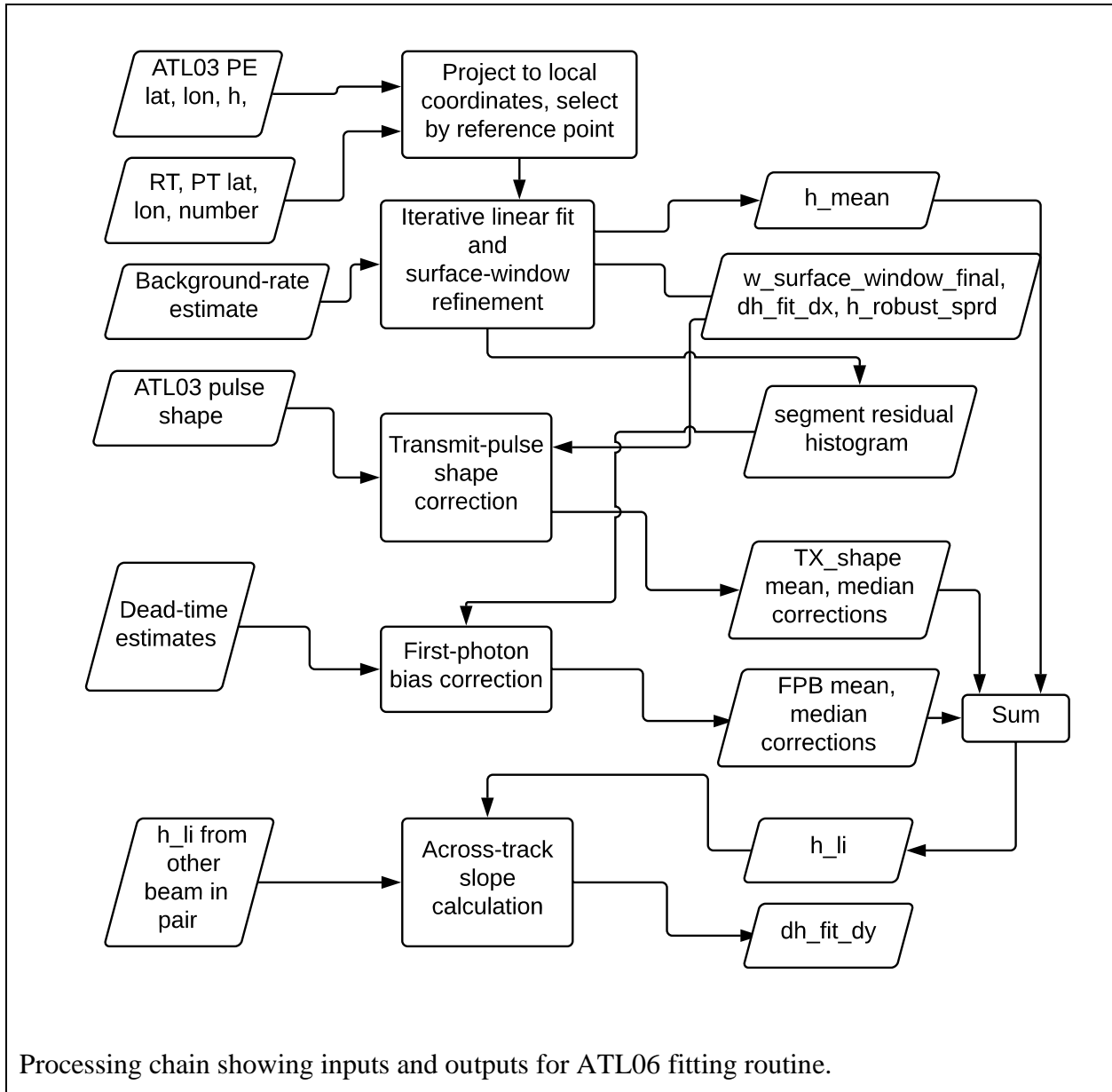
1230

1231 **5.4   Top-Level Fitting Routine**

1232   This routine calls the other routines in the processing chain to derive the final heights and
1233   corrections. It corresponds to all the steps described in 3.2.

1234

1235   **Inputs**, for each beam, for ATL03 segments *m-1* and *m*:

1236   *x_PE*: along-track coordinates of the land-ice PEs, meters

1237   *y_PE*: across-track coordinates of the land-ice PEs, meters

1238   *h_PE*: heights of the PE, meters

1239   *t_PE:* times for PE.

1240   *Ice_confidence_flag* : Confidence with which the PE has been identified as coming from
1241   the surface, unitless

1242   *bckgrd* : estimated background PE rate for the current segment, counts/second

1243   *ch_deadtime*: Deadtime estimate for each channel

1244   *x0_seg* : along-track coordinate of the current reference point

1245   *bckgrd_rate:* 50-shot-resolution background rate, derived from ATL03, interpolated to
1246   the center of the segment.

1247   *Spacecraft_ground_speed:* The speed of the nadir point below the spacecraft as it moves
1248   along the geoid.

1249   *Podppd_flag:* ATL03 flag indicating high or low quality geolocation

1250   **Outputs** (repeated for left and right beams)

1251   *delta_time*: time offset with respect to the beginning of the granule

1252   *h_li*   : land-ice height, meters

1253   *h_li_sigma* : error in the ice-sheet height, meters

1254   *h_robust_sprd* : ice-sheet residual robust spread, meters

1255   *h_rms_misfit* : RMS residual for the residual spread, meters

1256   *n_fit_photons:* The number of photons used to define the segment.

1257   *w_surface_window*   : width of the refined window used to select PEs, meters

1258   *h_expected_rms* : expected standard deviation of PEs based on surface geometry and
1259   signal levels, meters

1260   *dh_fit_dx*   : along-track slope for the segment, unitless

1261   *signal_selection* parameters *:* parameters indicating how the initial PE were selected

1262   *fpb_corr_mean* : first-photon bias correction for the mean surface height, meters

1263   *fpb_corr_median*: first-photon bias correction for the median surface height, meters

1264   *tx_median_corr*: return-truncation correction to the median-based segment height

1265   *tx_mean_corr*: return-truncation correction to the mean-based segment height

1266   *fpb_n_corr* : corrected PE count from the first-photon bias, meters

1267   *y_seg_RGT*: segment across-track coordinate

1268   *lat_seg_center*: segment-center latitude

1269   *lon_seg_center*: segment-center longitude

1270   *tide* and *dac* parameters: geophysical parameters that are averaged and passed on from
1271   ATL03

1272   *SNR:* Estimated signal-to-noise ratio for the segment

1273   *atl06_quality_summary*: Summary parameter indicating whether a problem in the
1274   segment fitting was identified

1275   **Output** for both beams together:

1276   *dh_fit_dy* : across-track slope, unitless

1277   **Internal variable**, that is tracked through the fitting procedure:

1278   *h_ range_ input:* The range of heights provided as an input to the fitting algorithm.

1279   **Parameters:**

1280   *granule_start_time*: the starting time of the granule

1281   *dx_seg* = 40 meters

1282   *sigma_beam*: sigma value for pulse surface footprint (expected to be equal to 4.25 m)

1283   *SNR_F_table:* 3-d table giving the probability of finding a segment with the given SNR
1284   for noise-only inputs

1285   *PRF*: Pulse repetition frequency for ATLAS (equal to 10,000 s^{-1})

1286   **Procedure:**

1287   1. Select PE for the initial fit.

1288   1a. If the *podppd_flag* indicates degraded geolocation for any pulses, skip to the next
1289   segment.

1290   1b. For each beam, select PE with ATL03 segment_id of *m* or *m-1*. Set *h_range_input*
1291   equal to the difference between the maximum and minimum of the PE heights. Eliminate any
1292   photons that are identified by ATL03 as part of the TEP.

1293   1c. Set initial values for the geolocation and time parameters: set *lat_seg_center,*
1294   *lon_seg_center* and *delta_time* to the means of the corresponding reference photon values.

1295   1d. Calculate *n_seg_pulses* based on the spacecraft ground speed, and the lengths of
1296   segments *m-1* and *m*: n_seg pulses=(sum of segment lengths * PRF)/*spacecraft_ground_speed*.

1297   1e Based on the *ice_confidence_flag* values (see **PE selection based on ATL03 flags**),
1298   and assign values to *signal_selection_source, signal_selection_status_confident,* and
1299   *signal_selection_status_all*. If *signal_selection_source* is equal to 0 or 1, set *h_range input* equal
1300   to *H_win*.

1301   1f. If both *signal_selection_status_confident* and *signal_selection_status_all* are nonzero,
1302   select PE using the **backup PE selection** routine. If *signal_selection_status_backup* is greater
1303   than 1, skip fitting for the current beam and reference point, report invalid for *h_mean,* and for
1304   *n_fit_photons*. If *signal_selection_status_backup* is equal to 0 set *h_range_input* equal to
1305   *H_win*.

1306   Note: If *h_range_input* is not set in 1d or 1e, it remains equal to the value set in 1a: the
1307   difference between the maximum and minimum heights of all photons found in segments *m* and
1308   *m-1*.

1309

1310   Output values assigned: *signal_selection_source, signal_selection_status_confident,*
1311   *signal_selection_status_all, signal_selection_status_backup.*

1312   Internal values assigned: PE_selection_flag.

1313   2. For each beam, estimate the surface height and slope using the **iterative least-squares fitting**
1314   routine. Set *n_fit_photons* to the number of PE in the final selection. If the final selection
1315   includes fewer than 10 PE, or if the along-track spread is less than 20 m, or if the final window
1316   width is larger than 20 m, report an invalid fit and set *h_mean* to its invalid value (*NaN*) and
1317   return.

1318   Output values assigned, for each beam: *n_fit_photons, dh_fit_dx, h_mean, h_rms_misfit,*
1319   *h_robust_sprd, med_r_fit, w_surface_window_final, SNR.*

1320   Internal values assigned, for each beam: *h_mean, r_fit, selected_PE, h_range_input*

1321

1322   3. For each beam, calculate the first-photon bias correction

1323   For each beam, estimate the first-photon bias correction to the mean height, the first-
1324   photon-bias corrected median height, and the corrected return-time histogram based on the
1325   residuals to the segment heights calculated in step 3.

1326   3a. Run the first-photon-bias-correction routine on PE flagged with *selected_PE* (see
1327   below)

1328   Internal values assigned: fpb-corrected residual histogram, estimated gain.

1329   Output values assigned for each beam: *fpb_mean_corr, fpb_mean_corr_sigma,*
1330   *fpb_median_corr, fpb_median_corr_sigma , FPB_N_PE*

1331

1332   4. Calculate the pulse-truncation correction

1333   Based on the *h_robust_sprd* and *w_surface_window_final* values calculated in the last
1334   step of the iterative least-squares fit and the *SNR* calculated in step 2, calculate the pulse-
1335   truncation correction (See pulse-truncation-correction section).

1336   Output values assigned for each beam: *tx_med_corr, tx_mean_corr*

1337

1338   5. Calculate remaining output parameters

1339   5a. Calculate *h_li*:

1340 $$h\_li = h\_mean + fpb\_med\_corr + tx\_med\_corr$$

1341   Output values assigned: *h_li*

1342

1343   5b. Calculate *y_seg_RGT,* equal to the median of all *y_PE_RGT* values.

1344   <u>Output values assigned:</u> *y_seg_RGT*

1345   5c. Calculate *seg_time, lat_seg_center* and *lon_seg_center* by regressing (respectively)
1346   *time_PE*, *lat_PE* and *lon_*PE as a function of *x_PE* to *x0_seg* for selected PE. For those
1347   segments for which fitting has failed, but for which the other beam in the pair has a valid
1348   segment, report the latitude and longitude of the valid segment, displaced by 90 m to the left or
1349   right in the across-track direction (depending on which segment is valid).

1350   <u>Output values assigned:</u> *seg_time, lat_seg_center, lon_seg_center, delta_time*

1351   5d. Estimate the final cross-track slope, equal to the difference between the *h_li* values
1352   divided by the difference between the *y_seg_RGT* values for the two beams.

1353   <u>Output values assigned:</u> *dh_fit_dy*

1354   5e. Calculate error estimates for each beam.

1355   *i.* For each segment, calculate *h_expected_RMS* based on the footprint size, the along-
1356   track track slope, and the transmit pulse duration (equation 1):

1357   *h_expected_RMS = sqrt((dh_fit_dx sigma_beam)^2 + (c/2 sigma_xmit)^2)*

1358   *ii.* Add the effects of background noise to *sigma_expected* to calculate *sigma_PE_est.*

1359   *sigma_PE_est= ((N_signal h_expected_RMS^2+N_noise(0.287 H_win)^2)/N_tot)$^{1/2}$*

1360   *iii.* Calculate linear-fit-model errors. Multiply *h_mean_sigma_unit* and
1361   *dh_fit_dx_sigma_unit* by *max(sigma_PE_est, h_rms_misfit)* to obtain *h_mean_sigma* and
1362   *dh_fit_dx_sigma*.

1363   <u>Output values assigned:</u> *sigma_h_mean, sigma_dh_fit_dx, sigma_PE_est, h_rms_misfit.*

1364   5f. Set *h_li_sigma* equal to the maximum of *sigma_h_mean* and *fpb_med_corr_sigma.*

1365   <u>Output values assigned</u> for each beam: *h_li_sigma.*

1366   5g. Calculate the uncorrected reflectance, based on the first-photon-bias-corrected total
1367   PE count. Equation given in 3.4.3.3.

1368   <u>Output values assigned,</u> for each beam: *r_eff*

1369   5h. Calculate *SNR_significance*, by interpolating into the *SNR_F_table* as a linear
1370   function of the table parameters *BGR, SNR*, and *w_surface_window_initial*.

1371   <u>Output value assigned:</u> *SNR_significance*

1372   5i: calculate atl06_quality_summary: *atl06_quality_summary* is zero unless *h_li_sigma >*
1373   1 m or *SNR_significance > 0.02* or *N_fit_photons/w_surface_window_final < 4 (for strong*
1374   *beams)* or <1 (for weak beams) or *signal_selection_source > 1.*

1375   5j: Calculate pass-through parameters: For tide parameters, error parameters, and the *dac*,
1376   calculate ATL06 values from the average values for the ATL03 segments.

1377   5k: Calculate systematic error estimates: Based on geolocation error estimates and surface
1378   slope, calculate *h_li_sigma_systematic* based on equation 36.

1379   **5.5   Signal selection based on ATL03 flags**

1380   **Inputs**, from one beam only, for each PE

1381   *x_PE*: along-track coordinates of the land-ice PE for the current segment

1382   *h_PE*: height of PE for the current segment

1383   *Ice_confidence_flag*: ATL03 classification of the land-ice PE. 0=undetected, 1=PE in the
1384   pad region, but not identified as signal PE, 2=low confidence, 3=medium confidence, 4=high
1385   confidence.

1386   **Input**, one per segment:

1387   *x0*: the along-track location of the segment center.

1388   *BGR:* the interpolated background PE rate for the segment.

1389   **Parameters:**

1390   *Sigma_beam:* The one-sigma expected horizontal spread of the photons on the ground.
1391   Equal to 4.25 m (pre-launch estimate)

1392   *Sigma_xmit*: The one-sigma temporal duration of the transmit pulse.

1393   **Outputs**:

1394   *PE_selection*: binary flag, one per input PE, showing whether to use that PE in the initial
1395   fit.

1396   *Signal_selection_source*: parameter indicating the how the signal was selected. See
1397   Table 3-1 for values.

1398   *signal_selection_status_confident:* parameter indicating the success/failure of signal
1399   selection using low-or-better confidence PEs.

1400   *signal_selection_status_all:* parameter indicating the success/failure of signal selection
1401   using all flagged PEs.

1402   *H_win:* Height of the window around the best-fitting line used to select PE.

1403

1404   **Procedure:**

1405   1. If the inputs are empty (no PE are in the along-track window), set *signal_selection_source* to
1406   3, set *signal_selection_status_confident* to 3, set *signal_selection_status_all* to 3 set
1407   *signal_selection_status_backup* to 4, and return.

1408   2. Check if the confidently detected PE are adequate to define an initial segment.

1409   2a. Set *PE_selection* to true for all PE with *Ice_confidence_flag*>=2, to zero for all
1410   others

1411
1412

2b: If the difference in *x_PE* between the first and last PE in *PE_selection* is less than 20 m set *signal_selection_status_confident* to 1.

1413
1414

2c: If there are fewer than 10 true elements in *PE_selection*, but the spread between the first and last PE in *PE_*selection is greater than 20 m, set *signal_selection_status_confident* to 2.

1415
1416

2d. If there are fewer than 10 true elements in *PE_selection,* and the spread between the first and last PE is less than 20 m, set *signal_selection_status_confident* to 3.

1417

1418
1419

3. Check if the combination of confidently detected PE and the padded PE are adequate to define an initial segment. If *signal_selection_status_confident* is zero, skip this step.

1420

3a. Set *PE_selection* to true for all PE with non-zero *ice_confidence_flag*.

1421
1422

3b: If the difference in *x_PE* between the first and last PE in *PE_selection* is less than 20 m set *signal_selection_status_all* to 1.

1423
1424

3c: If there are fewer than 10 true elements in *PE_selection*, but the spread between the first and last PE in *PE_*selection is greater than 20 m, set *signal_selection_status_all* to 2.

1425
1426

3d. If there are fewer than 10 true elements in *PE_selection,* and the spread between the first and last PE is less than 20 m, set *signal_selection_status_all* to 3.

1427
1428

3e: If *signal_selection_status_all* is equal to zero, set *signal_selection_source* to 1 and proceed to step 4, otherwise set *signal_selection_source* to 2, and return.

1429
1430

4. Calculate the vertical spread of the selected PE, make the selection consistent with a vertical window around a sloping segment.

1431
1432

4a. Calculate the least-squares fit line between (x_PE-x_0) and h_PE for the selected PE. Internal variables set: *along_track_slope*, *seg_center_height.*

1433

4b. Calculate *r_PE,* the residual between the best-fitting line and *h_PE*.

1434
1435
1436

4c. Calculate *sigma_r*, the robust spread (accounting for noise) of *r_PE*, based on the background density, *BG_density,* with *z_min* and *z_max* set to the minimum and maximum values of *r_PE*. See the **robust_dispersion** section for description.

1437
1438

4d. Calculate the expected PE spread, *sigma_expected*, based on the current slope estimate:

1439

$$sigma\_expected=[(c/2\ sigma\_xmit)^2 + sigma\_beam^2 along\_track\_slope^2]^{1/2}$$

1440

4e. Calculate *H_win*:

1441

$$H\_win=max(H\_win\_min,\ 6\ sigma\_expected,\ 6\ sigma\_r)$$

1442
1443

4f. Select all PE that have *abs(r_PE) < H_win/2*. Report the number of selected PE as *N_initial*.

1444

5.6   Backup PE-selection routine.

1445

Inputs:

1446   *x_PE* : along-track coordinates of all PE for the current beam

1447   *h_PE*: heights of all PE for the current beam

1448   *x0*: along-track bin center for the current bin.

1449   *Ice_confidence_flag*: ATL03 classification of the land-ice PE. 0=undetected, 1=PE in the
1450 pad region, but not identified as signal PE, 2=low confidence, 3=medium confidence, 4=high
1451 confidence

1452   *signal_selection_source*: Flag indicating the how the signal was selected. See Table 3-1
1453 for values.

1454 **Outputs**:

1455   *PE_selection*: selected PE for the current bin.

1456   *signal_selection_source*: Flag indicating the how the signal was selected. See Table 3-1
1457 for values, updated based on the results of this algorithm

1458   *signal_selection_status_backup* flag indicating the success/failure of signal selection
1459 using backup selection algorithm

1460   *H_win:* Vertical extent of the selected window

1461 **Internal variables:**

1462   *Test_window_center:* Vector of test window centers

1463   *Window_center_height:* Estimated window center height

1464 **Procedure**:

1465 1. Attempt to center the window on any ATL03 flagged PE that are present.

1466   1a. If any padded or detected PE are found, set *w0* to the maximum of 10 m and the
1467 difference between the maximum and minimum selected PE heights, and set *PE_selection* to true
1468 for all PE that have heights within *5 m* of the median of the selected PE heights. Set *H_win*
1469 equal to 10 m.

1470   1b. If the horizontal spread in the PE marked in *PE_selection* is greater than 20 m, and if
1471 10 or more PE are selected, then set *signal_selection_status_backup* to zero, set
1472 *signal_selection_source* to 2, and return.

1473 2. Find the 80-m along-track by 10-m vertical bin that contains the largest number of PEs

1474   2a. Select all PE from ATL03 segments *m-2* to *m+1,* inclusive.

1475   2b. Loop over *test_window_center* values between *floor(min(h_PE))*+0.25 and
1476 *ceil(max(h_PE))* in 0.5 m steps. For each *test_window_center* value, count the PE in a 10-m
1477 (vertical) bin centered on the *test_window_center* value.

1478   2c. Find the maximum of the window counts, *Cmax*, and calculate its uncertainty,
1479 *Csigma=sqrt(Cmax).* If *Cmax* is less than 16, then set *PE_selection* to null (no selected PE) and
1480 skip to step 3.

1481   2d. Set *window_center_height* equal to the center of the range of *test_window_center*
1482   values that have a count greater than *Cmax-Csigma*. Set *H_win* to the difference between the
1483   minimum and maximum of *test_window_center* values that have a count greater than *Cmax-*
1484   *Csigma*, plus 10 m.

1485   2e. Set *PE_selection* to 1 for all PE in ATL03 segments *m*-1 and *m*, with a height within
1486   *H_win/2* of *window_center_height.*

1487   3. Evaluate the selection.

1488   3a. Set *signal_selection_status_backup* to 1.

1489   3b: If the difference in *x_PE* between the first and last PE in *PE_selection* is less than 20
1490   m set *signal_selection_status_backup* to 2.

1491   3c: If there are fewer than 10 true elements in *PE_selection*, but the spread between the
1492   first and last PE in *PE_*selection is greater than 20 m, set *signal_selection_status_backup* to 3.

1493   3d. If there are fewer than 10 true elements in *PE_selection,* and the spread between the
1494   first and last PE is less than 20 m, set *signal_selection_status_backup* to 4.

1495   3e. If *signal_selection_status_backup* is 1, set *signal_selection_source* to 2, if greater
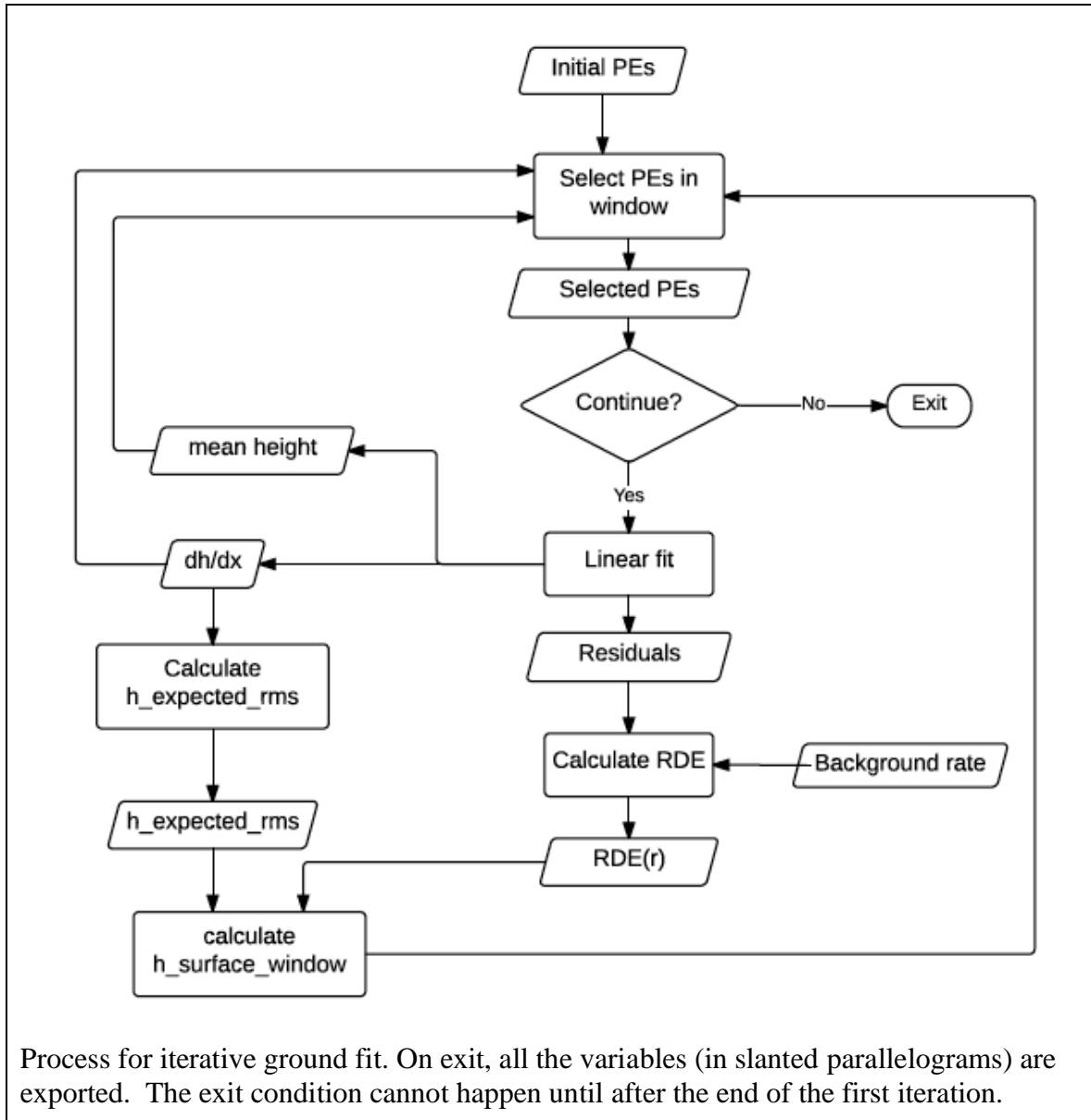1496   than 1, set *signal_selection_source* to 3.

1497

1498   **5.7   Iterative Least-Squares Fitting Routine**

1499   This routine performs the iterative least-squares fit to refine the surface window and determine
1500   the along-track slope. The process for this step is shown in Figure 5-2.

Figure 5-2. Flow chart for iterative ground fit

Process for iterative ground fit. On exit, all the variables (in slanted parallelograms) are exported. The exit condition cannot happen until after the end of the first iteration.

1501

1502 **Inputs:**

1503   *x_PE* : along-track coordinates of PE for the current beam

1504   *y_PE* : across-track coordinates of PE for the current beam

1505   *input_PE_selection:* Flag defining the PE selected by the initial selection routine

1506   *h_PE*: heights of selected PE for the current beam

1507   *x0*: along-track bin center for the current bin.

1508   *bckgrd:* Interpolated background-PE rate estimate for the segment

1509   *H_win*: Initial surface-window height.

1510   *signal_selection_source:* Flag indicating the source of the initial signal selection

1511   *N_it*: maximum number of iterations

1512   **Parameters:**

1513   *Sigma_xmit:* transmitted pulse duration (seconds)

1514   *Sigma_beam*: sigma value for pulse surface footprint (expected to be equal to 4.25 m)

1515   *L0*: Along-track length of the window

1516   *N_seg_pulses:* Number of pulses in a 40-meter segment (equal to 58 assuming 7 km/s
1517   ground-track speed)

1518   *H_win_min:* Minimum allowed surface window height, equal to 3m.

1519   **Outputs**:

1520   *H_win*: the height of the window around the best-fitting segment within which PE are
1521   selected.

1522   *dh_fit_dx:* The along-track slope of the best-fitting segment

1523   *h_mean:* The mean-based height of the best-fitting segment

1524   *PE_fit_flag*: A flag indiciating whether a particular PE has been selected based on the
1525   segment height and slope and *H_win.*

1526   *r0:* Residuals to the best-fitting segment

1527   *h_mean_sigma_unit:* Estimated error in *h_mean* per unit of PE-height error

1528   *dh_fit_dx_sigma_unit:* Estimated error in *dh_fit_dx* per unit of PE-height error.

1529   *N_signal* : Estimated number of signal PE

1530   *N_BG :* Estimated number of background PE

1531   *h_robust_sprd :* robust spread of residuals

1532   *h_rms_misfit*: RMS misfit of residuals

1533   *SNR:* signal-to-noise ratio for window.

1534   **Procedure:**

1535   1. Initialize the fit.

1536   1a. If *signal_selection_source* is zero or 1, eliminate all PE not marked as 1 in
1537   *input_PE_selection,* set *PE_fit_flag* to 1 for all remaining PE.

1538   1b. If *signal_selection_source* is nonzero, Set *PE_fit_flag* to 1 for all PE marked in
1539   *input_PE_selection,* zero for all others.

1540   1c. Calculate the vertical noise-photon density:

1541 $BG\_density = N\_seg\_pulses\ median(bckgrd) / (c/2)$

1542   2. Iterate the fit.

1543   2a. Check whether enough PE are selected to define a window. If fewer than 10 PE are
1544   selected in *PE_fit_flag*, set *H_win, dh_fit_dx, H_mean,* and *r0* to invalid, and return.

1545   2b. Calculate the least-squares linear fit between *h_PE* and *x_PE-x0* for the PE selected
1546   in *PE_fit_flag*. The intercept of the fit is *h_mean,* the slope is *dh_fit_dx*. Calculate the residual to
1547   this fit for the selected PE, *r0* and for all PE, *r*. If the along-track spread between the first and
1548   last selected PE is less than 10 m, fit for the height only, and set the along-track slope estimate to
1549   zero.

1550   2c. Calculate *sigma_r*, the robust spread (accounting for noise) of *r0*, based on the
1551   background density, *BG_density,* and current window height, *H_win*. The variables input to the
1552   ***robust dispersion including a background estimate*** routine are *z=r0, zmin=-H_win/2,*
1553   *zmax=H_win/2*, *N_BG=H_win BG_density*.   If the resulting *sigma_r* is greater than 5 m, set it to
1554   5 m.

1555   2d. Calculate the expected PE spread, *sigma_expected*, based on the current slope
1556   estimate:

1557 $sigma\_expected=[(c/2\ sigma\_xmit)^2 + sigma\_beam^2 along\_track\_slope^2]^{1/2}$

1558   2e. Save the value of *H_win* in *H_win_previous*, then calculate the window height from
1559   *sigma_expected* and *sigma_r*.

1560   *H_win=max(H_win_min, 6 sigma_expected, 6 sigma_r, 0.75 H_win_previous)*

1561   2f. Save the values of *PE_fit_flag* in *PE_fit_flag_last*.

1562   2g. Select PE within *H_win*/2 of the segment fit.

1563   *PE_fit_flag*= 1 for PE with *r<H_win*/2, 0 for PE with *r > H_win/2*

1564   2h. Evaluate the newly selected PE. If there are fewer than 10 selected PE, or if the
1565   along-track spread between the first and last PE is less than 20 m, set *PE_fit_flag* to
1566   *PE_fit_flag_last, H_win* to *H_win_previous*, and continue to step 3.

1567   2i. If fewer than *N_iterations* have been completed, and if the values for *PE_fit_flag* have
1568   changed since the previous iteration, return to step 2a. Otherwise continue to step 3.

1569   3. Propagate the error in the fit parameters assuming unit data errors (see 3.6, with $\sigma_{photon}=1$).
1570   This gives the unit errors *h_mean_sigma_unit*, *dh_fit_dx_sigma_unit*.

1571   4. Calculate the number of signal and background PE, and the SNR.

1572   *N_BG=bckgrd H_win 2/c N_seg_pulses*

1573   *N_signal=max(0, number of selected PE – N_BG)*

1574   *SNR=N_signal/N_BG*

1575   5. Calculate output error statistics:

1576   *h_rms_misfit=*RMS misfit of selected PE

1577   *h_robust_sprd = sigma_r* from the last iteration

1578   **5.8   Robust dispersion calculation from a collection of points, not including a background**
1579   **estimate**

1580   **Input**:

1581   z: sampled values

1582   **Output:**

1583   RDE : the robust dispersion estimate for z.

1584

1585   **Procedure**:

1586   1. Sort z. *zs* is equal to *z*, sorted in ascending order. Let *Nz* equal to the number of elements in *z*.

1587   2. Calculate an abscissa for *zs*,

1588   2a. Generate *ind*, equal to the sequence of integers between 1 and *Nz*.

1589   2b. Calculate *ind_N*, equal to *(ind-0.5)/Nz*.

1590   3. Interpolate the percentiles of *z*.   Interpolate the values of *zs* as a function of *ind_N* at values
1591   0.16 and 0.84. Half the difference between these values is *RDE*.

1592

1593   **5.9   Robust dispersion calculation from a collection of points, including a background**
1594   **estimate**

1595   **Inputs**:

1596   *z*: sampled values

1597   *zmin, zmax*: window from which the values in z are sampled

1598   *N_BG*: Estimate of the number of background events between *z_min* and *z_max*.

1599   **Output:**

1600   *RDE* : the robust dispersion estimate for z.

1601   **Parameter:**

1602   *Scale_factor*: equal to *sqrt(2)(erfinv(0.5)-erfinv(-0.5))*, where *erfinv( )* is the inverse error
1603   function, or 1.3490.

1604   **Procedure**:

1605   1. Estimate the background rate and signal count.

1606   1a. *bckgrd* is equal to *N_BG* divided by the difference between *zmax* and *zmin*.

1607   1b. *N_sig* is equal to the number of elements in *z*, minus *N_BG*.

1608   1c. If *N_sig<=1*, the RDE is equal to *(zmax-zmin)/(the number of elements in z)*, and the
1609   rest of the calculation is skipped.

1610   2. Sort z. *zs* is equal to *z*, sorted in ascending order. Let *Nz* equal to the number of elements in *z*.

1611   3. Calculate an abscissa for *zs*. Generate *ind*, equal to the sequence of integers between 1 and *Nz*,
1612   minus 0.5.

1613   4. Find the indices for the smallest potential percentiles of *z*.

1614   4a. *i0* is equal to the index of the greatest value of *ind* for which *ind<(0.25N_sig + (zs-*
1615   *zmin)bckgrd).*

1616   4b. *i1* is equal to the index of the smallest value of *ind* for which *ind>(0.75N_sig + (zs-*
1617   *zmin)bckgrd).*

1618   5. If *i1<i0*, reselect *i0* and *i1* to measure spread of the central *N_sig*/2 values of the distribution:

1619   5a: *i0* is equal to the index of the greatest value of *ind* for which *ind<Nz/2-Nsig/4.*

1620   5b: *i1* is equal to the index of the smallest value of *ind* for which *ind>Nz/2+Nsig/4.*

1621   6. Calculate *RDE*. *RDE* is equal to the difference between the *zs* values at *i0* and *i1*, divided by
1622   *scale_factor.*

1623   **5.10 First- Photon Bias Correction**

1624   These routines calculate the first-photon bias for a collection of residual photon heights. Most of
1625   the calculation is done as a function of time, and the results are converted back to height at the
1626   end of the routine.

1627

1628   **Inputs:**

1629   *r_p*: PE heights, corrected for the along-track segment fit, converted to time (multiplied by –2/c)

1630   *N_seg_pulses*: the number of pulses in the segment

1631   *N_px*: the number of pixels in the detector.

1632

1633   **Outputs:**

1634   *G_est*: the estimated detector gain

1635   *N_hist:* The uncorrected PE count histogram (in units of PE)

1636   *N_PEcorr*: the estimated PE count histogram (in units of PE)

1637   *t_full*: the time vector for the PE count histogram.

1638   *FPB_med_corr*: the FPB correction to the median height

1639   *Sigma_FPB_med_corr*: the error estimate for *FPB_med_corr*

1640   *FPB_mean_corr*: The FPB correction to the mean height

1641   *FPB_mean_corr_sigma*: the error estimate for *FPB_mean_corr*.

1642   *Fpb_N_photons*: the FPB-corrected estimate of the number of PE in the return.

1643

1644   **Parameters:**

1645   *t_dead* : the mean detector dead time for the beam.

1646   *N_seg_pulses*: the number of pulses in the segment

1647   *N_px*: the number of pixels in the detector.

1648   *dt*: duration of a histogram bin.

1649

1650   **Procedure:**

1651

1652   *1. Generate a residual histogram*

1653   Convert PE height residuals to time residuals (multiply by -2/c). Generate a histogram of time
1654   residuals, *N_hist*, in bins of size *dt.*

1655   *2. Calculate the gain from the histogram*

1656   *P_dead* for bin i is the sum over bins i-N_dead to i-1 of *N_hist,* divided by *N_seg_pulses N_px.*
1657   *G_est* is equal to 1- *P_dead, where N_dead* is the deadtime expressed in histogram bins.

1658   *3.* Check if the correction is valid. If the minimum value for *G_est* is less than 2/(*N_seg_pulses*
1659   *N_px*), set all return values equal to invalid (*NaN*) and return.

1660   *4. Calculated the corrected histogram:*

1661   *N_PEcorr* is equal to *N_hist* divided by *G_est.*

1662   *5. Calculate height statistics*

1663   Calculate the gain-corrected mean and median and their errors for the segment, based on the full
1664   gain estimate and the full histogram:

1665   *FPB_med_corr*: -1/2c times the gain-corrected median time based on *N_PE* and *G_est.* See
1666   5.11.

1667   *Sigma_FPB_med_corr*: the error estimate for *FPB_med_corr*

1668   *FPB_mean_corr*: -1/2c times the gain-corrected mean time based on *N_PE* and *G_est.* See 5.12.

1669   *FPB_mean_corr_sigma*: the error estimate for *FPB_mean_corr*.

1670   *Fpb_N_photons*: the sum of *N_PEcorr*.

1671

1672

1673   **5.11 Gain-corrected median**

1674   Inputs:

1675   *N:* The uncorrected histogram

1676 *G*: The gain estimate,

1677 x: the abscissa for the bin centers, corresponding to N and G.

1678

1679 Outputs:

1680 *x_med*: the median of N based on G

1681 *sigma_x_med*: the error in *x_med*

1682

1683 **Procedure:**

1684 *1. Calculate the corrected histogram:*

1685 *N_corr* is equal to *N* divided by *G*.

1686

1687 *2. Calculate the CDF of N_corr*

1688 The CDF, *C*, is calculated at the bin centers, and at each bin center, *j*, is equal to the sum of all
1689 values of *N_corr* for bin centers $i < j$. *C* is normalized so that its last value is equal to 1.

1690

1691 *3. Calculate the 40th, 50th, and 60th percentiles of N_corr*

1692 *C* is treated as a function that increases linearly across each bin, such that the upper edge of the
1693 ith bin is greater than the lower edge of the ith bin by N_i. The abscissa for *C* runs from zero at
1694 $x_1-dx/2$, to $x_m+dx/2$, where x_1 is the first bin center, x_m is the last bin center, and *dx* is the spacing
1695 between bin centers. The 40th, 50th, and 60th percentiles of *N_corr* are calculated by interpolating
1696 into the vector of bin edges as a function of *C*. If more than one bin has a CDF within numerical
1697 precision of the calculated percentile, report the mean x value of all such bins.

1698

1699 *4. Calculate the error in the CDF at the 50th percentile*

1700 The error in any value of *N_corr* (*sigma_N_corr*) is the inverse gain value for that bin times the
1701 square root of *N* for that bin. *sigma_CDF* for any x is found by calculating the RSS of all
1702 *sigma_N_corr* values for bins less than x, and dividing by the sum of *N_corr*.

1703 The value for *sigma_CDF* at the 50th percentile is found by interpolating *sigma_CDF* as a
1704 function of *C* at a *C* value of 0.5.

1705

1706 5. calculate *sigma_x_med*

1707 Sigma_x_med is found:

$$sigma\_x\_med = \frac{dz_{60} - dz_{40}}{0.2} \sigma_{cdf}(dz_{med})$$

1708

1709   Here dz_{60} and dz_{40} are the 40th and 60th percentiles of N_corr from step 3.

1710

1711   **5.12   Gain-corrected mean**

1712   Inputs

1713   *N:* The uncorrected histogram

1714   *G*: The gain estimate

1715   x: the abscissa for the bin centers, corresponding to N and G.

1716

1717   **Outputs:**

1718   *x_mean*: the mean of N based on G

1719   *sigma_x_mean*: the error in *x_mean*

1720

1721   *1. Calculate the corrected histogram:*

1722   *N_corr* is equal to *N* divided by *G*.

1723

1724   *2. Calculate the corrected mean:*

1725   Calculate the mean:

$$x\_mean = \sum \frac{N_{corr,i}}{N_{tot}} x_i$$

1726

1727   *3. Calculate the error in the corrected histogram:*

$$\sigma_{N,corr,i} = \frac{N_{0,i}^{1/2}}{G_i}$$

1728

1729   4. Calculate the error in the corrected mean:

$$sigma\_x\_mean = \left[\sum \left(\sigma_{N,corr,i} \frac{x_i - x\_mean}{N_{corr,tot}} \right)^2 \right]^{1/2} \qquad 49$$

1730

1731 **5.13 Transmit-pulse-shape correction**

1732 This routine uses the most recent estimate of the transmit-pulse shape calculated from the
1733 transmitter-echo pulse to calculate median and mean offsets for a windowed, truncated received
1734 pulse. This correction depends the shape of the transmit pulse, and on three parameters that are
1735 unique to each segment: the estimated width of the return pulse, the refined surface-window
1736 height, and the signal-to-noise ratio.

1737

1738 **Inputs:**

1739 -Transmit-pulse-shape estimate (t_tx, P_tx). The time vector, t_tx is shifted so that P_tx has a
1740 zero centroid (see 5.15).

1741 -Received-pulse width estimate (W_rx)

1742 -Surface-window time duration (dt_W)

1743 -Signal-to-noise ratio estimate within the truncated window (SNR)

1744 **Outputs:**

1745 Height offsets for the mean and median transmit-pulse-shape correction.

1746

1747 **Procedure:**

1748 This correction works by generating a synthetic return pulse that matches the width of the actual
1749 return pulse, and truncating it in the same way that the return pulse has been truncated. The
1750 median and the mean of the synthetic pulse are then calculated.

1751

1752 *1. Calculate the time by which the received pulse was broadened*

1753 The spreading needed to broaden the transmitted pulse to match the received pulse is equal to
1754 *$W\_spread=sqrt(max(0.01e-9^2, W\_RX^2 – W\_TX^2))$.*

1755

1756 *2. Generate a synthetic received pulse*

1757 *2a: Calculate the shape of the expected spread pulse:*

1758 The synthetic received pulse is generated by convolving the transmitted pulse with a Gaussian
1759 function of with a sigma parameter equal to *W_spread*. The Gaussian should have enough
1760 samples to include at least *$4*W\_spread$* worth of samples on either side of its center. The
1761 synthetic pulse and its time vector are *$N\_hist\_synthetic$* and *$t\_synthetic$*.

1762

1763 *2b: Calculate the median of the broadened synthetic pulse:*

1764 Calculate the median of the synthetic received pulse, *$t\_synthetic\_med$*, and set
1765 *$t\_ctr=t\_synthetic\_med$.*

1766

1767   *2c: Normalize the waveform and add an estimated noise signal:*

1768   *N_hist_synthetic* is normalized so that its sum is equal to 1, and a background count of 1/*SNR*
1769   (*dt/dt_W*) is added to *N_hist_synthetic*.

1770

1771   *3. Calculate the centroid of the synthetic received pulse*

1772   To find the centroid of the truncated synthetic waveform, an iterative procedure is used:

1773   *3a: Calculate the centroid of the synthetic waveform*

1774   *t_ctr* is set to the centroid of the truncated synthetic received waveform, windowed by *t_ctr -*
1775   *dt_W/2* and *t_ctr +dt_W/2*

1776   *3b: Check for convergence and iterate*

1777   Unless the current and previous values of *t_ctr* are consistent to within 0.1 mm (0.00067 ns) or if
1778   50 iterations are complete, return to *4a*.

1779

1780   *4. Calculate the median of the synthetic received pulse*

1781   The median of the synthetic received waveform is calculated the synthetic received waveform
1782   from 4b, windowed by *t_ctr -dt_W/2* and *t_ctr +dt_W/2*

1783

1784   5. The corrections for the median and mean heights are equal to c/2 times the median and mean
1785   time offsets.

1786   **5.14 Residual_histogram calculation**

1787   **Inputs:**

1788   *Segment_lat* : latitude for each segment center

1789   *Segment_lon* : longitude for each segment center

1790   *Segment_x_*ATC: along-track (x) coordinate for each segment center

1791   *Segment_h_mean:* mean-based land-ice height for each segment center

1792   *Segment_slope*: along-track slope for each segment center

1793   *Segment_SNR*: SNR values for segment fits

1794   *Segment_BGR:* Background rate estimate for each segment

1795   *N_seg_pulses* Number of pulses in each segment (including those contributing no PE to the fit).

1796   *x_pe*: along-track(x) coordinates for all ATL03 PE in the segment

1797   *h_pe:* ATL03 surface height for all PE in the segment.

1798   **Parameters:**

1799   *N_hist:* Number of groups of segments in the histogram (number of horizontal divisions)

1800   *N_bins***:** Number of vertical bins in the residual histogram

1801   *bin_top_h:* Tops of the histogram bins, listed from bottom to top

1802   **Outputs:**

1803   *Count*: *N_bins* x *N_hist*-element array giving the number of residual photons in each bin
1804   (*N_bins* is the vertical dimension, *N_hist* is the horizontal dimension)

1805   *bckgrd_per_m: 1xN_hist-vector giving the expected background count per vertical*
1806   *meter in each column of the histogram based on the observed background rate (bckgrd) and the*
1807   *number of segments included in the histogram*

1808   *Segment_id_list:* 10 x *N_hist*-element array list of segment IDs included in the histogram

1809   *Lat_mean: N_hist*-element list giving the mean latitude of all segments included in each
1810   horizontal histogram bin

1811   *Lon_mean: N_hist*-element list giving the mean longitude of all segments included in
1812   each horizontal histogram bin

1813   *x_ATC_mean: N_hist*-element list giving the mean along-track (x) coordinate of all
1814   segments included in each horizontal histogram bin

1815   **Procedure**

1816   1. Calculate the bin-edge heights. There are N_bins+1 edges. The second through last edges are
1817   equal to the input *bin_top_h* values. The first (lowest) edge is 1 m lower than the second (i.e.
1818   equal to the first value of *bin_top_h* -1).

1819   2. Group segment centers into 10-segment groups: For each RGT, segments 1-10 would be in the
1820   first group, 11-20 in the second, etc.

1821   3. For each group, gather all valid segments that have high-quality surface-height estimates
1822   (*ATL06_quality_summary=0*). If any high-quality segments are present, calculate the histogram
1823   count. Otherwise, report the histogram count as all zeros, and report *lat_mean*,
1824   *lon_mean*,_*x_atc_mean*, and *segment_id_list* as invalid.

1825   3a. For each valid segment, calculate the histogram and background count.

1826   3a.1: Gather the PE that have *x_segment* -10 m < *x_pe* <= 10 m.

1827   3a.2: Calculate the residual between the segment and the gathered PE: *r=h-*
1828   *h_mean_segment- (x_pe- segment_x_ATC) × segment_slope.*

1829   3a.3: For each vertical bin in the histogram, count the PE with residuals that fall
1830   into the bin

1831   3a.4: For each valid segment, add the expected background count per vertical
1832   meter, as estimated from the segment background count to the total background-per-meter
1833   (*bckgrd_per_m*) for the segment. The contribution for each segment is: *segment_BGR ×*
1834   *N_seg_pulses / 2 /(c/2). [N.B. The factors of 2 in the previous statement cancel, leaving* :
1835   *segment_BGR × N_seg_pulses /c.]*

1836   3b. Add the segment histograms together to calculate the 10-segment histogram

1837   3c. Calculate the mean values for latitude, longitude, and *x_ATC* for the segment. List
1838 the selected segments in *segment_id_list*

1839

1840 **5.15 Transmit-echo-pulse initialization**

1841 This calculation centers the transmit-echo-pulse reported by ATL03 on its centroid, after using
1842 an iterative edit to distinguish between signal and noise. It should be performed each time a new
1843 night-time TEP estimate of the waveform becomes available. The TEP consists of the power
1844 (*tep_hist*) and time (*tep_hist_x*) that are input from ATL03. Two TEP histograms are available,
1845 obtained for laser spot 1 and 3. The ATL03 *tep_valid_spot* parameter specifies with which TEP
1846 histogram is used for each of the ground tracks, and the ATL03 *tep_range_prim* parameter
1847 specifies the valid range of times for each TEP histogram.

1848 **Inputs:**

1849 -*tep_hist_x* : Time for the Transmit-pulse-shape estimate

1850 -*tep_hist*: power (or signal count) for the transmit-pulse-shape estimate

1851 The time-sampling interval these is *dt_input*. The transmit pulse is sampled so that at least the
1852 first 5 ns and the last 10 ns are representative of the background noise for the transmit pulse.

1853 **Outputs:**

1854 -*t_tx*: time vector for the transmit pulse estimate, shifted such that *P_tx* has a zero centroid

1855 -*P_tx*: Power for the transmit-pulse estimate,

1856 **Algorithm:**

1857 *1. Identify noise-only and signal samples:* mark index *noise_samples* as true for the first 5 ns
1858 and last 10 ns of samples in *tep_hist*. Set *sig_samples* to the inverse of *noise_samples*

1859 *2. Calculate the noise value for the transmit pulse:* N_tx = the mean of *tep_hist* for the samples
1860 in *noise_samples*. Subtract N_tx from *tep_hist* to give *P_tx*.

1861 *3. Calculate the centroid of the transmit pulse: $T0\_tx = sum(\ P\_tx*\ t\_tx)\ /sum(P\_tx)$.* *The sum*
1862 *is carried out over the samples in sig_samples.*

1863 *4. Calculate the RDE of the transmit pulse*: The width of the transmitted pulse (W_TX) is equal
1864 to half the difference between the 84th percentile and the 16th percentile of the portion of *P_tx* in
1865 *sig_samples.*

1866 *5. Re-establish the noise-only samples:* mark *noise_samples* as true for all samples with times
1867 more than 6 W_TX away from *T0_tx,* set *sig_samples* to the inverse if *noise_samples.* If
1868 *sig_samples* has changed from its previous values, and if fewer than 10 iterations have taken
1869 place, return to *1b*.

1870 *6. Center the transmit pulse on its centroid:* Subtract *T0_tx* from *t_tx_input* to give *t_tx*.

1871

1872

1873 **6   TEST DATA AND SOFTWARE REQUIREMENTS**

1874 This section describes a very simple test data set that has been derived to verify the performance
1875 of the ATL06 surface code.

1876 **6.1   ATL06 Test Data Setup**

1877 The ATL06 test data are a set of synthetic data generated based on a planar, sloping surface with
1878 a slope of 0.02. Separate data sets are generated for surface reflectance values between 1/16 and
1879 1, and for surface roughness values between zero and 2 m. A detector model with a dead time of
1880 3.2 ns is used to simulate the effects of the first-photon bias. For each segment, a full set of
1881 ATL06 parameters are generated using the Matlab prototype code, and with the ASAS
1882 production code, and the two are compared. Small numerical differences between the codes can
1883 produce different results in the early stages of the signal-finding code, so the most valid
1884 comparisons between the results of the two codes are for segments with moderate signal strength
1885 (reflectance greater than 0.25). We consider the two codes to produce equally valid results when
1886 the difference between the results for any parameter is not significantly different from zero, and
1887 when the spreads of the two sets of parameters are not significantly different from one another
1888 for segments based on the same number of photons with the same surface window size.

1889 **7   BROWSE PRODUCTS AND Q/A STATISTICS**

1890 **7.1   Browse Products**

1891   Browse products include two kinds of plots: Data-quality maps, and profile plots.

1892   Data-quality maps are based on the *signal_selection_source* parameter. Each map shows a
1893   background image based on the MODIS mosaics of Greenland or Antarctica (Scambos and
1894   others, 2007), with color-coded points showing the mean segment location for each kilometer of
1895   the beam track, with the color showing the largest bit in signal_selection_source that is set for
1896   more than 50% of all segments in that kilometer of data, assuming that for segments with no
1897   data, all bits are set. The plots are made separately for the strong and weak beams, because the
1898   two beams are, at the granule scale, very close to one another and would otherwise overlap.

1899   Profile plots are generated separately for each beam pair in the granule. Each plot shows the
1900   surface height as a function of along-track distance, and the height for each beam in the pair. A
1901   second set of axes, aligned with the first, shows the number of PE per segment (*N_fit_photons*)
1902   and the height error estimate, *h_li_sigma*.

1903   **7.2   Q/A Statistics**

1904   Quality assessment statistics are provided for each beam, for each 10-km increment along track.
1905   For each increment we provide:

1906   A synopsis of the *signal_selection_source* parameter:

1907   -The fraction of possible segments with *signal_selection_source* equal to zero.

1908   -The fraction of segments with *signal_selection_source* equal to 1.

1909   -The fraction of segments with *signal_selection_source* equal to 2.

1910   -The fraction of segments with *signal_selection_source* equal to 3.

1911   [Add parameters for the entire file]

1912

1913

1914 **8   APPENDIX A: GLOSSARY**

1915 This appendix defines terms that are used in ATLAS ATBDs, as derived from a document
1916 circulated to the SDT, written by Tom Neunann.   Some naming conventions are borrowed from
1917 **Spots, Channels and Redundancy Assignments** (ICESat-2-ATSYS-TN-0910) by P. Luers.
1918 Some conventions are different than those used by the ATLAS team for the purposes of making
1919 the data processing and interpretation simpler.

1920

1921 **Spots.** The ATLAS instrument creates six spots on the ground, three that are weak and three that
1922 are strong, where strong is defined as approximately four times brighter than weak. These
1923 designations apply to both the laser-illuminated spots and the instrument fields of view. The
1924 spots are numbered as shown in Figure 1. At times, the weak spots are leading (when the
1925 direction of travel is in the ATLAS +x direction) and at times the strong spots are leading.
1926 However, the spot number does not change based on the orientation of ATLAS. The spots are
1927 always numbered with 1L on the far left and 3R on the far right of the pattern. Not: beams,
1928 footprints.

1929

1930 **Laser pulse (pulse for short).** Individual pulses of light emitted from the ATLAS laser are
1931 called laser pulses. As the pulse passes through the ATLAS transmit optics, this single pulse is
1932 split into 6 individual transmit pulses by the diffractive optical element. The 6 pulses travel to
1933 the earth's surface (assuming ATLAS is pointed to the earth's surface). Some attributes of a laser
1934 pulse are the wavelength, pulse shape and duration. Not: transmit pulse, laser shot, laser fire.

1935

1936 **Laser Beam.** The sequential laser pulses emitted from the ATLAS instrument that illuminate
1937 spots on the earth's surface are called laser beams. ATLAS generates 6 laser beams. The laser
1938 beam numbering convention follows the ATLAS instrument convention with strong beams
1939 numbered 1, 3, and 5 and weak beams numbered 2, 4, and 6 as shown in the figures. Not:
1940 beamlet.

1941

1942 **Transmit Pulse.** Individual pulses of light emitted from the ICESat-2 observatory are called
1943 transmit pulses. The ATLAS instrument generates 6 transmit pulses of light from a single laser
1944 pulse. The transmit pulses generate 6 spots where the laser light illuminates the surface of the
1945 earth. Some attributes of a given transmit pulse are the wavelength, the shape, and the energy.
1946 Some attributes of the 6 transmit pulses may be different. Not: laser fire, shot, laser shot, laser
1947 pulse.

1948

1949 **Reflected Pulse.** Individual transmit pulses reflected off the surface of the earth and viewed by
1950 the ATLAS telescope are called reflected pulses. For a given transmit pulse, there may or may
1951 not be a reflected pulse. Not: received pulse, returned pulse.

1952

1953   **Photon Event.** Some of the energy in a reflected pulse passes through the ATLAS receiver
1954   optics and electronics. ATLAS detects and time tags some fraction of the photons that make up
1955   the reflected pulse, as well as background photons due to sunlight or instrument noise. Any
1956   photon that is time tagged by the ATLAS instrument is called a photon event, regardless of
1957   source. Not: received photon, detected photon.

1958

1959   **Reference Ground Track (RGT).** The reference ground track (RGT) is the track on the earth at
1960   which a specified unit vector within the observatory is pointed. Under nominal operating
1961   conditions, there will be no data collected along the RGT, as the RGT is spanned by GT2L and
1962   GT2R (which are not shown in the figures, but are similar to the GTs that are shown). During
1963   spacecraft slews or off-pointing, it is possible that ground tracks may intersect the RGT. The
1964   precise unit vector has not yet been defined. The ICESat-2 mission has 1387 RGTs, numbered
1965   from 0001xx to 1387xx. The last two digits refer to the cycle number. Not: ground tracks, paths,
1966   sub-satellite track.

1967

1968   **Cycle Number.** Over 91 days, each of the 1387 RGTs will be targeted in the polar regions once.
1969   In subsequent 91-day periods, these RGTs will be targeted again. The cycle number tracks the
1970   number of 91-day periods that have elapsed since the ICESat-2 observatory entered the science
1971   orbit. The first 91-day cycle is numbered 01, the second 91-day cycle is 02, and so on. At the
1972   end of the first 3 years of operations, we expect the cycle number to be 12. The cycle number
1973   will be carried in the mid-latitudes, though the same RGTs will (in general) not be targeted more
1974   than once.

1975

1976   **Sub-satellite Track (SST).** The sub-satellite track (SST) is the time-ordered series of latitude
1977   and longitude points at the geodetic nadir of the ICESat-2 observatory. In order to protect the
1978   ATLAS detectors from damage due to specular returns, and the natural variation of the position
1979   of the observatory with respect to the RGT throughout the orbit, the SST is generally not the
1980   same as the RGT. Not: reference ground track, ground track.

1981

1982   **Ground Tracks (GT).** As ICESat-2 orbits the earth, sequential transmit pulses illuminate six
1983   ground tracks on the surface of the earth. The track width is approximately 10m wide. Each
1984   ground track is numbered, according to the laser spot number that generates a given ground
1985   track. Ground tracks are therefore always numbered with 1L on the far left of the spot pattern
1986   and 3R on the far right of the spot pattern. Not: tracks, paths, reference ground tracks, footpaths.

1987

1988   **Reference Pair Track (RPT).** The reference pair track is the imaginary line half-way between
1989   the planned locations of the strong and weak ground tracks that make up a pair. There are three
1990   RPTs: RPT1 is spanned by GT1L and GT1R, RPT2 is spanned by GT2L and GT2R (and may be
1991   coincident with the RGT at times), RPT3 is spanned by GT3L and GT3R. Note that this is the
1992   planned location of the midway point between GTs. We will not know this location very
1993   precisely prior to launch. Not: tracks, paths, reference ground tracks, footpaths, pair tracks.

1994

1995 **Pair Track (PT).** The pair track is the imaginary line half way between the actual locations of
1996 the strong and weak ground tracks that make up a pair. There are three PTs: PT1 is spanned by
1997 GT1L and GT1R, PT2 is spanned by GT2L and GT2R (and may be coincident with the RGT at
1998 times), PT3 is spanned by GT3L and GT3R. Note that this is the actual location of the midway
1999 point between GTs, and will be defined by the actual location of the GTs. Not: tracks, paths,
2000 reference ground tracks, footpaths, reference pair tracks.

2001

2002 **Pairs.** When considered together, individual strong and weak ground tracks form a pair. For
2003 example, GT2L and GT2R form the central pair of the array. The pairs are numbered 1 through
2004 3: Pair 1 is comprised of GT1L and GT1R, pair 2 is comprised of GT2L and GT2R, and pair 3 is
2005 comprised of GT3L and 3R.

2006

2007 **Along-track.** The direction of travel of the ICESat-2 observatory in the orbit frame is defined as
2008 the along-track coordinate, and is denoted as the +x direction. The positive x direction is
2009 therefore along the Earth-Centered Earth-Fixed velocity vector of the observatory. Each pair has
2010 a unique coordinate system, with the +x direction aligned with the Reference Pair Tracks.

2011

2012 **Across-track.** The across-track coordinate is y and is positive to the left, with the origins at the
2013 Reference Pair Tracks.

2014

2015 **Segment.** An along-track span (or aggregation) of PE data from a single ground track or other
2016 defined track is called a segment. A segment can be measured as a time duration (e.g. from the
2017 time of the first PE to the time of the last PE), as a distance (e.g. the distance between the
2018 location of the first and last PEs), or as an accumulation of a desired number of photons.
2019 Segments can be as short or as long as desired.

2020

2021 **Signal Photon.** Any photon event that an algorithm determines to be part of the reflected pulse.

2022

2023 **Background Photon.** Any photon event that is not classified as a signal photon is classified as a
2024 background photon. Background photons could be due to noise in the ATLAS instrument (e.g.
2025 stray light, or detector dark counts), sunlight, or mis-classified signal photons. Not: noise
2026 photon.

2027

2028 **h_**.** Signal photons will be used by higher-level products to determine height above the
2029 WGS-84 reference ellipsoid, using a semi-major axis (equatorial radius) of 6378137m and a
2030 flattening of 1/298.257223563. This can be abbreviated as 'ellipsoidal height' or 'height above
2031 ellipsoid'. These heights are denoted by h; the subscript ** will refer to the specific algorithm

2032 used to determine that elevation (e.g. is = ice sheet algorithm, si = sea ice algorithm, etc…). Not:
2033 elevation.

2034

2035 **Photon Cloud.** The collection of all telemetered photon time tags in a given segment is the (or
2036 a) photon cloud. Not: point cloud.

2037

2038 **Background Count Rate.** The number of background photons in a given time span is the
2039 background count rate. Therefore a value of the background count rate requires a segment of PEs
2040 and an algorithm to distinguish signal and background photons. Not: Noise rate, background
2041 rate.

2042

2043 **Noise Count Rate.** The rate at which the ATLAS instrument receives photons in the absence of
2044 any light entering the ATLAS telescope or receiver optics. The noise count rate includes PEs
2045 due to detector dark counts or stray light from within the instrument. Not: noise rate,
2046 background rate, background count rate.

2047

2048 **Telemetry band.** The subset of PEs selected by the science algorithm on board ATLAS to be
2049 telemetered to the ground is called the telemetry band. The width of the telemetry band is a
2050 function of the signal to noise ratio of the data (calculated by the science algorithm onboard
2051 ATLAS), the location on the earth (e.g. ocean, land, sea ice, etc…), and the roughness of the
2052 terrain, among other parameters. The widths of telemetry bands are adjustable on-orbit. The
2053 telemetry band width is described in Section 7 or the ATLAS Flight Science Receiver
2054 Algorithms document. The total volume of telemetred photon events must meet the data volume
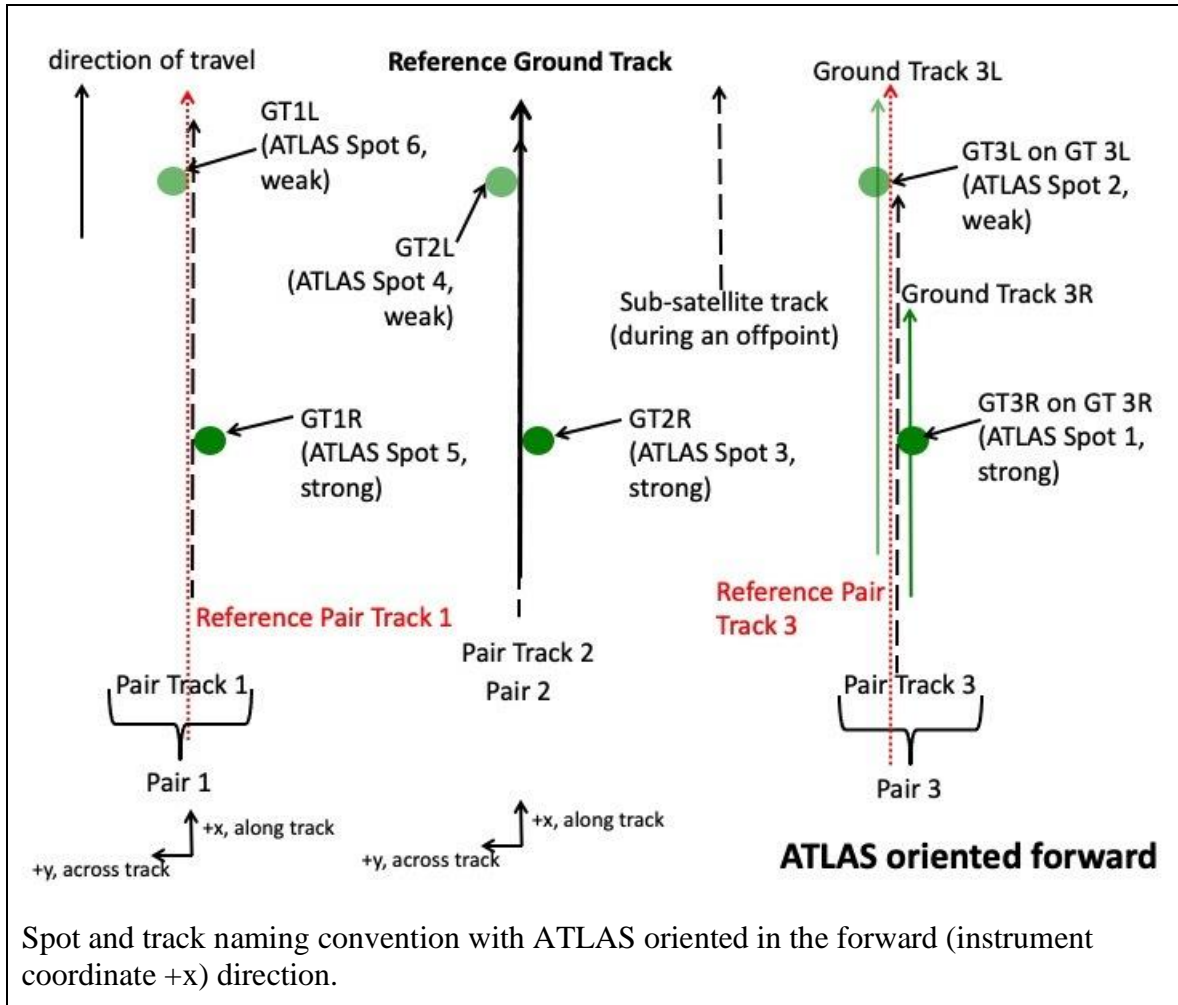2055 constraint (currently 577 GBits/day).

2056

2057 **Window, Window Width, Window Duration.** A subset of the telemetry band of PEs is called a
2058 window. If the vertical extent of a window is defined in terms of distance, the window is said to
2059 have a width. If the vertical extent of a window is defined in terms of time, the window is said to
2060 have a duration. The window width is always less than or equal to the telemetry band.
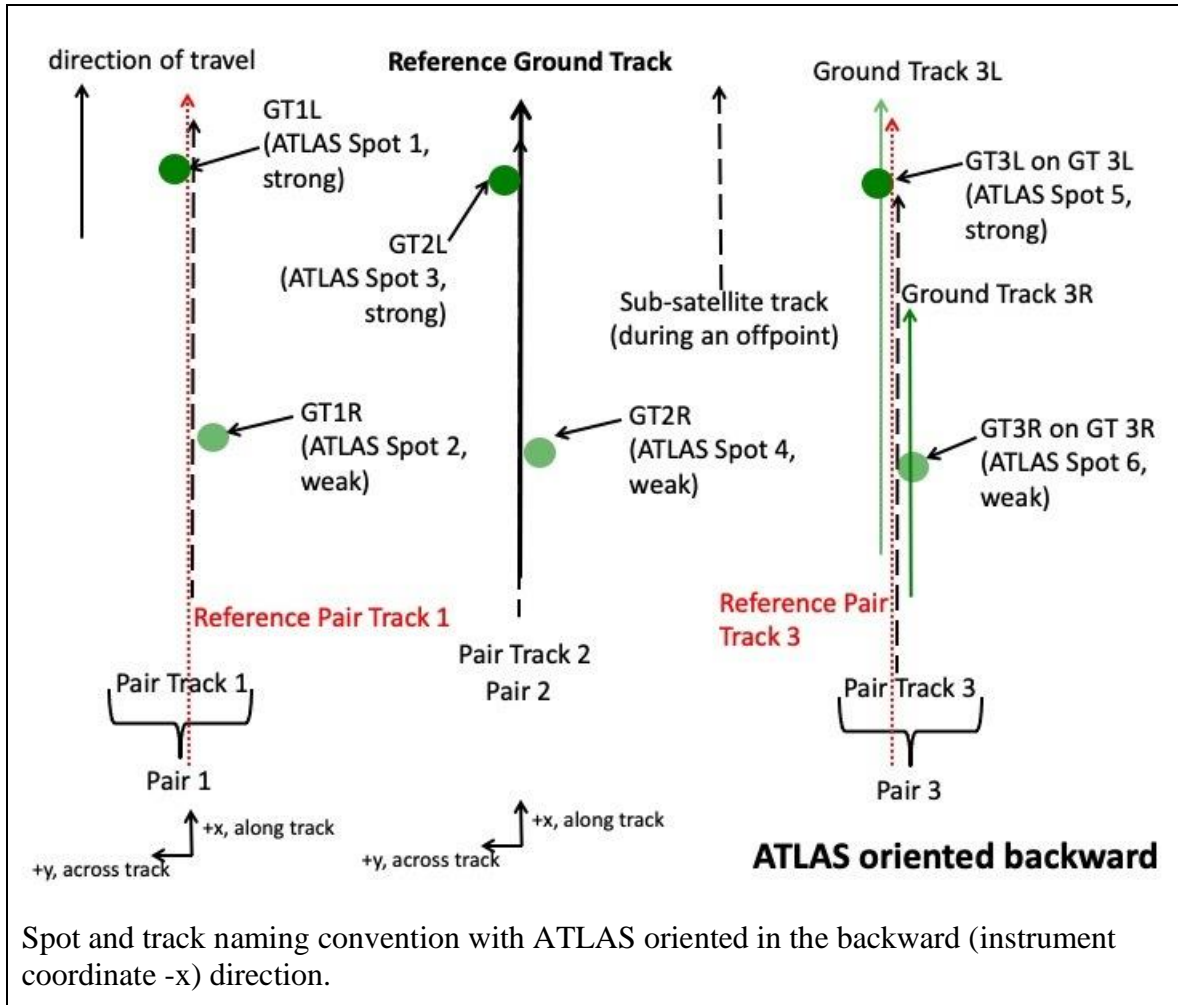
2061

Figure 8-1. Spots and tracks, forward flight

Spot and track naming convention with ATLAS oriented in the forward (instrument coordinate +x) direction.

2062

2063

Figure 8-2. Spots and tracks, forward flight

Spot and track naming convention with ATLAS oriented in the backward (instrument coordinate -x) direction.

2064

2065   **Glossary/Acronyms**

ASAS	ATLAS Science Algorithm Software
ATBD	Algorithm Theoretical Basis Document
ATLAS	ATLAS Advance Topographic Laser Altimeter System
CDF	Cumulative Distribution Function
DEM	Digital Elevation Model
GSFC	Goddard Space Flight Center
GTs	Ground Tracks
ICESat-2	Ice, Cloud, and Land Elevation Satellite-2
MABEL	Multiple altimeter Beam Experimental Lidar
MIS	Management Information System
NASA	National Aeronautics and Space Administration
PE	Photon Event
POD	Precision Orbit Determination
PPD	Precision Pointing Determination
PRD	Precise Range Determination
PSO	ICESat-2 Project Science Office
PTs	Pair Tracks
RDE	Robust Dispersion Estimate
RGT	Reference Ground Track
RMS	Root Mean Square
RPTs	Reference Pair Tracks
RT	Real Time
SCoRe	Signature Controlled Request

SIPS   ICESat-2 Science Investigator-led Processing System

TBD   To Be Determined

TL/DR   Too Long/Didn't Read.

References

2066

2067 Bamber, J.L., J.L. Gomez-Dans and J.A. Griggs 2009. A new 1 km digital elevation model of the
2068 Antarctic derived from combined satellite radar and laser data - Part 1: Data and methods.
2069 *Cryosphere*, **3**(1): 101-111.

2070 Menke, W. 1989. *Geophysical data analysis: discrete inverse theory.* San Diego, CA, Academic
2071 Press.

2072 Scambos, T.A., T.M. Haran, M.A. Fahnestock, T.H. Painter and J. Bohlander 2007. MODIS-
2073 based Mosaic of Antarctica (MOA) data sets: Continent-wide surface morphology and snow
2074 grain size. *Remote Sensing of Environment*, **111**(2-3): 242-257.

2075 Warren, S.G., R.E. Brandt and T.C. Grenfell 2006. Visible and near-ultraviolet absorption
2076 spectrum of ice from transmission of solar radiation into snow. *Applied Optics*, **45**(21): 5320-
2077 5334.

2078 Yang, Y., A. Marshak, S.P. Palm, T. Varnai and W.J. Wiscombe 2011. Cloud Impact on Surface
2079 Altimetry From a Spaceborne 532-nm Micropulse Photon-Counting Lidar: System Modeling for
2080 Cloudy and Clear Atmospheres. *Ieee Transactions on Geoscience and Remote Sensing*, **49**(12):
2081 4910-4919.

2082 Yang, Y., A. Marshak, S.P. Palm, Z. Wang and C. Schaaf 2013. Assessment of Cloud Screening
2083 With Apparent Surface Reflectance in Support of the ICESat-2 Mission. *Ieee Transactions on*
2084 *Geoscience and Remote Sensing*, **51**(2): 1037-1045.

2085 Yi, D.H. and C.R. Bentley 1999. Geoscience Laser Altimeter System waveform simulation and
2086 its applications. *Annals of Glaciology, Vol 29, 1999*, **29**: 279-285.

2087